Silesian University of Technology
Faculty of Environmental
Engineering and Energy

Institute of Thermal Technology

Clausthal University of Technology
Faculty of Energy and Management

Institute of Energy Process Engineering
and Fuel Technology

Ph.D. Thesis

Investigation of Fixed-Bed Combustion Process in Small Scale Boilers

Rafał Buczyński

This thesis was realized in the frame of the agreement between Silesian University of Technology and Clausthal University of Technology

Supervisors: prof. Andrzej Szlęk, prof. Roman Weber

Gliwice - Clausthal-Zellerfeld, 2011

Contents

1 Introduction **1**

2 Small scale retort boilers **6**
2.1 Low-emission retort boilers 6
2.2 Fuel for retort boilers 7
2.3 Environmental emission standards 9

3 Objectives **12**

4 Scope of the work **13**

5 Process model of fixed-bed combustion **14**
5.1 Coal structure 14
5.2 Coal decomposition during the combustion process 15
5.3 Thermal conductivity 16
5.4 Specific heat 18
5.5 Density and porosity of sold fuels 19
5.6 Rates of physical and chemical processes during combustion of solid fuel . . 21
5.7 Heat exchange between phases 24
5.8 Radiation of the gaseous phase 27
5.9 Pressure drop across the fixed - bed 29
5.10 Modeling of combustion and gasification in fixed beds 29

6 Mathematical model **31**
6.1 Gas phase free-board combustion model 31
6.1.1 The continuity equation 31
6.1.2 Momentum conservation equations 32
6.1.3 The conservation equation of chemical species 33
6.1.4 The energy conservation equation 33
6.1.5 Turbulences 34
6.1.6 Equation of state 36
6.1.7 Gas phase combustion model 36
6.1.8 Radiative heat transfer 38
6.2 Fixed - bed combustion model 38
6.2.1 Properties of EKORET coal 39
6.2.2 Flow of gas through a bed of solid fuel 40
6.2.3 Basic equations of the fixed - bed model 43
6.2.4 Diffusion of gaseous species 55
6.2.5 Structure of fuel bed 56
6.2.6 Thermal conductivity 57
6.2.7 Specific heat of the fuel bed 61

6.2.8 Heat transfer coefficient 63

7 Validation of the fixed-bed model 67
7.1 Composition and calorific value of the EKORET fuel 67
7.2 Measurements for validation of the fixed-bed model 69
7.3 Numerical simulations of the fixed-bed reactor 71
7.4 Comparison of the model predictions against the measured data 76
7.5 Correlation between model predictions and measured data 78
7.6 Sensitivity analysis of the fixed - bed model 79
7.7 Overall assessment of the fixed - bed model 81

8 Simulations of the combustion process in a small - scale retort boiler. 82
8.1 Boiler geometry and dimensions 82
8.2 Material properties 85
8.3 Boundary conditions 86
8.4 Results of the calculations 86
8.4.1 Fixed-bed results 87
8.4.2 Free-board results 88
8.5 Sensitivity analysis 91
8.5.1 Sensitivity to mesh density 91
8.5.2 Sensitivity to physical parameters 92

9 Validation of the numerical model 96
9.1 Procedure of experimental measurements 96
9.2 Comparison of calculations with experimental results 97

10 Improvements to the boiler design 101
10.1 Influence of deflector on flue gas composition 103
10.2 Influence of the air distribution 109
10.3 Influence of the combustion chamber shape 113
10.4 Improvements related to emission of solid particles 116
10.5 Comparison of the modifications 117
10.6 Efficiency of the retort boiler 122

11 Summary and Conclusions 125

List of Figures

1.1 Word Primary Energy Demand. 1
1.2 World Coal Production by Regions (4595 Mt in 2000) 2
1.3 Prognosis of World Coal Production by Regions (6954 Mt in 2030) 2
2.1 Typical design of retort boiler with screw feeder 6
2.2 Small scale retort boiler 8
5.1 Thermal conductivity of coal (B - effective thermal conductivity, A, W - thermal conductivity) 16
5.2 Specific heat of coal 19
5.3 Predicted variation of true density with temperature. Heating rate, 3 K/min 20
5.4 Variation of porosity during carbonization 20
5.5 Effective heat transfer coefficient - comparison ($t_s = 1000^oC$) 26
5.6 Heat transfer coefficient as a function of gas velocity 27
5.7 Pressure drop across the fixed - bed (d_p=0.02 m - the upper curve, d_p=0.04 m - the lower curve) 29
6.1 EKORET coal 39
6.2 EKORET coal – in shipping bags 39
6.3 Measurements of the pressure drop across the bed of the EKORET coal – the reactor 41
6.4 Pressure drop across the bed of the EKORET coal - experimental investigations 41
6.5 Mass sources and sinks 46
6.6 Energy sources and sinks 49
6.7 Determination of the contact surface area between solid fuel and the gaseous phase 51
6.8 Determination of the surface area for internal pores 53
6.9 Specific surface area as a function of char conversion degree 54
6.10 Total area of the contact surface between particles and gaseous phase 55
6.11 Concentration of gaseous substrates at surfaces of solid particles 55
6.12 Porosity variation within the fixed - bed 56
6.13 Thermal conductivity in the bed of solid fuel 57
6.14 Effective thermal conductivity (particulate charge) 58
6.15 Effective thermal conductivity (coke charge) 59
6.16 Effective thermal conductivity vs. temperature 60
6.17 Specific heat for coal components 61
6.18 Predicted variation of specific heat within the fixed - bed 62
6.19 Effective heat transfer coefficient 64
7.1 Geometry of the reactor 70
7.2 Photo of the reactor 70
7.3 Geometry of the numerical model 72

7.4 Model predictions along the center-line of the fixed-bed - B (τ =1800 sec.) 73
7.5 Model predictions along the center-line of the fixed-bed - A (τ =1800 sec.) 74
7.6 Model predictions along the center-line of the fixed-bed - C (τ =1800 sec.) 75
7.7 Flue gas composition . . . 76
7.8 Coal bed temperature . . . 77
7.9 Sensitive analysis - fuel temperature (parameters increased by 20%) . . . 80
8.1 Coal in the retort . . . 82
8.2 The retort boiler considered in this work . . . 83
8.3 The sketch of the whole boiler . . . 83
8.4 Geometry of the model . . . 84
8.5 Dimensions of the geometry of radiation section . . . 84
8.6 The air distribution to the combustion chamber . . . 85
8.7 Boundary conditions . . . 86
8.8 Solid bed temperature inside the retort . . . 87
8.9 Mass fraction of char, volatiles and moisture in the coal bed . . . 88
8.10 Temperature profile . . . 89
8.11 Path lines colored by temperature . . . 89
8.12 Path lines colored by oxygen mole fraction . . . 90
8.13 Path lines colored by CO mole fraction . . . 90
8.14 Sensitivity factor for temperature with a respect to mesh size . . . 92
8.15 Temperature sensitivity factor with a respect to excess air ratio . . . 93
8.16 Temperature sensitivity factor with a respect to walls temperature . . . 93
8.17 Temperature sensitivity factor with a respect to walls emissivity . . . 93
9.1 Measurement ports located on the side wall of the boiler . . . 96
9.2 Location of the measurement ports in the boiler – side view . . . 97
9.3 Location at the measurement ports in the boiler – top view . . . 97
9.4 Measurement planes inside the combustion chamber . . . 98
10.1 Temperature distribution inside the combustion chamber . . . 101
10.2 Path lines colored by temperature . . . 102
10.3 Distribution of gases in the combustion chamber . . . 102
10.4 Case A . . . 104
10.5 Case B . . . 104
10.6 Case C . . . 105
10.7 Case D . . . 105
10.8 Case E . . . 106
10.9 Case F . . . 106
10.10 Case G . . . 107
10.11 Case H . . . 107
10.12 Case I and Case J . . . 108
10.13 Case J . . . 108
10.14 Case K . . . 109

10.15Case L 110
10.16Case M 111
10.17Case N 112
10.18Case O 112
10.19Case P 114
10.20Case R - The best design 115
10.21Comparison of the cases - particles tracks 117
10.22Comparison of the best cases 119
10.23Temperature profiles (cross-section C and D) 120
10.24The boiler unit 124

List of Tables

2.1 Main Parameters of Retort Boilers . . . 6
2.2 Main Parameters of Coal . . . 7
2.3 Emission standards - PN-EN 12809 . . . 9
2.4 Emission standards - PN - EN 303-5 . . . 9
2.5 Emission standards - "Ecological Safety Mark" . . . 10
2.6 Emission limit values for boilers with solid fuels . . . 10
2.7 Typical flue gas and dust emission from retort boiler . . . 11
5.1 Kinetics of the processes during coal combustion . . . 21
6.1 Proximate and ultimate analysis of EKORET coal . . . 40
7.1 Proximate and ultimate analysis of raw coal - EKORET and substitute coal 67
7.2 Initial and boundary conditions for numerical calculations . . . 71
7.3 Correlation coefficients - Temperatures . . . 78
7.4 Correlation coefficients - Gas composition . . . 79
7.5 Average logarithmic sensitivity factor for the fixed - bed model . . . 81
8.1 Properties of steel . . . 85
8.2 Properties of the ceramics of the deflector . . . 85
8.3 Boundary condition . . . 87
8.4 Average logarithmic sensitivity factors . . . 94
9.1 VALIDATION of the model - plane a . . . 98
9.2 VALIDATION of the model - plane b . . . 99
9.3 Correlation coefficient between measurements and calculations . . . 100
10.1 Comparison of the deflector modifications. . . . 109
10.2 Comparison of air distribution modifications. Predictions of the mathematical model at the exit of the radiative section . . . 113
10.3 Comparison of the boiler construction modifications. Predictions of the mathematical model at the exit of the radiative section . . . 114
10.4 Comparison of the cases-particles emissions . . . 116
10.5 Size distribution . . . 116
10.6 Comparison of the cases considered in this study . . . 118
10.7 Residence time - comparison of the cases . . . 121
10.8 Measurements of retort boiler efficiency . . . 123
10.9 Comparison of predicted and measured data . . . 123

List of Symbols

Greek

α	heat transfer coefficient, $\frac{W}{m^2 \cdot K}$
α_k	convective heat transfer coefficient, $\frac{W}{m^2 \cdot K}$
α_r	radiative heat transfer coefficient, $\frac{W}{m^2 \cdot K}$
ΔH^o	standard state enthalpy, $\frac{J}{kmol}$
Δn	bed height, m
ΔS^o	standard state entropy, $\frac{J}{kmolK}$
ΔT_{g-s}	temperature difference between the phases, K
ϵ	turbulent dissipation rate of energy, $\frac{m^2}{s^3}$
η	stoichiometric coefficient
γ^*	destruction time of the Kolmogorov structure (reaction time scale), s
$\mathbb{E}$	the rate of strain tensor, $\frac{1}{s}$
$\mathbb{I}$	identity matrix
$\mathbb{T}$	stress tensor
μ	dynamic viscosity, $Pa \cdot s$
μ_t	turbulent viscosity, $Pa \cdot s$
ν	kinematic viscosity, $\frac{m^2}{s}$
Ω	solid angle, sr
Φ	phase function
ψ	structural parameter of pores
ρ	fluid density, $\frac{kg}{m^3}$
$\rho_{x,y}$	correlation coefficient
σ	Stefan – Boltzmann constant, $\frac{W}{m^2 \cdot K^4}$
σ_s	scattering coefficient
σ_t	Reynolds stress tensor
σ_{ij}	stress tensor, $\frac{N}{m^2}$

σ_x standard deviation for variable x

σ_y standard deviation for variable y

τ^* length fraction of the fine scales

$\triangle$ the rate of expansion of the flow, $\frac{1}{s}$

ε_s emissivity of external surfaces of particles

ε_g emissivity of gas

ρ_g gas density, $\frac{kg_f}{m^3}$

ρ_s coal density, $\frac{kg_s}{m_s^3}$

Roman

a absorption coefficient

a_d mass fraction of ash in dry coal, $\frac{kg_{ash}}{kg}$

A_s specific area of the contact surface between the gaseous and solid phases, $\frac{m^2}{m^3}$

A_w specific surface area of particle internal pores, $\frac{m^2}{g}$

A_z specific surface area of particles, $\frac{m^2}{m^3}$

$ALSF$ average logarithmic sensitivity factor

B_i pre-exponential factor, $\frac{m}{s}$

c equivalent specific heat, $\frac{J}{kg \cdot K}$

C_2 internal resistance, $\frac{1}{m^2}$

C_i concentration of the gaseous component „i", $\frac{kmol_i}{m^3 s}$

c_i specific heat of moisture, volatile parts, char and ash, $\frac{J}{kg \cdot K}$

c_w specific heat of moisture in coal, $\frac{J}{kg \cdot K}$

c_c specific heat of char, $\frac{J}{kg \cdot K}$

C_g substrate concentration nearby the solid material surface, $\frac{kmol}{m^3}$

$c_{p,i}$ specific heat of the component „i", $\frac{J}{kg_i \cdot K}$

c_{pa} specific heat of ash, $\frac{J}{kg \cdot K}$

c_{pp} specific heat of combustible part of coal, $\frac{J}{kg \cdot K}$

c_{pz} specific heat of dry coal, $\frac{J}{kg \cdot K}$

c_{v1}, c_{v2} specific heat of volatile matter, $\frac{J}{kg \cdot K}$

D binary diffusion coefficient, $\frac{m^2}{s}$

d_h hydraulic diameter, m

D_o diffusion coefficient at reference parameters T_o, p_o, $\frac{m^2}{s}$

d_s characteristic length, m

D_t turbulent diffusivity, $\frac{m^2}{s}$

$D_{(i,m)}$ diffusion coefficient for species „i" within the mixture, $\frac{m^2}{s}$

E activation energy, $\frac{J}{kmol}$

E total fluid energy, $\frac{J}{kg}$

e coal porosity, $\frac{m_f^3}{m^3}$

e' effective porosity of fixed - bed, $\frac{m_f^3}{m_c^3}$

e_o initial porosity of particle, $\frac{m_f^3}{m_c^3}$

e_{ex} external porosity within the coal bed, $\frac{m_{f,ex}^3}{m_c^3}$

e_{in} internal porosity within the coal bed, $\frac{m_{f,in}^3}{m_c^3}$

F_i mass forces of component i, $\frac{N}{m^3}$

g gravitational acceleration, $\frac{m}{s^2}$

g_i mass fraction of the component „i", $\frac{kg_i}{kg}$

g_i^* mass fraction of species „i" in fine - structure τ^*, $\frac{kg_i}{kg}$

g_i^o initial mass fraction of the species „i", $\frac{kg_i}{kg}$

$G_{char,o}$ initial mass of char, kg

G_{char} instantaneous mass of char,kg

g_{char} mass fraction of char in coal, $\frac{kg_{char}}{kg}$

$g_{moist.}$ mass fraction of moisture in coal, $\frac{kg_{moist.}}{kg}$

$g_{vol.}$ mass fraction of volatiles in coal, $\frac{kg_{vol.}}{kg}$

h specific enthalpy, $\frac{J}{kg}$

h_g physical enthalpy of gas, $\frac{J}{kg_f}$

h_i specific enthalpy of component „i", $\frac{J}{kg_i}$

h_s physical enthalpy of the solid body, $\frac{J}{kg_s}$

$h^0_{T_{ref,i}}$ formation enthalpy of species „i" at the reference temperature T_{ref}, K

I radiation intensity, $\frac{W}{sr \cdot m^2}$

J_i the diffusive flux of substance i, $\frac{kg_i}{m^2 \cdot s}$

k reaction rate constant, (units vary)

k turbulent kinetic energy, $\frac{kg \cdot m^2}{s}$

k_g gas thermal conductivity, $\frac{W}{m \cdot K}$

k_o the pre-exponential factor, $\frac{m}{s}$

k_r reaction rate constant of heterogeneous reaction, $\frac{m}{s}$

$k_{b,j}$ reverse reaction rate constant of „j" reaction, (units vary)

k_{dev} the pre-exponential factor of devolatilization process, $\frac{1}{s}$

k_{eff} effective thermal conductivity of solid fuel, $\frac{J}{mK}$

$k_{f,j}$ forward reaction rate constant of „j" reaction, (units vary)

k_{vap} the pre-exponential factor of vaporisation process, $\frac{1}{s}$

LSF logarithmic sensitivity factor

m_p particle mass , kg

M_{char} molecular weight of char, $\frac{kg_{char}}{kmol_{char}}$

$M_{vol.}$ molecular weight of volatile matter (assumed), $\frac{kg_{vol.}}{kmol_{vol.}}$

$MQ_{r,char}$ amount of heat generated during combustion reactions of char, $\frac{J}{kmol_{char}}$

$MQ_{r,vol.}$ amount of heat generated during combustion reactions of volatile matter, $\frac{J}{kmol_{vol.}}$

N number of chemical species that enter into the specific reaction „j"

n reaction order

n refractive index

Nu Nusselt number

p pressure, Pa

p_a air pressure, Pa

p_p	partial pressure of gas, Pa
Q_{vapour}	evaporation heat of moisture (latent heat), $\frac{J}{kg_{moist.}}$
R	gas constant, $\frac{J}{kmol \cdot K}$
r	characteristic dimension (radius) of internal pores , m
R_i	source term of species „i", $\frac{kg_i}{m^3 \cdot s}$
r_r	reaction rate of heterogeneous reaction,$\frac{kmol}{m^3 s}$
Re	Reynolds number
s	average optical distance within the gas area, m
S_h	source element of energy balance, $\frac{W}{m^3}$
S_i	energy source for corresponding chemical and physical processes, $\frac{W}{m^3}$
S_k, S_ϵ	source terms for $k-\epsilon$ equations, $\frac{kg}{s^3 \cdot m^3}$, $\frac{kg}{s^4 \cdot m^3}$
S_m	source term of the equation for continuity, $\frac{kg}{m^3 \cdot s}$
S_o	initial surface area of internal pores, m^2
S_s	contact surface between solid and gaseous phases, m^2
$S_{in,o}$	initial surface area, m^2
$S_{particle}$	surface area of a particle, m^2
Sc_i	Schmidt number
Sc_t	turbulent Schmidt number
Sh	Sherwood number
T	gas temperature, K
T_a	air temperature, K
T_g	gas temperature, K
T_o	reference temperature, K
T_s	coal surface temperature, K
T_w	temperature of water jacket walls , K
$T_{ref,i}$	reference temperature, K
u	component associated i-th fluctuations of the gas velocity , $\frac{m}{s}$

V_c	total volume of the bed, m_c^3
V_f	volume of the continuous phase in the bed, m_f^3
V_i	volume of an individual element within the numerical mesh , m^3
V_m	total volume of elements for the entire numerical mesh, m^3
V_s	volume of solid phase in the bed, m_s^3
V_{daf}	mass fraction of volatile matter in the dry and ash-free coal, $\frac{kg_{vol}}{kg_{daf}}$
V_{gas}	volume of empty cavities between particles (void - space),m^3
$V_{por,o}$	initial volume of internal pores,m^3
V_{por}	total volume of internal pores , m_f^3
w_∞	superficial velocity, $\frac{m}{s}$
w_2	mass fraction of moisture in coal $\frac{kg_w}{kg_c}$
w_s	velocity of coal bed, $\frac{m}{s}$
X_c	degree of char conversion.
Y_i	mass fraction of the specific component of gas, $\frac{kg_i}{kg_f}$
Y_m	source element for the equation defining transfer of kinetic energy for turbulences k associated with the effect of gas compressibility,$\frac{W}{m^3}$
r_{dev}	devolatilization rate, $\frac{kg_{vol}}{s \cdot m^3}$
r_{vap}	evaporation rate, $\frac{kg_w}{s \cdot m^3}$
G_i	source term associated with chemical and physical processes,$\frac{kg_i}{m^3 s}$
e	porosity of fixed - bed, $\frac{m_f^3}{m_c^3}$
LCV	lower calorific value of fuel, $\frac{J}{kg}$
$c_{p,g}$	specific heat of gas that flows throughout the bed, $\frac{J}{kg \cdot K}$
k_r	radiative part of the effective thermal conductivity, $\frac{W}{m \cdot K}$
k_{s+g}	thermal conductivity of the solid material and pores filled with gas, $\frac{W}{m \cdot K}$
S_{in}	surface area of internal pores, m^2
t	time,s
S_{ex}	external surface area of particle, m^2

Rest

$\mathbf{F}$	vector of body forces (per unit volume), $\frac{N}{m^3}$
$\dot{V}_a$	volumetric flow rate of air , $\frac{m_a^3}{s}$
$\frac{1}{z}$	viscous resistance, $\frac{1}{m}$
$\mathbf{r}$	vector of position, m
$\mathbf{s}$	vector of direction, sr
$\boldsymbol{w}$	vector of fluid velocity, $\frac{m}{s}$
$[C_{a,j}]$	molar concentration of species „a" in „j reaction, $\frac{kmol}{m^3}$
$\overline{U}$	average value for the gas velocity , $\frac{m}{s}$
$\mathbf{s}'$	scattering direction vector

Acknowledgments

I would like to express my appreciations to my promoters, Prof. Roman Weber and Prof. Andrzej Szlęk, for enabling me the opportunity to develop this PhD thesis, for understanding and patience during the progress of the work as well as for kind advice and valuable remarks.

Particular credit goes to those people who supported me during four years of PhD studies and were with me for better and for worse.

This research would not have been possible without the financial assistance of the:

- Project of Polish Ministry of Science and Higher Education (3902/B/T02/2009/36),
- European Commission Marie Curie INSPIRE Network (MRTN-CT-2005-019296),
- "Elaboration of low emission combustion technology of solid fuels - coal and biomass in small capacity boilers and strategy of their implementation", project of Ministry of Science and Higher Education in Poland (R06 009 03).

1 Introduction

Nowadays hard coal is one of the most important sources of energy used by humans (Figure 1.1). The widespread availability of that fuel presents one of its most important advantages. More than 70 countries of the word are capable to excavate coal at the industrial scale. General accessibility to that source of power makes it difficult or even unfeasible to consider the available resources as a measure of political or economic pressure. It is also the reason for which it seams unrealistic that leading suppliers of that fossil fuel can set up 'coal OPEC' (Organization of the Petroleum Exporting Countries) and decide about coal prices just as it happened with crude oil [1].

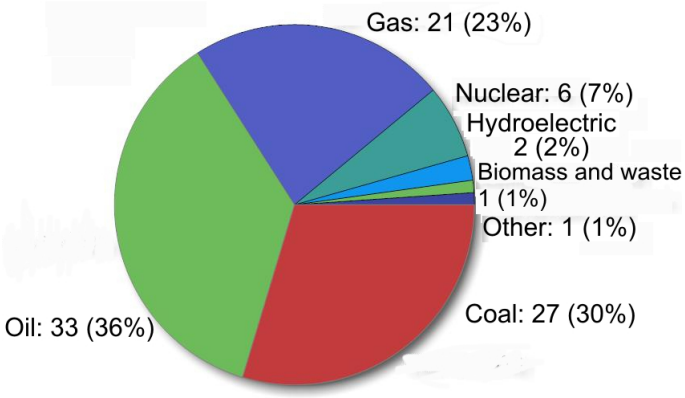

Figure 1.1: Word Primary Energy Demand [1].

The largest already documented deposits of crude oil are located in the countries of unsteady political systems (Iraq, Iran, Nigeria, Venezuela) or in the countries of the former Soviet Union. These deposits make up about 74% of all the available reserves. On the contrary, deposits of coal are uniformly distributed, which nearly eliminates the hazard that supplies can be disrupted. According to the information from the World Coal Institute 5990 million tonnes (Mt) of hard coal were extracted worldwide in 2009. The largest amounts of coal are extracted in China (Figure 1.2) [1, 2, 3, 5, 6, 7]. In consequence, nearly 78% of the power generation in that country comes from coal. The country that takes the second place in the world production of coal is the USA. Coal extraction in that country maintains the steady level with a slight trend of growth. It is the fuel that plays an important role in the American policy of energy coverage as it is considered a safeguarding factor for the case when supplies of crude oil and natural gas from politically unsteady regions of the world might be cut off [1, 2, 4, 5].

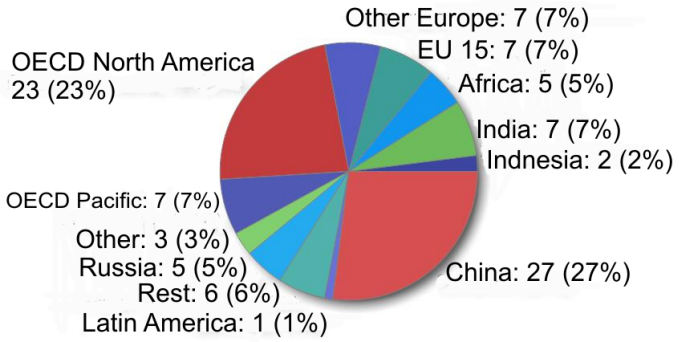

Figure 1.2: World Coal Production by Regions (4595 Mt in 2000) OECD - Organisation for Economic Co-operation and Development [1].

The demand for coal in the European Union is gradually decreasing, which is caused by the adopted environmental policy, where ecology is considered one of the most crucial factors in all respective EU Action Programs. Nowadays, The Sixth Environment Action Program of the European Community is in progress with the title: 'Environment 2010: Our Future, Our Choice'. The aim of the program is to reduce emission of greenhouse gases by 8% during the years 2008 – 2012. To achieve the assumed goal it is necessary to support the consumption of renewable energy sources. It is also planned to improve the efficiency of the natural resource utilization and reduce the amount of wastes by 20% by the year 2010.

Substantial reduction of coal utilization can be witnessed in such countries of the European Union as Germany, France, Turkey or Spain whilst the reverse trend occurs in the United Kingdom and Italy. Coal consumption permanently grows in Russia and Ukraine. For countries from Eastern Europe coal still remains a very important source of energy. Similar situation takes place in South Africa and India [1, 6].

Nearly all countries worldwide, except for very few Arabic countries, as well as EU generate power through coal combustion. The electricity generation from coal is well established and cheap. Prognosis of coal production are shown in (Figure 1.3). When considering prices of fossil fuels, it is necessary to make reference to reports of European Commission that predict substantial increase of natural gas and crude oil prices until 2030. The same forecast envisages that coal prices shall be maintained on the same level [2].

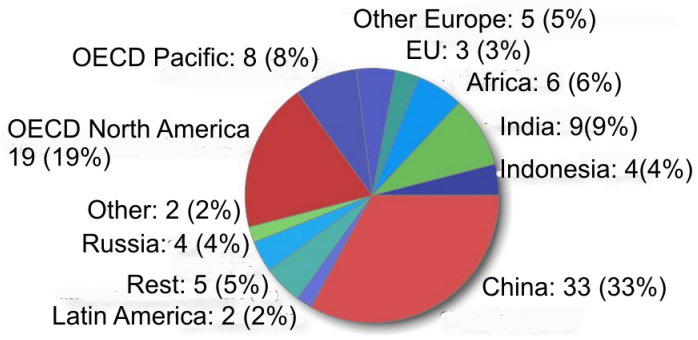

Figure 1.3: Prognosis of World Coal Production by Regions (6954 Mt in 2030) [1]

Poland is the largest producer of hard coal in Europe. Hard coal together with brown coal (lignite) is the main source of energy in Poland. Despite the current vogue for other sources of power, coal shall keep its dominating role during the oncoming years. The forecasts predict that the world demand for that fuel shall increase by 53% by 2030. It is also expected that the demand in European Union shall make a leap as well, perhaps by as much as 100%. It results from the need to generate electric power at low costs [8].

Prospects for coal seem to be quite promising for several reasons. Expenditures for coal extraction make up about one-fourth of expenses necessary to win crude oil and one-fifth of those for natural gas production. The price of coal seems to be really steady and there are no indications that would suggest substantial variation of the prices in the nearest future. Vast deposits of that fuel at the present level of extraction, should be sufficient for about 200 years. In particular Poland is rich in deposits of hard and brown coal that will surely be sufficient for many years to come [8, 9, 10]. Nearby the town of Legnica the vast deposits of brown coal were found and rated among the largest in Europe or, possibly, worldwide and are estimated to amount to 35 billion tons [11].

The negative attitude to coal is caused by its harmful effect on natural environment. The emissions of such substances as carbon oxide, nitrogen oxides, sulphur oxides, as well as the emission of dust substantially affect health of humans, flora and fauna. However, nowadays the coal-based power engineering is no longer the main source of pollutants harmful to human beings. Advanced methods of flue gas treatment make the detrimental effect of power engineering onto natural environment much smaller than it used to be in the past. The only significant problem that is to be resolved is the emission of carbon dioxide, which may be responsible for climatic changes in the world. It is believed that this hindrance shall be eliminated by underground storage of carbon dioxide captured from the flue gas.

The phenomenon of so called 'low emission' still remains a serious ecological problem in Poland. The low emission is understood as pollution of environment by household heating boilers that are fired with coal. The combustion process in such appliances frequently runs without appropriate supervision, which results in excessive emission of substances that are hazardous to humans and the environment. Effects of that emission are clearly visible on urban agglomerations, where a huge number of such boilers operate on relatively small areas. Flue gases from such small heating units are usually released to the atmosphere by means of stacks that are of low height and therefore are unsuitable. It leads to air pollution that is comparable with the industrial one or is even higher during winter periods [12].

The problem of 'low emission' can be resolved in several ways, among them application of heating units with higher efficiency seems to be a very promising idea. In addition, such units should be fired with appropriately prepared and environment-friendly fuel. On the Polish market the partly automated retort boilers are available where the fossil fuel is supplied from the storage reservoir (fuel container) to the combustion chamber by means of a screw or a piston reciprocal feeder. The amount of fuel and air delivered to the appliance is adjusted by means of an attached microprocessor controller with pre-programmed

optimized settings. The attendance is reduced to topping up the coal reservoir once per 3-5 days and to removing ash from the ash pan. Owing to automatic control of the combustion process, the retort boilers can achieve efficiency as high as 85% [13].

However, even the most advanced household boilers cannot meet the current environmental regulations. In order to meet very stringent ecological standards that have been implemented since Poland joined the European Union, it is necessary to use purposefully prepared coal. The fuels that are most suitable to fire retort coal boilers are such ones as 'ekogroszek' (eco-peas), 'ekofins', ekoret', etc. These fuels demonstrate low content of sulphur ($< 0.6\%$), ash ($< 12\%$) and relatively high calorific value ($> 25\frac{MJ}{kg}$) as well as suitable physical and chemical properties that guarantee reliable and fault-free operation of both the feeder and the furnace (relevant granulation, lack of mechanical pollutants, low sinter ability, high temperature of ash sintering and softening ($>1250^oC$) as well as moisture content of coal less than 12%) [14, 15, 16].

The use of coal and other fossil fuels to heat households, even if fuels are completely combusted (with no flammable remnants), cannot solve the problem of CO_2 emission. The carbon dioxide, similarly to other triatomic gases, is responsible for the so called 'greenhouse effect', i.e. retention of heat that is delivered by sun radiation. It is an effect that leads to heating up of our globe with subsequent climatic changes. The only method suitable for reduction of CO_2 emission is combustion of biomass in such boilers. In Western Europe, boilers with purposefully prepared biomass are gaining more and more popularity, which is associated with increasing concern about natural environment, much higher than in new member countries of EU [17]. The biomass is suitable for combustion in automated household boilers but must be initially pre-processed in appropriate manner, where such raw material as timber wastes, sawdust, cuttings, chips and similar stuff are dried and disintegrated. In the subsequent step the material is heated up so that lignin and cellulose contained in the processed material glue together. After such preparation the biomass is subject to granulation to produce the so called pellets [18].

Application of pre-treated biomass as a fuel dedicated to household boilers is considered as an environmental friendly solution due to the so called zero emission of CO_2. The amount of carbon dioxide produced during the process of biomass combustion is just the same as the amount of CO_2 adsorbed from the environment during the growth period of plants that make up the biomass. As compared to carbon combustion, use of biomass pellets results in virtually no emission of SO_x. Heating of dwelling houses with the use of biomass is more expensive than coal-fired systems but is cheaper than application of natural gas or fuel oil. The Polish biomass granulate is rated among the best products of that type in Europe; thus, in 2007 nearly $350,000$ tons of pellets were produced in Poland, whilst as much as 83% was exported and only $60,000$ were purchased by domestic consumers. Nearly $35,000$ tons were combusted in low-power boilers (with the heating power below $20kW$) that heat single-family houses, while the remaining amount was utilized by larger boiler houses as well as electric power of thermal power plants [17].

Poland, being a member country of EU, is obliged to respect the environmental pro-

gram, where development of renewable energy sources is introduced as a must. According to that program shares of renewable energy sources should constantly increase and reach the level of 12% by 2010. In the future, even a higher share of such energy sources, amounting to as much as 30% is anticipated. Nowadays, the share of renewable energy sources in Poland is at the level of 1.5%. That is why biomass that is also rated among the group of renewable energy may soon become a really desirable fuel also in Poland [18].

In Germany, the use of biomass (especially wood) as a fuel in domestic heating systems is rising due to high prices of natural gas and heating oil. There are currently about 14 million small scale biomass and coal fired boilers. These installations (similarly to Poland) cause considerable air pollution problems, mainly dust, PAH (Polycyclic Aromatic Hydrocarbons). Those harmful substances are usually emitted at high rates in residential areas. Considered boilers are often operated at part load. It leads to increased emissions [142].

Design principles of coal-fired and pellet-fired domestic boilers are very similar and their operating principle is exactly the same. Designs of such appliances are usually based on experience and intuition of manufacturers. Boilers are designed and put on the market by small companies without research and development necessary to optimize engineering features of boilers in terms of their efficiency and ecological qualities. There is no doubt that importance and market share of heating units fired with solid fuels will increase over the next years due to relatively low and steady price of coal and ecological properties of biomass.

2 Small scale retort boilers

In Poland more than 40% of heat consumed by both communal and household sectors is produced from coal. It leads to combustion of ca. 8 million tons of coal per year and Poland is becoming the largest consumer of that fuel, as far as the market of low-power boilers is concerned [19, 21].

2.1 Low-emission retort boilers

The technology of low-emission automatic coal-fired boilers with retort burners appeared on the domestic market in mid 90's. The major advantages of these boilers, as compared to units of older design, include high efficiency, automated operation and meeting requirements of emission standards that enable operation of such boilers in EU countries [21, 20].

Rated power	(15-1800) kW
Thermal efficiency	(80-85) %
Power consumption (electricity)	(0.4-1.0) % of rated power
Maximum operating pressure	(0.2-0.4) MPa
Maximum water temperature	(70-95) ^oC
Minimum water temperature	(1-2) ^oC
Coal bunker refilled	ones every 3-4 days

Table 2.1: Main Parameters of Retort Boilers [19]

Retort boilers are suitable for heating houses for one or two families, farm buildings, large municipal facilities, industrial plants, etc. They also provide hot water for home use. Figure 2.1 shows a typical design of such a boiler.

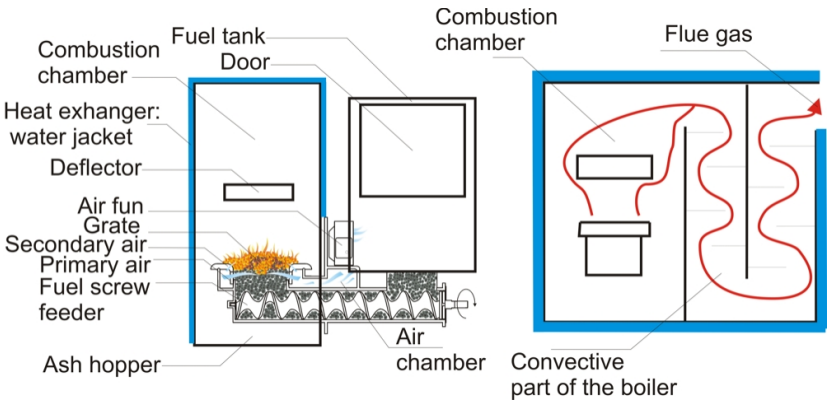

Figure 2.1: Typical design of retort boiler with screw feeder

The feeder supplies appropriately prepared fuel from a fuel bunker to a retort burner located in the heating part of the boiler. Air is supplied into the combustion chamber

by means of a fan. Inside the air duct the air stream is split into a primary air that is delivered directly to the coal bed and a secondary air delivered to the area above the bed. Combustion is controlled by means of an electronic controller that controls the amount of supplied fuel and air. Safe operation of boilers is assured by appropriate sensors that indicate any faults or deficiencies. Retort boilers are furnished with a very specific component, the so called deflector that is suspended at some height above the retort and is intended to prolong presence of combustion products in the zone of high temperatures. Such a design guarantees more complete combustion [19].

Operation of such appliances is limited to refilling the fuel bunker once per three or four days and to removing ash that is formed during boiler operation and falls down to a special ash-pan drawer being pushed down and expelled by new fuel supplied to the furnace. The ash-pan drawer is located in the bottom part of the boiler and must be emptied as needed. From time to time the entire boiler must be cleaned from soot and ash that deposits on inner walls of the boiler. Access to inner parts of the boilers is possible via purposefully designed inspection flaps. The boiler presented in Figure 2.2 is the subject matter of this study [19].

2.2 Fuel for retort boilers

Reliable and fault free operation of retort boilers is only possible with the use of adequately prepared fuel. Such a fuel must have appropriate physical and chemical properties to enable smooth operation and long lifetime (proper granulation, lack of mechanical contamination, low sintering power, high temperature of ash sintering and softening) combined with low content of sulphur, ash and relatively high calorific value. The most popular coal grades meant for application in small retort heating boilers are offered with their commercial brands EKORET and EKOFINS (Table 2.2). These coal mixtures are produced on the basis of selected coal grades, chiefly from collieries of The Coal Holding of Katowice (KHW) plc. EKORET and EKOFINS are offered either loose or in bags of 25 kg each [20].

Name	EKORET	EKO-FINS
Granulation	(5-30) mm	(0-35) mm
LHV	>26 MJ / kg	>25 MJ/ kg
Ash content	(4-10) %	(4-12) %
Sulphur content	< 0,6 %	< 0,6 %
Moisture content	< 10 %	< 10 %
Sintering power RI	Under 10	Under 12

Table 2.2: Main Parameters of Coal [20]

Owing to specially prepared fuel and appropriate combustion process, the environmental burdensomeness of retort boilers is much less than in case of old-type boilers. Unfortunately, when compared to gas boilers, efficiency values of thermal units are still lower

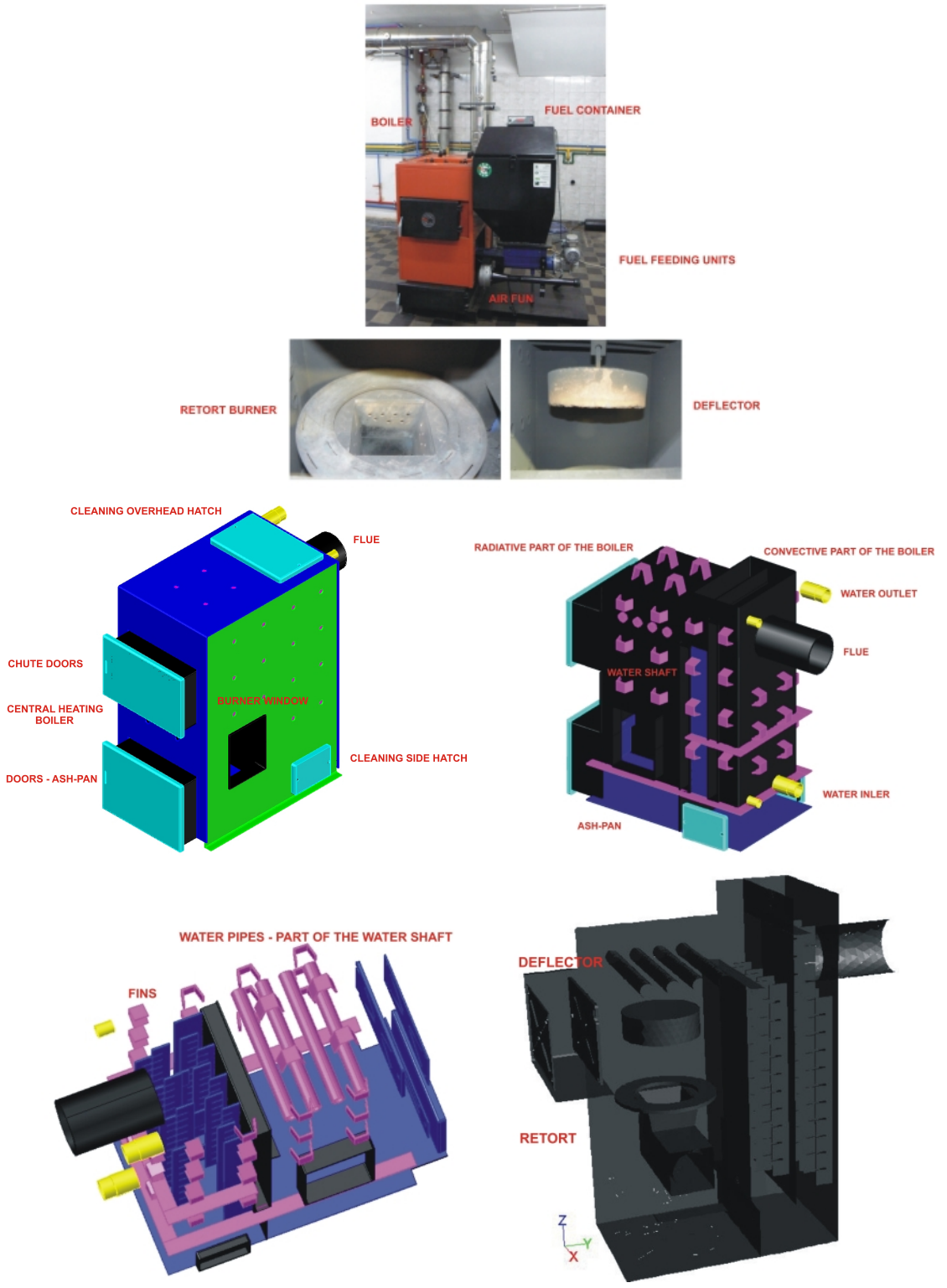

Figure 2.2: Small scale retort boiler.

whilst emission of hazardous compounds is much higher.

2.3 Environmental emission standards

Three emission standards for small scale boilers (installations capacity below 1MW) exist in Poland [139, 141]:

- PN - EN 12809 "Residential independent boilers fired by solid fuel - Nominal heat output up to 50 kW - Requirements and test methods",
- PN - EN 303-5. Part 5. "Heating boilers for solid fuels, hand and automatically stoked, nominal heat output of up to 500 kW - Terminology, requirements, testing and marking",
- system of certification of the heating equipment and solid fuel. The certificate of "Ecological Safety Mark" (from Institute for Chemical Processing of Coal - ICHPW).

The emission regulations - "Ecological Safety Mark" are the most restrictive criterion but only PN- EN 12809 standards are obligatory in Poland. The emission standards - PN- EN 12809 are shown in Table 2.3.

PN - EN 12809		
Class	Emisssion limits - CO	
	(13% O_2), %	(10% O_2), mg/m^3
1	0.3	5156
2	0.8	13750
3	1.0	17188

Table 2.3: Emission standards - PN-EN 12809 [137].

The PN - EN 303-5 regulations contain emission limits for carbon monoxide, total organic carbon (TOC) and dust (Table 2.4).

PN - EN 303-5									
Rated thermal capacity, kW	Emission limits[1], mg/m^3(10% O_2)								
	carbon monoxide			TOC (organic)[2]			dust		
	class			class			class		
	1	2	3	1	2	3	1	2	3
hand stoked									
<50	25 000	8 000	5 000	2 000	300	150	180	150	125
50 - 150	12 500	5 000	2 500	1 500	200	100	180	150	125
150 - 300	12 500	2 000	1 200	1 500	200	100	180	150	125
automatically stoked									
<50	15 000	5 000	3 000	1 750	200	100	180	150	125
50 - 150	12 500	4 500	2 500	1 250	150	80	180	150	125
150 - 300	12 500	2 000	1 200	1 250	150	80	180	150	125

Table 2.4: Emission standards - PN - EN 303-5 ([1] - in dry gas, [2] - total organic carbon)[138].

The standards proposed by ICHPW are presented in Table 2.5.

ICHPW							
Boiler type	Class	Emission rate[1] (10% O_2)					
		CO mg/m^3	[2]NO_2 mg/m^3	dust mg/m^3	organic mg/m^3	PAH mg/m^3	B(a)P $\mu g/m^3$
hand stoked (periodically)	B	< 5 000	< 400	< 200	< 150	< 15	< 150
	A	< 1 200	< 400	< 125	< 75	< 5	< 75
automatically stoked (continious)	B	< 3 000	< 600	< 150	< 100	< 5	< 100
	A	< 1 200	< 400	< 125	< 75	< 5	< 75

Table 2.5: Emission standards - "Ecological Safety Mark" ([1] - in dry gas, [2] - total nitric oxides)[140].

In Germany small scale combustion installations (also retort boilers) are covered by the emission regulations on small and medium size combustion units. In the case of coal fired boilers (considered in this PhD work), this applies for installations with a rated thermal input of up to 1MW. The above mentioned ordinance is shown in Table 2.6 [142].

		Rated thermal output kW	dust mg/m^3	CO mg/m^3
(13% O2)	currently in place	15 - 50 50 - 150 150 - 500 > 500	150 150 150 150	4000 2000 1000 500
(11% O2)	step 1: after entry into force of the ordinance	4 - 500	60 (bimass) 100 (other)	1000
		>500	60 (bimass) 100 (other)	600
	step 2: instalations put into operation after 31 January 2014	>4	20	600

Table 2.6: Emission limit values for boilers with solid fuels [142, 143].

Typical flue gas composition and dust emission from coal - fired retort boiler with its thermal power about 25 kW is shown in Table 2.7.

Fuel	LCV	Q^a_i	kJ/kg	28549	
	Fuel flow rate	kg/h	kg/h	3.83	
Exhaust	Temperature	t_{sp}	°C	225.11	
	Chimney draft	p_k	Pa	4.6	
	CO_2	z_{CO2}	%	12.85	11.0
	O_2	z_{O2}	%	8.15	10.0
	CO	C_{CO}	mg/m_n^3	2291.4	1426.2
	SO_2	C_{SO2}	mg/m_n^3	654.44	407.33
	NO	C_{NO}	mg/m_n^3	295.68	184.04
	TOC	C_{TOC}	mg/m_n^3	6.449	4.014
	dust	C_{dust}	mg/m_n^3	35	
Thermal efficiency	79.6%				
Thermal capacity	25.65 kW				

Table 2.7: Typical flue gas and dust emission from retort boiler [145].

3 Objectives

The major objective of this study is to gain a comprehensive understanding of the combustion process that takes place in low-power (small-scale) boilers. In particular, the detailed objectives are as follows:

- deeper and wider investigation of processes that take place in beds of combusted solid fuel (fixed - bed combustion),
- development of a methodological approach for modeling of the combustion process that takes place in both, the fixed - bed and in the combustion chamber above the retort,
- identification of parameters and design features that are responsible for incomplete combustion,
- suggestion of design alterations intended to increase efficiency of the coal-fired retort boilers,
- suggestion of methods and design alterations to decrease emissions of pollutants.

4 Scope of the work

The research work has been divided into the following tasks.

The first and very important task of the study is to develop a mathematical model that describes the process of coal combustion in the retort (fixed - bed combustion). The newly developed algorithm is then used for modeling of the processes that take place in low-power boilers.

The next step is the validation of the developed model against experimental data generated in an associated PhD project [56].

The third task is to incorporate the fixed - bed model into the CFD (Computational Fluid Dynamics) Fluent code to allow for numerical simulations of the whole boiler unit consisting of the retort and the combustion chamber.

During the subsequent task, the overall boiler model (the retort + combustion chamber) is validated against the experimental results collected during measurements in a real 25 kW boiler.

The final task is to find out means of improving the efficiency of the boiler and suggest methods to decrease pollutants emissions. To this end the whole boiler model is used.

5 Process model of fixed-bed combustion

The phenomena that occur in the fixed - bed are sophisticated and difficult for mathematical description. Even the structure of the solid fuel itself is hard to determine. Heating of coal leads to its physical and chemical transformation. During the transformation the thermal properties of fuel, its thermal conductivity and specific heat, are subject to alterations. The porous material, which is in fact the coal bed, is considered as a good thermal insulator, although its thermal conductivity increases typically by a factor of three during both heating and transformation.

As far as the specific heat of solid matter is concerned, one has to consider not only the effect of temperature but also composition that is subject to rapid changes. The alteration to the coal structure substantially affects rates of heterogeneous reactions that take place on the coal surface. The contact area between the solid fuel and the gaseous phase varies as the temperature increases as a result of changing both porosity and density of solid phase during the combustion process. It is wrongly to assume that the temperatures of solid and gaseous phases are the same during combustion of solid fuel in a fixed - bed where diameters of particles are larger than several millimeters. There is a temperature difference that results in transfer of heat between the two phases. Not only the convective heat transfer coefficient is of importance but the amount of transferred heat depends also on the contact surface between the solid and the gaseous phase as well as on the structure of the solid material.

There seems to be neither papers nor textbooks that deal with modeling of processes that take place in small heating boilers. Still, there are numerous studies that contain information that is relevant to this PhD study in terms of modeling physical and chemical processes that occur in beds of solid fuels. These studies are reviewed in a few subparagraphs below.

5.1 Coal structure

During thermal decomposition the solid fuel releases liquid and gaseous products of chemical reactions. The only material that remains in the solid phase is the so called coke consisting of char and ash. The coke is the remnant after evaporation of moisture and devolatilization of volatile matter. Volatiles are the substances that originate during the pyrolysis process and are released from the solid fuel as a result of temperature increase. They include liquid hydrocarbons (tar) released during primary carbonization as well as gases (mainly $H_2, CO, CO_2, H_2O, N_2, O_2, CH_4$ and other hydrocarbons) that are results of secondary carbonization. Moisture can be classified as hygroscopic and transient one. The transient moisture is the moisture of random origin [22, 23]. Coal matter can be split into combustible part (volatiles and char) and the mineral part that remains in solid combustion products as ash. A small portion of the ash may also evaporate [22].

5.2 Coal decomposition during the combustion process

Investigation of physical and chemical processes that occur during the process of coal combustion in fixed - beds is a crucial issue for modeling of the combustion phenomena. The temperature range from 100^oC to 200^oC is associated with the evaporation of moisture. At temperature of about 350^oC coal is subject to depolymerization and transformation into the unsteady phase, becoming a sticky liquid. That phase, referred to as the softening phase, may occur or not, depending on the fuel grade, heating rates, dimensions of particles and composition of the gaseous atmosphere where the fixed - bed is placed. The plastic (soft) phase is associated with the phenomenon of coal particle swelling when the particles expand their volume by several times. It is the phenomenon that can be observed during heating up at high rates. At temperature of about 500^oC coal undergoes resolidification, which is accompanied by emission of liquid hydrocarbons. In consequence of the coal softening phase the agglomeration takes place. In the temperature range, from 400^oC to 700^oC, coal gives off gases such as CO, CO_2, H_2, H_2O and hydrocarbons. When temperature of around 800^oC is reached, the combustion reaction of the remaining coal (char) in the solid phase is initiated. A further increase of the combustion temperature leads to endothermic reactions that cool down surface of the solid body (fuel). The most important reactions that take place on coal surface are the following [22]:
exothermic reactions:

$$\mathrm{C} + \mathrm{O_2} \rightarrow \mathrm{CO_2} \tag{5.1}$$

$$\mathrm{C} + \frac{1}{2}\mathrm{O_2} \rightarrow \mathrm{CO} \tag{5.2}$$

$$\mathrm{C} + 2\mathrm{H_2} \rightarrow \mathrm{CH_4} \tag{5.3}$$

and endothermic reactions:

$$\mathrm{C} + \mathrm{H_2O} \rightarrow \mathrm{CO} + \mathrm{H_2} \tag{5.4}$$

$$\mathrm{C} + \mathrm{CO_2} \rightarrow 2\mathrm{CO} \tag{5.5}$$

Beside incompletely burnt char, the second remnant of the combustion process is ash. The non-combustible part of coal is chiefly made up of minerals such as carbonates, sulfides, oxides and hydroxides. The largest portion are alumina - silicates that make up more than 50% of mineral substances. Not the whole mineral components remain in ash, a part of them (about 10%) evaporates. Due to high temperature (about 1100^oC) ash particles may sinter it means partial melting of their surfaces occurs with aggregation (gluing) of individual grains into a porous matter. The sintering effect is a disadvantageous phenomenon during the combustion process. Sintered material may prevent penetration of air into the coal bed and lead to failures of fuel feeders [22, 23, 27].

5.3 Thermal conductivity

The coefficient of thermal conductivity is one of the most important fuel properties with regard to modeling of the combustion process in a solid fixed - bed. For hard coal the coefficient of thermal conductivity at 25^oC ranges from 0.1 to 0.5 $\frac{W}{mK}$ (depending on the coal grade) and even after substantial heating (up to 1000^oC) only slightly grows to the value of 0.8 - 1.0 $\frac{W}{mK}$. Coal beds are good insulators and reluctantly convey heat by thermal conduction. Resistances to heat transfer occur at contact surfaces between solid and gaseous phases as well as in pores and fissures between grains that trap air (gas of thermal conductivity about 0.025 $\frac{W}{mK}$). When the fixed - bed temperature exceeds 600^oC, the radiation process between surfaces of coal particles prevails, which increases the heat transfer rate several times. Figure 5.1 shows the effect of radiation on the effective thermal conductivity.

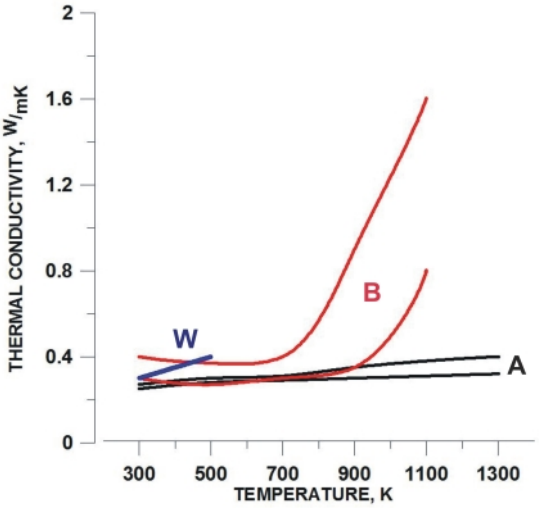

Figure 5.1: Thermal conductivity of coal (B - effective thermal conductivity, A, W - thermal conductivity) (compilated by Tomeczek [23])

There exists a considerable body of literature on the effect of radiative transfer on heat transfer rates inside solid layers. In majority of works the so called effective thermal conductivity is used, where the component responsible for the effect of radiative heat transfer is included beside the coefficient of thermal conductivity associated with presence of solid materials and pores filled with gas [24, 25, 26, 27, 28, 29].

$$\mathsf{k_{eff}} = \mathsf{k_{s+g}} + \mathsf{k_r} \qquad \frac{\mathsf{W}}{\mathsf{mK}} \tag{5.6}$$

where:

k_{s+g} - thermal conductivity for the solid material and pores filled with gas, $\frac{W}{mK}$,

k_r - the radiative part of the effective thermal conductivity, $\frac{W}{mK}$.

Establishing the relationship for calculating the amount of heat transfered by radiation is a sophisticated problem. One reason for that is the complex structure of fixed - bed that varies during the combustion process. It is difficult to estimate shapes and dimensions of pores where the radiation process takes place. Many publications simplify the sophisticated structure of the fixed - bed and restrict the analysis to idealized geometrical forms and structures that are made up of spherical particles. The simplification leads to the situation that calculation results may differ from the reality [26]. It has been established that the heat transfer rate depends on such parameters as [24, 25, 26]:

- particle diameter and emissivity of their surfaces,
- dimensions, sizes and types of pores – porosity of the fixed - bed,
- temperature of the solid fuel.

The study of Hütter and Kömle [25] established that the effect of radiation is substantial when the temperature of coal bed exceeds 600^oC and diameters of coal particles are not smaller than 1 mm. Computations of Schotte [26] examine the effect of pore sizes and porosity of the fixed - bed on the value of the radiative part of thermal conductivity. The work demonstrates that larger contact surfaces between the solid and gaseous phases lead to more intense transfer of heat via radiation. In fact it is the case when porosity of the bed is high and the pores are small.

The research report of Atkinson and Merrick [27] describes in a very accurate and detailed manner how heat is transferred in coal beds. The study is important as it deals with the bed of hard coal, very similar to the fuel that is fired in small scale retort boilers. After determination of the effective coefficient of thermal conductivity that also takes account of convective heat exchange in pores of the fuel as well as heat transfer by radiation, attention is paid to amendments in coal structure and composition during the combustion process. Authors of the mentioned study distinguish three basic forms of solid bed. For the first, original form, one assumes that particles are not porous which means that the fixed-bed contains only external pores. The second and third forms (plastic and sintered forms) not only comprise external pores but also internal ones that are created during physical transformation of coal as well as during coal devolatilization. After final extraction of tar and volatiles the bed achieves its final form. The remaining char cracks due to the effect of high temperature that leads to formation of pores of very specific shapes. The mentioned study distinguishes two major zones to enable mathematical description of heat transfer by conduction and radiation. The zones are as follow:

- the zone where only external pores exist (conventionally referred to as the particulate charge),
- the zone where the both types of porosity exist (conventionally referred to as the coke charge).

Heat transfer proceeds in the two zones in different ways. In the first zone one can identify thermal conduction in coal and moisture, conduction in pores and radiation between fuel particles. Within the char zone the effective thermal conductivity must be determined using a different procedure due to the fact that two types of porosity (internal and external ones) exist in that zone. The pores have different shapes as compared to space between particles. Alteration of both shapes and dimensions of pores affect the characteristic dimension that is used to determine the radiative part of thermal conductivity. The char zone features heat conduction in coke or gas, radiation across internal pores as well as along cracks. The approach proposed in [27] describes the heat transfer within the fixed - bed in a strict and accurate manner, as the authors adopted the model that takes account of such important phenomena as alteration of solid fuel structure during the combustion process. This approach enables to achieve results that are quite close to reality.

The method proposed in [27] is used in this study to calculate the effective heat conduction coefficient. Mathematical relationships and the detailed description is given in Paragraph 6.2.6.

5.4 Specific heat

Another property of coal that is very important for this study is the specific heat. Composition of the solid fuel mixture is subject to substantial variations due to evaporation, devolatilization and eventually combustion and gasification of char. Each component of the fuel (moisture, volatiles, char and ash) passes a specific heat that is different for each component. It leads to obvious variations of specific heat with fuel composition. The next parameter that affects the value of specific heat attributable to each component and product that originates during coal decomposition is the fixed - bed temperature. Vast majority of the published papers uses the so called equivalent specific heat where coal is considered as the mixture of moisture, volatiles, char and ash [23, 30].

$$\mathsf{c} = \sum_{\mathsf{i}=1}^{3} \mathsf{g_i c_i} \qquad \frac{\mathsf{J}}{\mathsf{kgK}} \tag{5.7}$$

where:

c	- equivalent specific heat,	$\frac{J}{kgK}$,
g_i	- mass fraction of moisture, volatiles, char and ash,	$\frac{kg_i}{kg}$,
c_i	- specific heat of moisture, volatile parts, char and ash,	$\frac{J}{kgK}$.

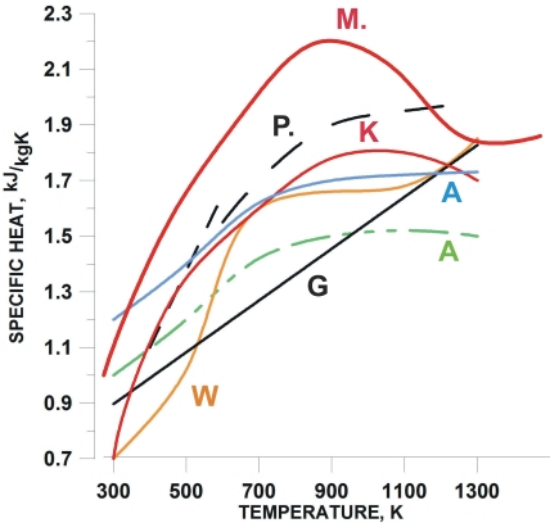

Figure 5.2: Specific heat of coal (A - [106, 107], G - [108], K - [109], P - [110],W - [111], M - [30] (See also [144]) (compiled by the author of this PhD)

Figure 5.2, which originates from the report of Atkinson and Merrick [30], shows the effect of temperature on specific heat for a number of coals. Experimental investigations as well as calculations have demonstrated that the specific heat of the analyzed fuel reaches its maximum $c = 2200\frac{J}{kgK}$ at temperatures around 500^oC. A further temperature increase leads to a drop of the specific heat. The drop is caused by releasing substances with the highest values of specific heat, such as volatiles. The authors of the mentioned study [30] notice that the relationship between the specific heat of coal and its temperature may serve as an indication that endothermic reaction may actually not occur at temperatures below 700^oC. Tomeczek [23] proposes an experimental relationships that determine the effect of the temperature on the specific heat for moisture,volatiles, char and ash. The suggested method reproduces actual variations of thermal capacity during combustion of solid fuel and confirms observations reported in [30].

In this PhD study the dependence of specific heat during coal combustion is described follows references [109, 23]. The formulas are given in Chapter Paragraph 6.2.7.

5.5 Density and porosity of sold fuels

Similarly to thermal conductivity and specific heat, also density of solid fuels is subject to variations during the combustion process. The increase of the bed temperature results in an increase of fuel density as chemical compounds with relatively low density, such as water and volatiles are released to gas phase (vaporisation, devolatilization). The solid phase contains then more char and ash. The relationship between the coal density and temperature is shown in Figure 5.3.

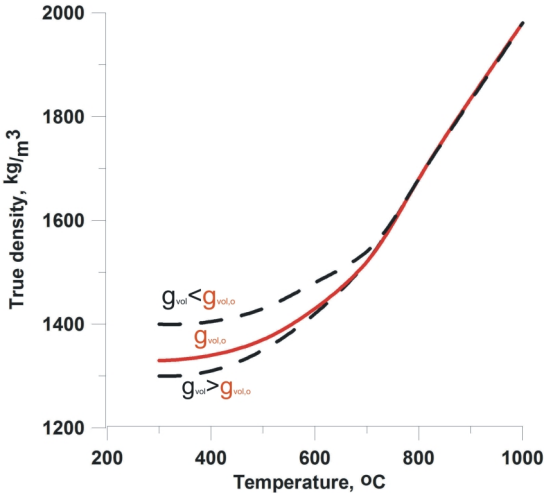

Figure 5.3: Predicted variation of true density with temperature. Heating rate, 3 K/min [54]

Figure 5.4 shows changes to the structure of pores during the combustion process. The overall volume of the solids with respect to the total volume of fuel increases with temperature from about 35% to about 70%. After reaching the softening conditions, the porosity increases rapidly, while at temperature above 500^oC the bed resolidification starts. The fuel undergoes sintering while additional pores appear in the form of cracks and fissures.

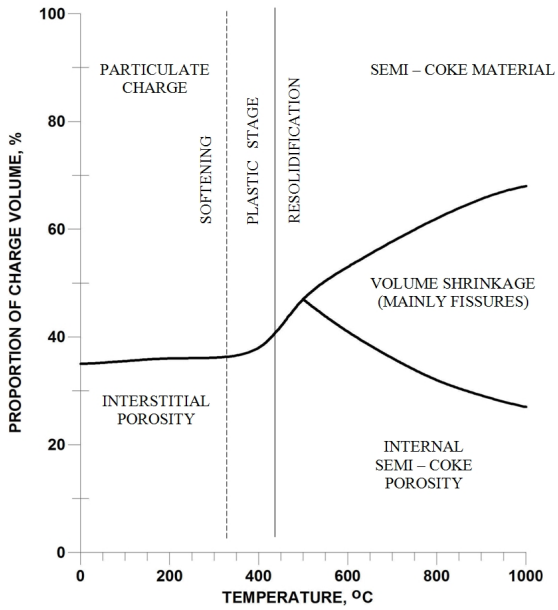

Figure 5.4: Variation of porosity during carbonization [54]

The transformation of the bed structure during the combustion process results in an increase of the bed porosity, but also type and shapes of pores that occur within the bed are subject to alterations. The described changes substantially affect rates of heat transfer in the fixed - bed and therefore they are taken into account in the model developed in this

thesis. Appropriate formula are given in Paragraph 6.2.6.

5.6 Rates of physical and chemical processes during combustion of solid fuel

Combustion of solid fuel is associated with a number of sophisticated physical and chemical processes. In the literature on coal and biomass combustion, rates of various phenomenon are described using Arrhenius equations listed in Table 5.1. The equations describe the rate of evaporation, devolatilization, char combustion, oxidation and char gasification.

	Vaporization	Devolatilization	Char Combustion $C+O_2 \rightarrow CO_2$	Char Gasification $C+CO_2 \rightarrow 2CO$	Description
I	$1.6 \cdot 10^{27} \exp(-25000/T)$	$1.3 \cdot 10^{8} \exp(-16875/T)$	$1.715 \cdot T \cdot \exp(-9000/T)$	$3.42 \cdot T \cdot \exp(-15000/T)$	biomass
II	-	$1.56 \cdot 10^{10} \exp(-16600/T)$	$8620 \cdot \exp(-15900/T)$	-	straw
III	$4.01 \cdot \exp(-14{,}4/RT)$	$1.4 \cdot 10^{5} \exp(-105.9/RT)$	$11000 \cdot \exp(-113/RT)$	$790000 \cdot \exp(-214/RT)$	brown coal
IV	$5.13 \cdot 10^{10} \exp(-88/RT)$	$1.52 \cdot 10^{7} \exp(-139.7/RT)$	-	$3.42 \cdot \exp(-130/RT)$	biomass d_p – (3 - 15) mm
V	-	-	$860 \cdot \exp(-18000/T)$	$10400 \cdot \exp(-178/RT)$	coal char d_p = 20 mm
VI	$1.6 \cdot 10^{27} \exp(-25000/T)$	$1.3 \cdot 10^{8} \exp(-16875/T)$ $2.2 \cdot 10^{8} \exp(-16009/T)$ $1.1 \cdot 10^{7} \exp(-14602/T)$	$1.715 \cdot T \cdot \exp(-9000/T)$	$3.42 \cdot T \cdot \exp(-15000/T)$	wood d_p = (5 - 40) mm
VII	-	-	-	$1327 \cdot \exp(-10945/T)$	Australian coal dp = (0,8 - 4,1) mm
VIII		$2.6 \cdot 10^{11} \exp(-204/RT)$ $10^{7} \exp(-159/RT)$ $10^{13} \exp(-230/RT)$ $10^{12} \exp(-272/RT)$ $492 \cdot \exp(-45/RT)$ $320 \cdot \exp(-41.5/RT)$			CH_4 n=2 heating rate = 0,05 K/s, p=1,1 MPa CH_4, n=2 heating rate = 0,05 K/s, p=0,1 MPa CH_4, n=1 heating rate = (100- 10000) K/s, p=0,1 MPa CH_4, n=1 heating rate = (100- 10000) K/s, p=0,1 MPa CH_4, n=1 heating rate = 210 K/s, p=9 MPa CH_4, n=1 heating rate = 230 K/s, p=9 MPa
IX			$150 \cdot \exp(-83.8/RT)$ $140000 \cdot \exp(-132/RT)$ $5000 \cdot \exp(-97.6/RT)$ $1600000 \cdot \exp(-148.7/RT)$ $1000 \cdot \exp(-85.1/RT)$ $15000000 \cdot \exp(-243/RT)$ $4000 \cdot \exp(-96.4/RT)$		small particles (400 - 2200)°C anthracite d_p= 15 mm, (600 - 800)°C anthracite, (600 - 860)°C ccal d_p= 15 mm, (600 - 800)°C coal coal d_p= 15 mm, <2000°C char d_p– 15 mm, (600 - 800)°C
X			$410000 \cdot \exp(-247.6/RT)$ $890 \cdot \exp(-115.2/RT)$ $3000 \cdot \exp(-167.62/RT)$ $6940 \cdot \exp(-185.4/RT)$ $1100 \cdot \exp(-176/RT)$ $4450 \cdot \exp(-135.8/RT)$		coal

Table 5.1: Kinetics of the processes during coal combustion (I - [113], II - [65], III - [114], IV - [116, 115], V - [117], VI - [118, 113], VII - [119], VIII - [120, 23, 121, 122], IX - [123], X - [123, 22]) (Compilation of the author)

Evaporation

First and foremost, the bed of solid fuel heats up and gets dried whilst the encapsulated moisture evaporates. Even through evaporation of moisture is a physical phenomenon, the evaporation rate is described using an Arrhenius equation of the following form:

$$r_{vap} = k_{vap} \exp\left(-\frac{E}{RT_s}\right) \cdot \rho_s \cdot g_w \qquad \frac{kg_w}{m^3 s} \tag{5.8}$$

where:

r_{vap}	- evaporation rate,	$\frac{kg_w}{m^3 s}$,
k_{vap}	- the pre-exponential factor of evaporation process,	$\frac{1}{s}$,
E	- activation energy,	$\frac{J}{kmol}$,
R	- gas constant,	$\frac{J}{kmol \cdot K}$,
T_s	- solid fuel temperature,	K,
ρ_s	- density of solid fuel,	$\frac{kg}{m^3}$,
g_w	- mass fraction of water in solid fuel,	$\frac{kg_w}{kg}$.

Actually, a full description of the evaporation process is much more complex and its rate depends on a number of factors. However, due to a small amount of water in solid fuels as well as due to high rate of the process, as compared with other phenomena, such a simplification is acceptable.

Devolatilization

At a sufficiently high temperature, coal starts to release hydrocarbons along with gas that contains oxygen, nitrogen, carbon oxide, carbon dioxide, hydrogen, etc. For each of the chemical compounds the release process takes place at different temperatures and with different rates. The combination of foregoing chemical processes that results in release of volatiles from coal is referred to as the devolatilization process. The studies that deal with the phenomenon of coal devolatilization frequently use an Arrhenius equation of the following form:

$$\dot{m}_{dev} = k_{dev} \exp\left(-\frac{E}{RT_s}\right) \cdot \rho_s \cdot g_{vol}^n \qquad \frac{kg_{vol}}{m^3 s} \tag{5.9}$$

where:

r_{dev}	- devolatilization rate,	$\frac{kg_{vol}}{s \cdot m^3}$,
k_{dev}	- the pre-exponential factor of devolatilization process,	$\frac{1}{s}$,
E	- activation energy,	$\frac{J}{kmol}$,
R	- gas constant,	$\frac{J}{kmol \cdot K}$,
ρ_s	- density of solid fuel,	$\frac{kg}{m^3}$,
g_{vol}	- mass fraction of volatiles in solid fuel,	$\frac{kg_{vol}}{kg}$.

The parameters appearing in Equation 5.9, which are often called kinetic parameters, are determined experimentally [22, 23, 31]. There exists a large number of coal devolatilization models and they may be classified into single - equation models and multi - equation models (See for example [23]). The single-equation models are typically applicable for heating rates above $100\frac{K}{s}$. Under such circumstances devolatilization curves, plotted as a

function of temperature, usually have a single maximum or a plurality of maxima located very close to each other. In such a case the single-equation model provides a good fit to experiments. The multi-equation models are used when higher accuracy is required. The frequent assumption that makes the problem easier is considering the volatiles as a single chemical compound and the entire devolatilization process is then described by means of a single equation (Table 5.1).

The analysis of the devolatilization process provided in Merrick [31] shows that thermal effects may be of two types:

- endothermic that take place at temperatures up to $900K$, the thermal effect is about 200 $\frac{kJ}{kg}$ and can be neglected only when the oxygen content is sufficiently high,
- exothermic that take place at temperatures above $900K$, at the level of (200-400)$\frac{kJ}{kg}$.

It has also been reported in [31] that rapid heating of fuel brings about (300-1400)$\frac{kJ}{kg}$ energy released in exothermic reactions.

Char combustion and gasification

The next very important chemical process in a solid fuel bed is associated with reactions of char with the gaseous phase. These reactions that take place exclusively on contact surfaces between the solid and gaseous phases can be split into two groups: exothermic and endothermic ones. Understanding of basic mechanisms that govern chemical processes proceeding in a solid fuel bed is indispensable for developing an efficient model of the combustion process. It is extremely important to know kinetic parameters of the reactions, and these are usually determined by experiments. There are a large number of studies that deal with processes of coal combustion and gasification but they are frequently restricted to pulverized coal. Large coal particles of a solid fuel bed demonstrate different rates of reactions than those measured for pulverized coal. The scientific papers related to the issue of solid fuel combustion report that rates of heterogeneous reactions depend on such parameters as concentration of gaseous substrates, their diffusion rates, particle size as well as kinetic parameters [22, 23, 28, 32, 33, 34] (Table 5.1). In numerous studies the reaction of char combustion:

$$\mathsf{C} + \mathsf{O_2} \rightarrow \mathsf{CO_2} \tag{5.10}$$

is considered as the first order reaction [22, 23]:

$$\mathsf{r_r} = \mathsf{k_r A_z C_g} \qquad \frac{\mathsf{kmol}}{\mathsf{m^3 s}} \tag{5.11}$$

where:

r_r	- reaction rate of heterogeneous reaction,	$\frac{kmol}{m^3 s}$,
k_r	- reaction rate constant of heterogeneous reaction,	$\frac{m}{s}$,
A_z	- specific surface area of particles,	$\frac{m^2}{m^3}$,
C_g	- substrate concentration nearby the solid material surface,	$\frac{kmol}{m^3}$.

The reaction rate constant is usually determined using the Arrhenius equation [22, 23]:

$$\mathsf{k_r = k_o exp(-\frac{E}{RT_s})} \qquad \frac{\mathsf{m}}{\mathsf{s}} \tag{5.12}$$

where:

k_o	- the pre-exponential factor,	$\frac{m}{s}$,
E	- activation energy,	$\frac{J}{kmol}$,
R	- gas constant,	$\frac{J}{kmol \cdot K}$.

Similarly to char combustion, char gasification reaction:

$$\mathsf{C + CO_2 \rightarrow 2CO} \tag{5.13}$$

is also considered as first order with the rate expression identical to equation 5.11 and 5.12.

5.7 Heat exchange between phases

In the old publications on combustion of pulverized coal it is frequently assumed that the temperatures of both phases (gaseous and solid ones) are the same. Such an assumption is acceptable for small particles only. When particles are in millimeters or even centimeters size range this assumption is incorrect. Such large particles heat up quite slowly and, therefore, not only the temperature difference between both phases exists but also a significant temperature gradient in the solid material occurs. This effect is magnified by heating or cooling effect of heterogeneous reactions that occur at contact surfaces between both phases. In order to determine the heat exchange rate between the phases, it is necessary to determine the heat transfer coefficient. In publications [23, 33, 38, 39] the heat exchanged between a solid fuel bed and adjacent gas is considered. The heat transfer coefficient α is determined by means of the following formula:

$$\mathsf{Nu} = \frac{\alpha \cdot \mathsf{d_s}}{\mathsf{k_g}} \tag{5.14}$$

where:

d_s	- characteristic length,	m,
k_g	- thermal conductivity of the gas,	$\frac{W}{mK}$,
Nu	- Nusselt number,	
α	- heat transfer coefficient,	$\frac{w}{m^2K}$.

In case of forced convection, the dimensionless Nusselt number is determined by the relationship between the Reynolds and Prandtl numbers often called as Nusselt function:

$$\mathsf{Nu} = \mathsf{f}\{\mathsf{Re}, \mathsf{Pr}\} \tag{5.15}$$

Exact forms of Nusselt function, that can be used to determine Nusselt number, differ one from another depending on the assumed method and approach to the problem.

The PhD thesis of Bes [40] comprises quite a lot of literature informations on how to calculate the heat transfer coefficient between solid and gaseous phases. The author of the thesis outlines two models. The first model considers the case when gas flows around a single particle. Heat exchange between a single particle and the flowing gas is less intense than in the gas flowing through a fuel bed made up of particles. To take account of presence of other particles, the value of already determined Nusselt number is multiplied by an appropriate shape parameter, so corrections to the heat transfer coefficient are made. Another way, that is also described in the above mentioned thesis, is based on the hydraulic diameter of channels throughout which gas flows. For a porous bed, that diameter can be determined using the following relationship [40]:

$$\mathsf{d_h} = \left(\frac{\mathsf{e}}{1-\mathsf{e}}\right) \cdot \frac{\mathsf{V_s}}{\mathsf{S_s}} \qquad \mathrm{m} \tag{5.16}$$

where:

S_s	- contact surface area between solid and gaseous phases,	m^2,
V_s	- volume of solid phase in the fixed - bed,	m^3.

The bed porosity e is defined as a ratio of the pore volumes to the total volume of the bed [40]:

$$\mathsf{e} = \frac{\mathsf{V_c} - \mathsf{V_s}}{\mathsf{V_c}} \qquad \frac{\mathsf{m_g^3}}{\mathsf{m^3}} \tag{5.17}$$

where:

V_c	- total volume of the bed,	m^3,
V_s	- volume of solid phase in the fixed - bed,	m_s^3.

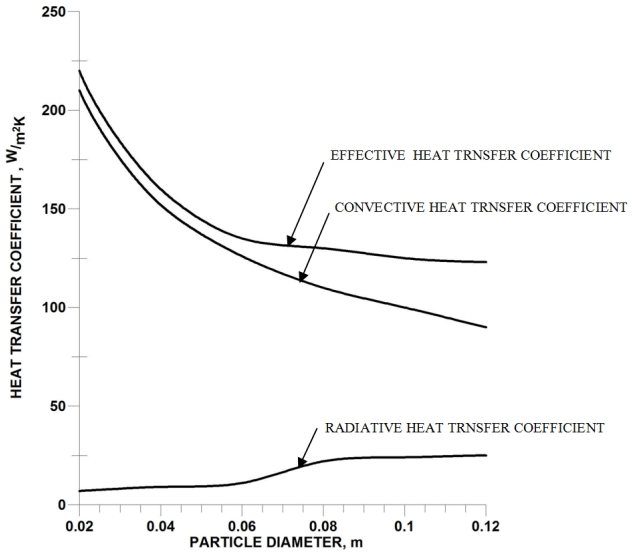

Figure 5.5: Effective heat transfer coefficient - comparison ($t_s = 1000^oC$) [40]

The porosity of coal beds usually ranges from 0.3 to 0.5. The porosity value depends on the particles arrangement and packing, their shapes and dimensions. The analyses presented in [40] demonstrate that the heat transfer coefficient determined by means of both models increases with gaseous phase temperature. Intensification of heat exchange occurs when particle size decreases. Values of the α coefficient for spheres (balls) with the diameter of $0.04m$ and temperature of 1000^oC reach about (100-200)$\frac{W}{m^2K}$ at the air velocity of (1-2)$\frac{m}{s}$.

For the bed of solid combustible fuel the so called effective heat transfer coefficient is frequently used. The effective heat transfer coefficient is the result of two basic thermal processes: radiation and convection, whereas the radiation effect is rather small as compared to heat convection (Figure 5.5). The amount of heat that is exchanged by radiation between the two phases is chiefly dependent on [40]:

- diameters of solid fuel particles,
- average optical path length,
- temperature of particle surface,
- concentration of such radiating gaseous components (CO_2, H_2O).

Figure 5.5 explains the effect of the particle size on the effective heat transfer coefficient. The diagram clearly shows that in general the contribution of radiation to heat transfer between the phases is rather insignificant. Its importance increases with particle diameter. In turn, Figure 5.6 shows that the larger the gas superficial velocity is, the more intense heat exchange between the two phases takes place. A more detailed procedure for calculating the effective heat transfer coefficient is outlined in the next section.

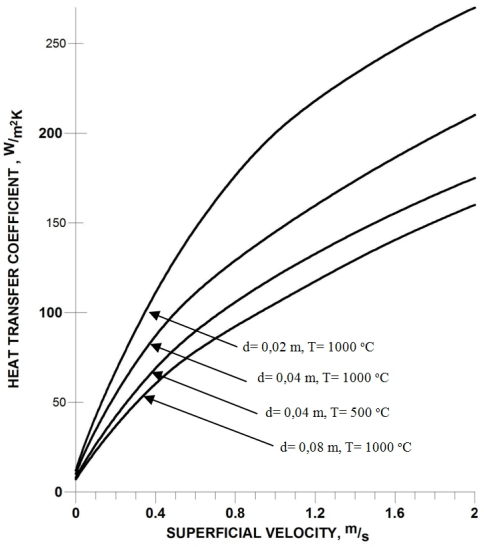

Figure 5.6: Heat transfer coefficient as a function of gas velocity [40]

5.8 Radiation of the gaseous phase

Heat transfer between the solid and gaseous phases take place not only by convection. A part of heat is emitted (by radiation) from the particle surfaces and then absorbed by the gaseous phase. The phenomenon is even more sophisticated when the gaseous phase contains dust. Bes [40] estimates the effect of emissivity of the gaseous phase on the heat transfer coefficient and, consequently on, the amount of heat exchanged between the two phases. The conclusion of Bes is that CO_2 and H_2O are the main molecules that participate in radiative exchange. Such gases as CO, SO_2, NH_3, CH_4 and higher hydrocarbons also absorb radiation but due to their low concentration in the flue gas they are of less importance. Major components of air, i.e. N_2 i O_2 are transparent to radiation. Emissivity of the gas that fills cavities in the solid bed depends on shapes and sizes of free space between particles. For the simplest example when particles are arranged in a cubical manner, the average optical distance within the gaseous area can be computed with sufficient accuracy by means of the following relationship [42].

$$\mathsf{s} = 0.9 \cdot \frac{4 \cdot \mathsf{V_{gas}}}{\mathsf{S_{particle}}} = \frac{\left(1 - \frac{\pi}{6}\right) \cdot \mathsf{d_s}}{\pi} \approx 0.152 \cdot \mathsf{d_s} \qquad \mathsf{m} \tag{5.18}$$

where:

V_{gas}	- volume of empty cavities between particles,	m^3,
$S_{particle}$	- surface area of a particle,	m^2,
d_s	- particle diameter,	m.

Emissivity of gas is described by the formula [42]:

$$\varepsilon_g = A \cdot e^{-BT} \tag{5.19}$$

$$A, B = f(p_p \cdot s) \tag{5.20}$$

where:

A, B - dimensionless coefficients,

T - gas temperature, K,

p_p - partial pressure of gas, Pa.

The radiative heat transfer coefficient α_r is calculated from the formula:

$$\alpha_r = 4 \cdot \frac{1}{\frac{1}{\varepsilon_g} + \frac{1}{\varepsilon_s} - 1} \cdot \sigma \cdot T^3 \qquad \frac{W}{m^2 K} \tag{5.21}$$

where:

ε_g - emissivity of gas,

ε_s - emissivity of external surfaces of particles,

T - gas temperature, K.

The study of Merrick [30] considers also the effect of particle size on the value of the radiative heat transfer coefficient. The coefficient increases with the temperature and reduction of particle sizes. For particle diameters ranging within the interval (0.01 - 0.02)m and the temperature below 1000^oC, the heat transfer coefficient amounts to about 5 $\frac{W}{m^2K}$. This value is so low as compared to the convective heat transfer coefficient ($120\frac{W}{m^2K}$), that it can be neglected. The analyses covered also the case where the gaseous phase contained dust. Even at high concentration of solid particles at the level of (30 - 100) $\frac{mg}{m^3}$ (typical values for low-power boilers [43]) the emissivity of the gas remained nearly constant with no substantial variations.

The foregoing analysis indicates that the amount of heat transferred by radiation and absorbed by the gaseous phase that fills cavities of a fixed - bed is negligibly low. This is so since the path lengths of the radiation rays are indeed small . On the contrary, in the combustion chambers the path length is substantially longer and therefore the gaseous phases containing CO_2, H_2O and dust participates in radiative exchange of heat.

The study of Roberts et al. [35] reveals a relationship between the flue gas emissivity and equivalent layer thickness of such gas. The relationship shows that at the temperature of $1500K$, and at the atmospheric pressure, the emissivity for dusty gas reaches the value of 0.5 when the average path of the ray is about $3m$. For small heating boilers such a distance never exceeds 1 m, which leads to the emissivity values at the level of 0.1.

5.9 Pressure drop across the fixed - bed

When one intends to develop a model for the flow of the gaseous phase throughout a bed of solid fuel, it is necessary to take account of pressure drop across the bed. Figure 5.7 taken from Bes [40] underlines that the pressure drop increases with the superficial gas velocity and with decreasing particle size. The figure shows that the pressure drop across the fixed - bed at the air velocity values from 1 to $2\frac{m}{s}$ at temperature of 600^oC and particle diameters from 0.01 to $0.04m$, reaches the value within the range from 100 to $1000\frac{Pa}{m}$.

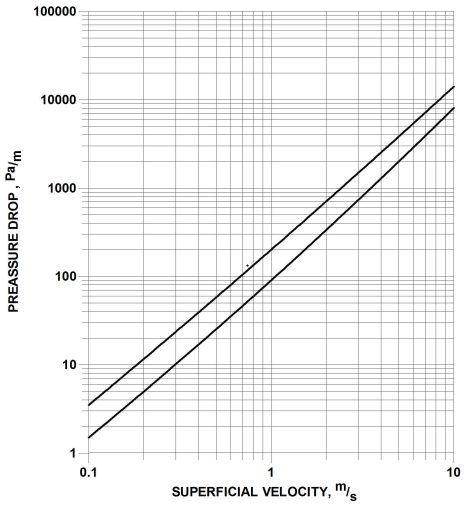

Figure 5.7: Pressure drop across the fixed - bed at temperature of 600^oC (d_p=0.02 m - the upper curve, d_p=0.04 m - the lower curve) [40].

5.10 Modeling of combustion and gasification in fixed beds

As it was mentioned in the beginning, there is only a scarce number of studies related to modeling of processes that take place in small-scale heating boilers [32, 56]. The available literature sources that deal with the subject tend to focus the attention on the gaseous phase with little interest in solid fuel combustion. These studies are mainly experimental.

A great deal of published papers undertakes problems related to specific phenomena that take place inside beds of solid fuel but they offer no models that are suitable for simulation of the combustion process in fixed - beds. For instance, the studies [22, 23, 27, 30, 31] provide detailed information on fundamentals of coal combustion and gasification. In particular, they precisely describe phenomena relevant to the process of solid fuel combustions. The mentioned developments cover also the methods meant to find out essential thermal properties of solid fuel beds and the heat transfer coefficient with the further possibility to determine the amount of heat exchanged within the fixed - bed between the solid and gas phases.

Predominant majority of mathematical models that deal with processes which occur in

fixed - beds are concerned with gasification processes [33, 34, 35, 66, 74, 78, 79, 82, 83, 89, 101].

More recently studies appeared which are related to the modeling of combustion processes for various types of biomass [65, 67, 69, 70, 72, 75, 76, 90, 99, 100, 102, 103, 104, 105, 133] and coal combustion [64, 68, 71, 73, 77, 80, 81, 84, 85, 87, 91]. One of such studies [58] deserves particular attention. The entire textbook is dedicated to the investigation of processes associated with solid fuel combustion in a steady (immobile) layer. The detailed mathematic model for the process in question is precisely described and compared with experimental results.

A substantial body of information relevant to the combustion and gasification in fixed - bed is available through the works on waste incineration on grates [134, 135, 136].

6 Mathematical model

This Chapter provides a detailed mathematical background to the modeling of a retort boiler with its nominal power of about 25 kW (fuel input of 30 kW). To perform numerical calculations the commercial Computational Fluid Dynamics (CFD) software package FLUENT is used.

Section 6.1 presents the essential balance equations and models for major phenomena that take place during the combustion process and are then used by the application (Fluent) software. However, the mentioned software package is insufficient to complete the task as the package does not posses a fixed - bed combustion sub-model. This is why the important objective of this study is to develop sub-model and implement it into the main software body by means of a subroutine developed in C language as the UDF (User Defined Function) module. The detailed description of the model developed by the author of this study is provided in Section 6.2. Reiterating, Section 6.1 provides already well established modeling approach provided by the CFD Fluent package while Section 6.2 presents the original contribution of the author.

6.1 Gas phase free-board combustion model

The mathematical model intended to describe processes that take place within the combustion space of low-power boilers is based on balances of mass, momentum, energy and individual chemical species [123, 124]. Phenomena that are relevant such as radiative heat transfer, turbulent combustion that take place among components of gas in a turbulent flow inside the combustion chamber, are considered in calculations by additional models described in this section. The Clapeyron equation for mixture of ideal gases is used as the state equation. Viscosity, specific heat and thermal conductivity are calculated using appropriate correlations.

6.1.1 The continuity equation

The continuity equation is the mathematical form of the mass conservation law. For a compressible and non-stationary flow (where density and velocity are functions of position and time), with mass sources, the continuity equation adopts the following form for the specific elementary volume dV:

$$\frac{\partial \rho}{\partial t} + div\left(\rho \cdot \boldsymbol{w}\right) = S_m \tag{6.1}$$

where:

ρ	- gas velocity,	$\frac{kg}{m^3}$,
t	- time,	s,
$\boldsymbol{w}$	- vector of gas velocity, $(\boldsymbol{w}_x, \boldsymbol{w}_y, \boldsymbol{w}_z)$,	$\frac{m}{s}$,
S_m	- source term,	$\frac{kg}{m^3 s}$.

The foregoing relationship contains three terms: the non-stationary, convective and the source term. The non-stationary term describes the rates of mass changes within the volume dV. The convective term represents the transport of fluid across borders of the volume dV. In turn, the S_m term stands for mass sources (or sinks) within the dV volume.

6.1.2 Momentum conservation equations

The Navier - Stokes equation is the relationship that describes motion of fluids. That equation is the balance of momentum for a fluid element:

$$\frac{\partial (\rho \cdot \boldsymbol{w})}{\partial t} + \nabla \cdot (\rho \boldsymbol{w} \boldsymbol{w}) = -\nabla p + \nabla \cdot \mathbb{T} + \rho \boldsymbol{g} + \boldsymbol{F} \tag{6.2}$$

where:

p	- pressure,	Pa,
g	- gravitational acceleration,	$\frac{m}{s^2}$,
$\boldsymbol{F}$	- vector of body forces (per unit volume),	$\frac{N}{m^3}$.

The N-S equation contains the following terms (from left to right): the non - stationary term, associated with accumulation of momentum (unsteady acceleration), the convective term that describes transfer of momentum (convective acceleration) and the pressure gradient term as well as stress term (surface forces) and finally the gravity and other body forces terms. The stress tensor for Newtonian fluids is related to the rate of strain. The dynamic viscosity μ acts as the proportionality coefficient. The stress tensor for Newtonian fluids is defined by the following formula:

$$\mathbb{T} = 2\mu \left(\mathbb{E} - \frac{1}{3} \triangle \mathbb{I} \right) \qquad \frac{\mathsf{N}}{\mathsf{m}^2} \tag{6.3}$$

where:

μ	- dynamic viscosity,	$Pa \cdot s$,
$\mathbb{E} = \frac{1}{2}(\nabla \boldsymbol{w}) + \frac{1}{2}(\nabla \boldsymbol{w})^T$	- the rate of strain tensor,	$\frac{1}{s}$,
$\triangle = \nabla \cdot \boldsymbol{w}$,	- the rate of expansion of the flow,	$\frac{1}{s}$,
$\mathbb{I}$	- 3×3 identity matrix.	

6.1.3 The conservation equation of chemical species

The conservation equation for the i-th component of the mixture reads:

$$\frac{\partial (\rho \cdot g_i)}{\partial t} + \nabla (\rho \boldsymbol{w} g_i) + \nabla \cdot \boldsymbol{J}_i = S_i + R_i \tag{6.4}$$

The above equation comprises the term that describes variation of the „i" component in time, the term associated with convection and diffusion of the „i" component, as well the source terms. The R_i stands for the effect associated with either formation or destruction of the species due to chemical reactions. The source S_i describes the mechanism of another type, e.g. by exchange of mass with another phase. The diffusion term describes the diffusion rate of „i" species in the mixture. The diffusive flux of the „i" substance can be determined using the relationship:

$$\boldsymbol{J}_i = -\left(\frac{\mu}{Sc_i} + \frac{\mu_t}{Sc_t}\right) \nabla g_i \tag{6.5}$$

where:

μ	- dynamic viscosity,	$Pa \cdot s$,
μ_t	- turbulent viscosity,	$Pa \cdot s$,
$Sc_i = \frac{\mu}{\rho \cdot D_i}$	- Schmidt number,	
$Sc_t = \frac{\mu_t}{\rho \cdot D_t}$	- turbulent Schmidt number,	
g_i	- mass fraction of species „i",	$\frac{kg_i}{kg}$,
$D_{i,m}$	- diffusion coefficient for species „i" within the mixture,	$\frac{m^2}{s}$,
D_t	- turbulent diffusivity,	$\frac{m^2}{s}$.

The most common practice in numerical calculations dedicated to mixtures made up of „n" components is to solve a system of n-1 balance equations. The mass fraction of the last component of the mixture is found from the complementary relationship stating that the sum of mass fractions for the mixture components must add up to 1. Usually the component with the largest mass fraction is selected as the one, for which the balance equation is not solved for. In case of fuel combustion in air it is nitrogen.

6.1.4 The energy conservation equation

The general form of the energy balance can be expressed in the following way:

$$\frac{\partial (\rho \cdot E)}{\partial t} + \nabla (\boldsymbol{w} (\rho E + p)) = \nabla \cdot \left(k_{eff} \nabla T - \sum_i h_i \boldsymbol{J}_i + (\mathbb{T}_{eff} \cdot \boldsymbol{w})\right) + S_h \tag{6.6}$$

where:

$E = h - \frac{p}{\rho} + \frac{\nu^2}{2}$	- specific fluid energy,	$\frac{J}{kg}$, and
$h = \sum g_i h_i$	- specific enthalpy of species „i",	$\frac{J}{kg}$.

$$h_i = h^0_{T_{ref,i}} + \int_{T_{ref,i}}^{T} c_{p,i} \cdot dT \tag{6.7}$$

where:

$c_{p,i}$	- specific heat of species „i",	$\frac{J}{kg \cdot K}$,
$h^0_{T_{ref,i}}$	- formation enthalpy of species „i" at the reference temperature T_{ref},	$\frac{J}{kg}$,
g_i	- mass fraction of species „i",	$\frac{kg_j}{kg}$.

The left hand side of the above equation contains both the accumulation and convection terms. The right-hand side includes, the heat conduction, diffusion as well as viscous dissipation terms. The last (source) term of the equation stands for the rate of heat generation per a volume unit.

6.1.5 Turbulences

The conventional approach to modeling of the turbulence effect is based on the concept proposed by Reynolds. According to that idea, the instantaneous velocity U of a turbulent flow can be considered as the sum of its mean value $\overline{U}$ averaged over time and its fluctuating component u. When this relationship is applied to the Navier-Stokes equation, one can obtain the Reynolds equation. For the non-compressive flow that relationship is simplified to the formula [46]:

$$\rho \left(\frac{\partial \overline{U}_i}{\partial t} + \overline{U}_j \frac{\partial \overline{U}_i}{\partial x_j} \right) = \frac{\partial}{\partial x_j} \sigma_{ij} + \overline{F}_i \tag{6.8}$$

where:

ρ	- fluid density,	$\frac{kg}{m^3}$,
F_i	- mass forces of component „i",	$\frac{N}{m^3}$,
σ_{ij}	- stress tensor „i",	$\frac{N}{m^2}$.

The stress tensor is determined by the relationship [46]:

$$\sigma_{ij} = -\overline{p}\delta_{ij} + \nu\rho \left(\frac{\partial \overline{U}_i}{\partial x_j} + \frac{\partial \overline{U}_j}{\partial x_i} \right) - \overline{\rho u_i u_j} \tag{6.9}$$

where:

ν - kinematic viscosity, $\frac{m^2}{s}$.

The above equation contains an additional term that does not appear in the Navier - Stokes equation. That terms is referred to as the Reynolds stress tensor [46]:

$$(\sigma_t)_{ij} = \rho\overline{u_i u_j} = \mu_t\left(\overline{u}_{ij} + \overline{u}_{ji}\right) - \frac{2}{3}\overline{\rho}k\delta_{ij} \tag{6.10}$$

$$\mu_t = \frac{\rho \cdot c_\mu \cdot k}{\varepsilon} \tag{6.11}$$

where k stands for the turbulent kinetic energy and c_μ is the constant parameter, ε denotes dissipation rate of turbulent energy. Appearance of two new variables $(k-\varepsilon)$ entails the need to seek for additional relationships to make the equation system closed. This deficiency can be replenished by implementation of the model of turbulences [46]. This study uses the $k-\varepsilon$ model proposed by Harlov and Nakayama [48]. It is a model that introduces two additional transport equations. The first one describes the transport of turbulent kinetic energy „k", while the second concerns turbulent dissipation rate „ε". The two transport equations adopt the form [47, 48]:

$$\frac{\partial(\rho k)}{\partial t} + \frac{\partial(\rho \cdot k \cdot u_i)}{\partial x_i} - \frac{\partial}{\partial x_j}\left(\left(\mu + \frac{\mu_t}{\mathrm{Pr}_k}\right)\frac{\partial k}{\partial x_j}\right) = P_k + P_b - \rho\cdot\varepsilon - Y_m + S_k \tag{6.12}$$

$$\frac{\partial(\rho\varepsilon)}{\partial t} + \frac{\partial(\rho\cdot\varepsilon\cdot u_i)}{\partial x_i} = \frac{\partial}{\partial x_j}\left(\left(\mu + \frac{\mu_t}{\mathrm{Pr}_\varepsilon}\right)\frac{\partial\varepsilon}{\partial x_j}\right) + C_{\varepsilon 1}\frac{\varepsilon}{k}\left(P_k + C_{\varepsilon 3}P_b\right) - C_{\varepsilon 2}\rho\cdot\frac{\varepsilon^2}{k} + S_\varepsilon \tag{6.13}$$

where:

$\varepsilon = \frac{\mu}{\rho}\cdot\overline{\frac{\partial u_i}{\partial x_j}}\cdot\overline{\frac{\partial u_j}{\partial x_i}}$		$\frac{m^2}{s^3}$,
μ_t	- turbulent viscosity,	$Pa\cdot s$,
	$k = \frac{1}{2}\cdot\overline{u_i\cdot u_j}$,	$\frac{m^2}{s^2}$,
u_i	- fluctuating velocity component,	$\frac{m}{s}$,
S_k, S_e	- source terms,	$\frac{kg}{s^3m^3}$, $\frac{kg}{s^4m^3}$,
Y_m	- parameter that incorporates effect of compressibility,	$\frac{W}{m^3}$,
$P_k = -\rho\overline{u_i u_j}\frac{\partial u_j}{\partial x_i}$		$\frac{kg}{s^3m^3}$,
$P_b = -\beta g_i\frac{\mu_t}{\mathrm{Pr}_t}\frac{\partial T}{\partial x_i}$		$\frac{kg}{s^3m^3}$,
$C_{1\varepsilon}$	- 1.44,	
$C_{2\varepsilon}$	- 1.92,	
C_μ	- 0.09,	
Pr_k	- 1.0,	
Pr_ε	- 1.3,	
$\beta = -\frac{1}{\rho}\left(\frac{\partial\rho}{\partial T}\right)_p$	- coefficient of thermal expansion,	$\frac{1}{K}$.

u_i stands for fluctuating velocity component, S_k, S_ε are source components, Y_m , incorporates effect of compressibility, P_k, refers to the effect of elasticity, P_b, is associated with the thermal expansion of gas.

6.1.6 Equation of state

The Clapeyron equation written in the following form:

$$\rho = \frac{\mathsf{p}}{\mathsf{R}\cdot\mathsf{T}\cdot\sum_{\mathsf{i}=1}^{\mathsf{n}}\frac{\mathsf{g_i}}{\mathsf{M_i}}} \qquad \frac{\mathsf{kg}}{\mathsf{m^3}} \tag{6.14}$$

where:

$R = 8.315$	- gas constant,	$\frac{kJ}{kmol\cdot K}$,
M_i	- molecular weight of species „i”,	$\frac{kg_i}{kmol}$,
g_i	- mass fraction of species „i”,	$\frac{kg_i}{kg}$,
p	- absolute pressure,	Pa.

serves as the equation of state.

6.1.7 Gas phase combustion model

The net source R_i of chemical species „i” describes its variation due to „n” chemical reactions and can be determined by means of the following formula:

$$\mathsf{R_i} = \mathsf{M_i}\sum_{\mathsf{j}=1}^{\mathsf{n}}\mathsf{r_{i,j}} \qquad \frac{\mathsf{kg_i}}{\mathsf{m^3 s}} \tag{6.15}$$

where:

M_i	- molecular weight of ,, i'' species,	$\frac{kg}{kmol}$,
$r_{i,j}$	- Arrhenius molar rate of creation/destruction of species „i” in reaction „j”,	$\frac{kmol}{m^3 s}$.

In order to determine the rate of change of species „i” in the „j” reaction the following relationship can be applied:

$$\mathsf{r_{i,j}} = \mathsf{k_{f,j}}\prod_{\mathsf{a}=1}^{\mathsf{N}}[\mathsf{C_{a,j}}]^{\eta_{\mathsf{f,a,j}}} - \mathsf{k_{b,j}}\prod_{\mathsf{a}=1}^{\mathsf{N}}[\mathsf{C_{a,j}}]^{\eta_{\mathsf{b,a,j}}} \qquad \frac{\mathsf{kmol_i}}{\mathsf{m^3 s}} \tag{6.16}$$

where:

$k_{f,j}$	- forward reaction rate constant of „j" reaction,	(units vary),
$k_{b,j}$	- backward reaction rate constant of „j" reaction,	(units vary),
$C_{a,j}$	- molar concentration of species „a" in „j" reaction,	$\frac{kmol}{m^3}$,
$\eta_{f,a,,j}$,$\eta_{b,a,j}$	- stoichiometric coefficient of species „a" in the „j" reaction,	
N	- number of chemical species that enter into the specific reaction „j".	

The rate constants of each reaction are related to the equilibrium constant:

$$\frac{\mathsf{k_f}}{\mathsf{k_b}} = \left(\frac{\mathsf{p}}{\mathsf{RT}}\right)^{\Delta\eta} \exp\left(\frac{\mathsf{\Delta S^o}}{\mathsf{R}} - \frac{\mathsf{\Delta H^o}}{\mathsf{RT}}\right) \tag{6.17}$$

where:

$\triangle\eta = \eta_b - \eta_f$,

$\triangle S^o$	- standard state entropy,	$\frac{J}{kmolK}$,
$\triangle H^o$	- standard state enthalpy,	$\frac{J}{kmol}$.

The rate of disappearance or creation of a species in a turbulent reacting flow is determined by two major mechanisms: the kinetics of the chemical reactions as well as by the transport (mixing). It will be shown later that for low power coal-fired boilers these both phenomena are of crucial importance and are responsible for incomplete combustion of such substances as CO or HC.

In this study the Eddy Dissipation Concept (EDC) model is used that takes account, in its description of chemical processes, of kinetics as well as turbulent mixing. The model has been developed by Magnussen et al. [126, 127, 128]. The originator assumes that chemical reactions take place exclusively in small turbulent structures (eddys) referred to as 'fine structures'. The reaction rate is determined by means of the following relationship:

$$\Re = \frac{\rho\,(\gamma^*)^2}{\tau^*\left[1-(\gamma^*)\right]^3}\left(\mathsf{g_i^*} - \mathsf{g_i^o}\right) \qquad \frac{\mathsf{kg_i}}{\mathsf{m^3 s}} \tag{6.18}$$

where:

$\tau^* = C_\tau \left(\frac{\nu}{\varepsilon}\right)^{\frac{1}{2}}$	- destruction time of the Kolmogorov structure,	s,
$\gamma^* = C_\gamma \left(\frac{\nu\cdot\varepsilon}{k^2}\right)^{\frac{1}{4}}$	- length fraction of the fine scales,	J,
ν	- kinematic viscosity,	$\frac{m^2}{s}$,
g_i^*	- mass fraction of species „i" in the fine structure,	$\frac{kg_i}{kg}$,

C_τ=0.4082,

C_γ=9.7687.

6.1.8 Radiative heat transfer

In the Discrete Ordinates DO model the radiative transfer equation is solved for a limited number of directions. The radiative transfer equation adopts the following form:

$$\frac{dI(\boldsymbol{r},\boldsymbol{s})}{ds} + (a+\sigma_s)\, I\left(\boldsymbol{r},\boldsymbol{s}\right) = an^2\frac{\sigma T^4}{\pi} + \frac{\sigma_s}{4\pi}\int_0^{4\pi} I\left(\boldsymbol{r},\boldsymbol{s'}\right)\Phi\left(\boldsymbol{s}\cdot\boldsymbol{s'}\right)d\Omega \tag{6.19}$$

where:

$\boldsymbol{r}$	- vector of position,	m,
$\boldsymbol{s}$	- vector of direction,	sr,
$\boldsymbol{s}'$	- scattering direction vector,	
a	- absorption coefficient,	
n	- refractive index,	
σ	- Stefan – Boltzmann constant,	$\frac{W}{m^2K^4}$,
σ_s	- scattering coefficient,	
I	- radiation intensity,	$\frac{W}{sr\cdot m^2}$,
T	- local temperature,	K,
Ω	- solid angle,	sr,
T	- local temperature,	K,
Φ	- phase function.	

The first term of Equation 6.19 describes the change of the radiation intensity at a given position r. When the radiation travels a ds distance, the intensity of radiation that passes throughout the specific volume dV is reduced by absorption and by out - scattering. The increase of the radiation intensity takes place owing to the emission and in - scattering. In the energy balance equation (Equation 6.6) the radiation appears as a source term.

6.2 Fixed - bed combustion model

Combustion of solid fuel in a fixed - bed is a sophisticated physical and chemical process. When one wishes to describe the process the attention must be paid to a number of phenomena, including flow of oxidizer through the bed, diffusion of oxidizer, evaporation of moisture, devolatilization of volatiles, thermal and chemical interactions between particles and the gaseous phase. Knowledge of thermal properties, such as specific heat and thermal conductivity is important. It is imperative to account for the effect of sizes, types and shapes of pores that can be found in the fixed - bed onto the chemical reactivity of fuel and rates of heat transport, both within the fixed - bed and between phases.

6.2.1 Properties of EKORET coal

Retort low-power boilers are fired with a prepared fuel. Such coal (Figure 6.1) must feature an appropriate granulation (see Table 2.2). Due to application of the automatic feeder (a screw or a piston one) the fuel must be free of mechanical contaminations. The coal must posses an adequate calorific value, sulfur content, sinterability, etc. (see Table 2.2).

Figure 6.1: EKORET coal

Appropriately prepared fuel is available in bags (Figure 6.2) so that the moisture content of the fuel remains constant during the storage period.

Figure 6.2: EKORET coal – in shipping bags

Table 6.1 shows the composition (ultimate, proximate analysis) and sieve analysis of EKORET coal.

EKORET fuel (as delivered)				
PROXIMATE ANALYSIS				
		a	d	daf
Total moisture(ar). %	7	6.1	-	-
Air dried moisture(ad). %	6	6.1	-	-
Ash. %	5.3	5.3	5.7	-
Combustisble substance. %	87.8	88.6	94.3	-
Volatile matter. %	31.5	31.9	31.9	35.9
HCV. kJ/kg	29 359	29 655	31 565	33 456
LCV. kJ/kg	28 235	28 545	30 540	32 370
ULTIMATE ANALYSIS				
carbon. %	73.64	74.38	79.17	83.91
hydrogen. %	4.37	4.41	4.69	4.98
oxygen. %	7.94	8.02	8.54	9.05
nitrogen. %	1.39	1.4	1.49	1.58
sulphur. %	0.43	0.43	0.46	0.49
chlorine. %	0.22	0.22	0.24	-
fluorine. %	0.002	0.003	0.003	0.003
ASH MELTING TEMPERATURES				
Sintering temperature. °C	1130			
Softening temperature. °C	1190			
Melting temperature. °C	1220			
Flow temperature. °C	1250			
Roga index RI	17			
SIEVE ANALYSIS				
mm	%			
>20	58.1			
20 - 10	41.4			
10 - 5.0	0.4			
5.0 - 3.0	0.0			
3.0 - 1.0	0.0			
1.0 - 0.5	0.0			
0.5 - 0.2	0.0			
< 0.2	0.1			

Table 6.1: Proximate and ultimate analysis of EKORET coal (a - air dried, d - dry, daf - dry ash free)

Table 6.1 provides the proximate and ultimate analysis of EKORET coal. Such parameters as the calorific value or coal composition are essential. The sieve analysis has demonstrated that EKORET coal is made up of particles with sizes that range within a narrow interval. The average diameter of the examined coal is 0.02 m. Particles of the investigated coal feature irregular shapes but in the further part of this study the assumption is made that they are spherical.

6.2.2 Flow of gas through a bed of solid fuel

The only one model from among very few ones closely associated with a fixed - bed and available for the employed software package is the model of flow through a porous volume. The model that is used for this study needs parameters related to properties of the fuel bed and they have been determined experimentally. These parameters include: viscous and internal resistance, as well as porosity. Knowledge of these parameters is essential for the pressure drop determination and calculation of velocity distribution within the bed.

In order to find out required resistance factors the measurement of pressure drop across the bed of EKORET coal is carried out. The research program covered measurements of pressure drop across the fuel bed for several values of air (superficial) velocity. The measurements are carried out in the reactor (Figure 6.3) with the internal diameter of 0.18m. The bed height during measurements is 0.1 m. The tests are performed for five values of air velocity ranging from 0 to 0.6 $\frac{m}{s}$. The measured pressure drop is presented in Figure 6.4.

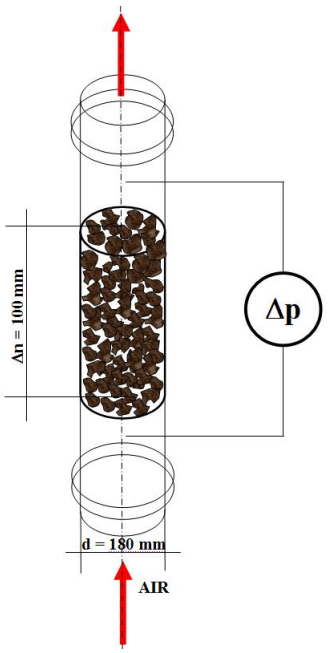

Figure 6.3: Measurements of the pressure drop across the bed of the EKORET coal – the reactor

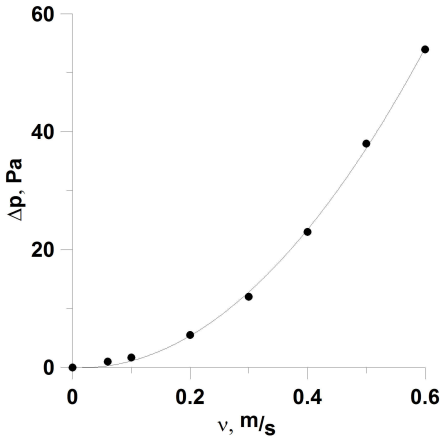

Figure 6.4: Pressure drop across the bed of the EKORET coal - experimental investigations

The measured data are least square fitted to provide the following relationship:

$$\Delta p = 158.92 w_\infty{}^2 - 5.022 w_\infty \qquad Pa \tag{6.20}$$

where:

w_∞ - superficial velocity $\frac{m}{s}$.

The effect of the bed presence (a porous volume) is modeled by means of an additional source term introduced to the momentum equation:

$$S_i = -\left(\frac{\mu}{z} w_\infty + C_2 \frac{1}{2} \rho w_\infty^2\right) \qquad \frac{Pa}{m} \tag{6.21}$$

where:

μ - dynamic viscosity, $Pa \cdot s$,
$\frac{1}{z}$ - viscous resistance, $\frac{1}{m}$,
C_2 - internal resistance, $\frac{1}{m^2}$.

Therefore, the pressure drop across the bed can be expressed by means of the formula:

$$\Delta p = -\left(\frac{\mu}{z} w_\infty \Delta n + C_2 \frac{1}{2} \rho w_\infty^2 \Delta n\right) \qquad Pa \tag{6.22}$$

where:

Δn - coal bed height, m.

The above equations enable calculation of resistance coefficients „a" and „b" that appear in:

$$\Delta p = a w_\infty{}^2 + b w_\infty \qquad Pa \tag{6.23}$$

and correspond to the parameters associated with the turbulent and viscous resistance. Using the measured data, one can find out that $a = 158.92, \frac{Pa \cdot s^2}{m^2}$, $b = -5.02, \frac{Pa \cdot s}{m}$. After substitution of the calculated values to the equations below one can finally find the desired resistance coefficients:

$$a = C_2 \frac{1}{2} \rho \Delta n \Rightarrow C_2 = 2605.24 \frac{1}{m^2} \tag{6.24}$$

$$b = \frac{\mu}{z} \Delta n \Rightarrow \frac{1}{z} = -2806527.33 \frac{1}{m} \tag{6.25}$$

where:

$\frac{1}{z}$	- viscous resistance,	$\frac{1}{m}$,
C_2	- internal resistance,	$\frac{1}{m^2}$,
μ	- dynamic viscosity of air,	$Pa \cdot s$,
ρ	- air density,	$\frac{kg}{m^3}$,
$\triangle n$	- coal bed height,	m,
$\triangle p$	- pressure drop across the bed,	Pa,
ν	- air velocity,	$\frac{m}{s}$.

The method proposed in Postrzednik et al. [59] has been used to determine the porosity of the coal bed. The measured value of the porosity is 35%.

6.2.3 Basic equations of the fixed - bed model

The solid phase

The newly developed model for solid (coal) phase is based on three species transport equations to calculate the moisture, volatiles, char content in the solid phase.

$$\frac{\partial}{\partial \mathsf{t}} \left[(1 - \mathsf{e}) \, \rho_{\mathsf{s}} \cdot \mathsf{g}_{\mathsf{w}} \right] + \nabla \cdot \left[(1 - \mathsf{e}) \, \rho_{\mathsf{s}} \mathsf{w}_{\mathsf{s}} \cdot \mathsf{g}_{\mathsf{w}} \right] = -\mathsf{G}_{\mathsf{vap}} \tag{6.26}$$

$$\frac{\partial}{\partial \mathsf{t}} \left[(1 - \mathsf{e}) \, \rho_{\mathsf{s}} \cdot \mathsf{g}_{\mathsf{vol}} \right] + \nabla \cdot \left[(1 - \mathsf{e}) \, \rho_{\mathsf{s}} \mathsf{w}_{\mathsf{s}} \cdot \mathsf{g}_{\mathsf{vol}} \right] = -\mathsf{G}_{\mathsf{dev}} \tag{6.27}$$

$$\frac{\partial}{\partial \mathsf{t}} \left[(1 - \mathsf{e}) \, \rho_{\mathsf{s}} \cdot \mathsf{g}_{\mathsf{char}} \right] + \nabla \cdot \left[(1 - \mathsf{e}) \, \rho_{\mathsf{s}} \mathsf{w}_{\mathsf{s}} \cdot \mathsf{g}_{\mathsf{char}} \right] = -\mathsf{G}_{\mathsf{char}} \tag{6.28}$$

where:

g_i	- mass fraction of the specific component of coal,	$\frac{kg_i}{kg}$.

The above three equations are accompanied by the continuity equation for the solid phase:

$$\frac{\partial}{\partial \mathsf{t}} \left[(1 - \mathsf{e}) \, \rho_{\mathsf{s}} \right] + \nabla \cdot \left[(1 - \mathsf{e}) \, \rho_{\mathsf{s}} \mathsf{w}_{\mathsf{s}} \right] = -\mathsf{G}_{\mathsf{char}} - \mathsf{G}_{\mathsf{vap}} - \mathsf{G}_{\mathsf{dev}} \tag{6.29}$$

where:

e	- coal porosity (initial value = 0.35),	$\frac{m_g^3}{m^3}$,
ρ_s	- coal density = 1300,	$\frac{kg_s}{m_s^3}$,
w_s	- velocity of coal bed,	$\frac{m}{s}$,
G_i	- source components associated with chemical and physical processes,	$\frac{kg_i}{m^3 s}$.

Ash g_{ash} is regarded as an inert substance and is calculated from the following relationship:

$$\mathsf{g_{ash}} = 1 - \mathsf{g_{char}} - \mathsf{g_{vol}} - \mathsf{g_w} \tag{6.30}$$

The energy balance for solids of the fixed - bed is as follows:

$$\frac{\partial}{\partial \mathsf{t}} \left[(1-\mathsf{e})\, \rho_\mathsf{s} \cdot \mathsf{h_s} \right] + \nabla \cdot \left[(1-\mathsf{e})\, \rho_\mathsf{s} \cdot \mathsf{w_s} \cdot \mathsf{h_s} \right] = \nabla \cdot (\mathsf{k_{eff}} \nabla \mathsf{T_s}) + \mathsf{S_{conv}} + \mathsf{S_{char}} - \mathsf{S_{vap}} - \mathsf{S_{dev}} + \mathsf{S_{fs}} \tag{6.31}$$

The gaseous phase

The continuity equation of the gas phase inside the fixed - bed reads:

$$\frac{\partial}{\partial \mathsf{t}} (\mathsf{e} \cdot \rho_\mathsf{g}) + \nabla \cdot [\mathsf{e} \cdot \rho_\mathsf{g} \cdot \mathsf{w_g}] = \mathsf{G_{char}} + \mathsf{G_{vap}} + \mathsf{G_{dev}} \tag{6.32}$$

where:

ρ_g - gas density, $\frac{kg_g}{m_g^3}$,

w_g - gas velocity, $\frac{m}{s}$.

The following components exist in the gaseous part of the fixed - bed: volatiles, oxygen, nitrogen, carbon monoxide, carbon dioxide and water vapour. Five equations (for volatiles, CO, CO_2, O_2 and H_2O) are solved for. The balance equation for individual gaseous components Y_i takes the form:

$$\frac{\partial}{\partial \mathsf{t}} (\mathsf{e} \cdot \rho_\mathsf{g} \cdot \mathsf{Y_i}) + \nabla \cdot [\mathsf{e} \cdot \rho_\mathsf{g} \cdot \mathsf{w_g} \cdot \mathsf{Y_i}] = \nabla \cdot [\mathsf{e} \cdot \rho_\mathsf{g} \cdot \mathsf{D_{i,eff}} \nabla \mathsf{Y_i}] + \mathsf{G_i} \tag{6.33}$$

where:

Y_i - mass fraction of the i-th gas component, $\frac{kg_i}{kg_g}$.

The energy balance for gas inside the fixed - bed reads:

$$\frac{\partial}{\partial \mathsf{t}} [\mathsf{e} \cdot \rho_\mathsf{g} \cdot \mathsf{h_g}] + \nabla \cdot [\mathsf{e} \cdot \rho_\mathsf{g} \cdot \mathsf{w_g} \cdot \mathsf{h_g}] = \nabla \cdot (\mathsf{e} \cdot \mathsf{k_g} \nabla \mathsf{T_g}) - \mathsf{S_{conv}} + \mathsf{S_{fg}} \tag{6.34}$$

where:

$h_g = \int_{T_o}^{T_g} c_p dT$	- physical enthalpy of gas,	$\frac{J}{kg_g}$,
$h_s = \int_{T_o}^{T_s} c \cdot dT$	- physical enthalpy of solid body,	$\frac{J}{kg_s}$,
S_i	- energy sources term for respective chemical and physical processes,	$\frac{W}{m^3}$,
Y_i	- mass fraction of the i-th gas component,	$\frac{kg_i}{kg_g}$,
k_g	- thermal conductivity for gas,	$\frac{J}{mK}$,
k_{eff}	- effective thermal conductivity for solid fuel,	$\frac{J}{mK}$,
T_g, T_s	- temperatures of gas and solid fuel,	K.

The implemented model assumes that the two following homogeneous reactions take place in gaseous phase:

- combustion of volatiles released from the solid fuel:

$$[\mathrm{volatiles}] + 1.21\mathrm{O_2} \rightarrow 1.05\mathrm{CO} + 2.11\mathrm{H_2O} + 0.038\mathrm{N_2} \tag{6.35}$$

- combustion of carbon monoxide:

$$\mathrm{CO} + 0.5\mathrm{O_2} \rightleftarrows CO_2 \tag{6.36}$$

In the last case one has also to take account of the reverse reaction that is important at high temperatures (above 1200 K). The rates of reaction 6.35 is calculated as [94]:

$$\mathrm{k_{co}} = 2.5 \cdot 10^8 [\mathrm{CO}][\mathrm{O_2}]^{0.3}[\mathrm{H_2O}]^{0.5} \exp\left(-\frac{8052}{\mathrm{T_g}}\right) \tag{6.37}$$

while the rate of volatiles oxidation as [92, 93]:

$$\mathrm{k_{volatiles}} = 4.4 \cdot 10^{11} [\mathrm{volatiles}]^{0.5}[\mathrm{O_2}]^{1.25} \exp\left(-\frac{15098}{\mathrm{T_g}}\right) \tag{6.38}$$

The volatile matter is assumed to have the following composition:

$$[\mathrm{volatiles}] - \mathrm{C_{1.05}H_{4.22}O_{0.74}N_{0.0761}} \tag{6.39}$$

which is obtained considering the proximate and ultimate analysis of the coal used (see Paragraph 7.1). The molar mass of volatiles is:

$$\mathrm{M_{volatile}} = 30 \frac{\mathrm{kg}}{\mathrm{kmol}} \tag{6.40}$$

Mass sources and sinks

In the balance equations for both phases a number of source terms appear. They are associated with the four basic phenomena:

- evaporation of moisture,
- devolatilization of volatile matter,
- char combustion,
- char gasification.

Figure 6.5 shows all the source terms in the mass balance equations. They are considered below, one by one.

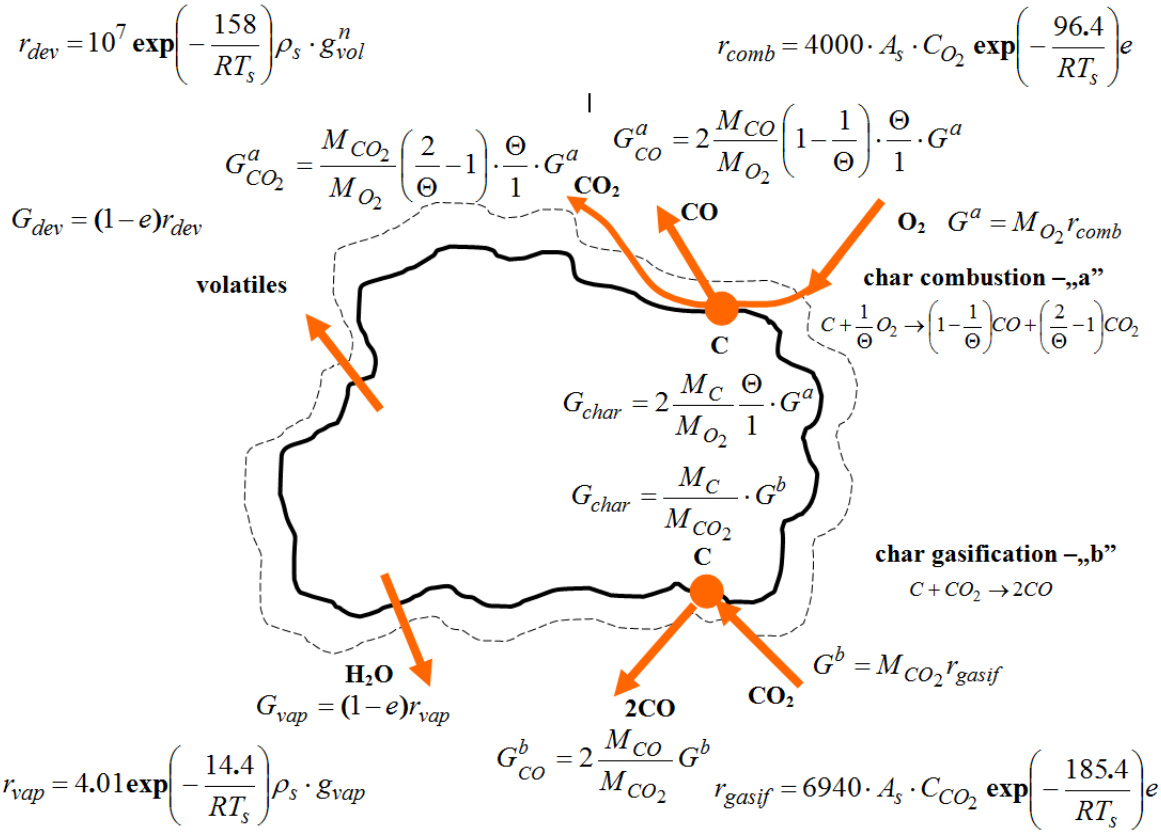

Figure 6.5: Mass sources and sinks

Due to a low moisture content of the considered fuel as well as fast rates of the evaporation process, the assumption is made that water encapsulated in coal is given off into the gaseous phase in accordance with the relationship [114]:

$$\mathsf{r_{vap}} = 4.01 \cdot \exp\left(-\frac{14.4}{\mathsf{RT_s}}\right)\rho_s \cdot \mathsf{g_w} \qquad \frac{\mathsf{kg_w}}{\mathsf{m_s^3 s}} \tag{6.41}$$

and

$$\mathsf{G_{vap}} = (1-\mathsf{e})\,\mathsf{r_{vap}} \qquad \frac{\mathsf{kg_w}}{\mathsf{m^3 s}} \tag{6.42}$$

where:

- g_w - mass fraction of moisture in fuel, $\frac{kg_w}{kg_s}$,
  T_s - surface temperature of solid fuel, K.

After drying and upon further heating, the volatiles included in coal are given off into the gaseous phase. The rate of the devolatilization process is described using the relationship [120]:

$$\mathsf{r_{dev}} = \mathsf{B_{vol}} \cdot \exp\left(-\frac{\mathsf{E_{a,dev}}}{\mathsf{RT_s}}\right) \rho_\mathsf{s} \cdot \mathsf{g_{vol}^n} \qquad \frac{\mathsf{kg_{vol}}}{\mathsf{m_s^3 s}} \tag{6.43}$$

and

$$\mathsf{G_{dev}} = (1 - \mathsf{e})\, \mathsf{r_{dev}} \qquad \frac{\mathsf{kg_{vol}}}{\mathsf{m^3 s}} \tag{6.44}$$

where:

$B_{vol} = 10^7$ - $\frac{1}{s}$,

$E_{a,vol} = 158$ - $\frac{kJ}{mol}$,

$n = 2$,

g_{vol} - mass fraction of volatile matter, $\frac{kg_{vol}}{kg_s}$.

After drying and devolatilization the solid fuel contains the char which is assumed to be pure carbon. The char that remains in the solid phase is oxidized to carbon oxides according to the following overall reactions:

$$\mathsf{C} + \frac{1}{\Theta}\mathsf{O_2} \rightarrow 2\left(1 - \frac{1}{\Theta}\right)\mathsf{CO} + \left(\frac{2}{\Theta} - 1\right)\mathsf{CO_2} \tag{6.45}$$

$$\mathsf{C} + \mathsf{CO_2} \rightarrow 2\mathsf{CO} \tag{6.46}$$

The first reaction defines the char combustion process. Char reacts with oxygen and may form either CO or CO_2. The CO/CO_2 ratio can be determined using the relationship [98]:

$$\mathsf{s} = \frac{\mathsf{CO}}{\mathsf{CO_2}} = 2500 \cdot \exp\left(-\frac{6240}{\mathsf{T_s}}\right) \tag{6.47}$$

Using the above formula one can calculate the stoichiometric coefficient appearing in Equation 6.45:

$$\Theta = \frac{1 + \frac{1}{\mathsf{s}}}{\frac{1}{2} + \frac{1}{\mathsf{s}}} \tag{6.48}$$

The rate of consumption of oxygen in the oxidation reaction (Equation 6.45) is calculated as:

$$\mathsf{G^a} = \mathsf{M_{O_2}} \cdot \mathsf{r_{comb}} \qquad \frac{\mathsf{kg_{O_2}}}{\mathsf{m^3 s}} \tag{6.49}$$

where

$$\mathsf{r_{comb}} = \mathsf{A_s} \cdot \mathsf{B_{comb}} \cdot \mathsf{C_{O_2}} \cdot \exp\left(-\frac{\mathsf{E_{a,comb}}}{\mathsf{RT_s}}\right) \cdot \mathsf{e} \qquad \frac{\mathsf{kmol_{O_2}}}{\mathsf{m^3 s}} \tag{6.50}$$

and $\mathsf{B_{comb}} = 4000\frac{\mathsf{m}}{\mathsf{s}}$, $\mathsf{E_{a,comb}} = 96.4\frac{\mathsf{kJ}}{\mathsf{mol}}$.

The second heterogeneous reaction is the reaction of char gasification (Equation 6.46). The rate of consumption of CO_2 in this reaction is:

$$\mathsf{G^b = M_{CO_2} \cdot r_{gasif}} \qquad \frac{\mathsf{kg_{CO_2}}}{\mathsf{m^3 s}} \tag{6.51}$$

where

$$\mathsf{r_{gasif} = A_s \cdot B_{gasif} \cdot C_{CO_2} \cdot \exp\left(-\frac{E_{a,gasif}}{RT_s}\right) \cdot e} \qquad \frac{\mathsf{kmol_{CO_2}}}{\mathsf{m^3 s}} \tag{6.52}$$

and $\mathsf{B_{gasif} = 6940 \frac{m}{s}}$, $\mathsf{E_{a,gasif} = 185.4 \frac{kJ}{mol}}$.

Therefore the net rate of carbon dioxide production which is generated in reaction 6.45 and consumed in reaction 6.46 is:

$$\mathsf{G_{CO_2} = \frac{M_{CO_2}}{M_{O_2}} \left(\frac{2}{\Theta} - 1\right) \cdot \frac{\Theta}{1} \cdot G^a - G^b} \qquad \frac{\mathsf{kg_{CO_2}}}{\mathsf{m^3 s}} \tag{6.53}$$

The formation rate of carbon monoxide as a result of incomplete combustion and gasification of char is:

$$\mathsf{G_{CO} = 2\frac{M_{CO}}{M_{O_2}} \left(1 - \frac{1}{\Theta}\right) \cdot \frac{\Theta}{1} \cdot G^a + 2\frac{M_{CO}}{M_{CO_2}} G^b} \qquad \frac{\mathsf{kg_{CO}}}{\mathsf{m^3 s}} \tag{6.54}$$

Finally, the source or rather sink term in the solid phase equation for char is:

$$\mathsf{G_{char} = \frac{M_c}{M_{O_2}} \frac{\Theta}{1} G^a + \frac{M_c}{M_{CO_2}} G^b} \qquad \frac{\mathsf{kg_c}}{\mathsf{m^3 s}} \tag{6.55}$$

It is stressed again that the kinetic parameters for reactions 6.45 and 6.46 originate from the publications of Tomeczek [22] and Wiljenskij et al. [123].

Energy sources and sinks

Energy sources and sinks discussed in this paragraph are shown in Figure 6.6.

The moisture evaporation process requires energy (latent heat) needed for transformation of liquid water into a gaseous state:

$$\mathsf{S_{vap} = G_{vap} \cdot [\Delta H_{vap} + c_{p,w,g} \cdot (T_s - T_o)]} \qquad \frac{\mathsf{W}}{\mathsf{m^3}} \tag{6.56}$$

where:

$c_{p,w,g}$	- specific heat of water vapour,	$\frac{J}{kgK}$,
$T_o = 298.15K$	- reference temperature,	K,
$\Delta H_{vap} = 2257$	- latent heat at 373 K,	$\frac{kJ}{kg}$.

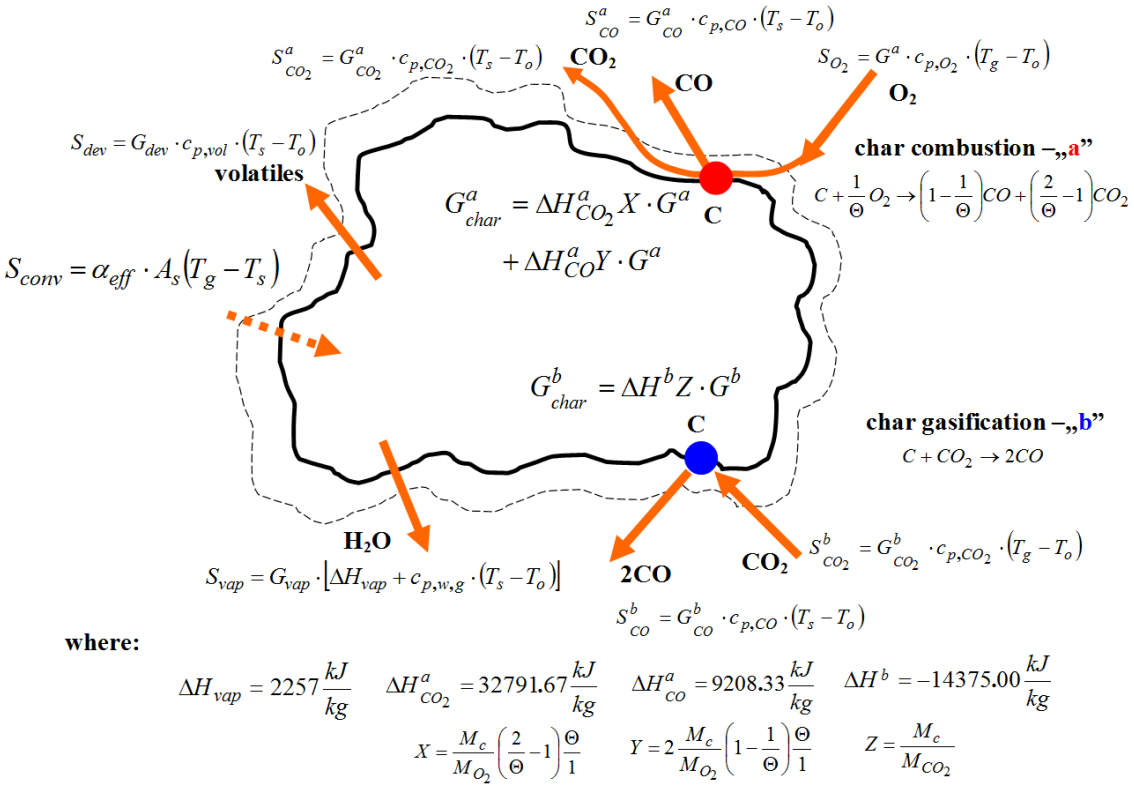

Figure 6.6: Energy sources and sinks (for mass sources see Figure 6.5)

In the mathematical model developed in this study, the rate of devolatilization is described using a single Arrhenius relationship (Equation 6.43), Here the assumption is made that the devolatilization effect is subject to similar kinetic mechanism as in case of methane release from coal. For description of the coal decomposition process it is additionally presupposed that the process is accompanied with no further thermal effects. With reference to [30, 31], all thermal effects of endothermic nature that may occur during the mentioned process can be explained by variation of the specific heat within the range from 400 to 600^oC. With consideration to the foregoing assumptions, the source term for devolatilization reads:

$$\mathsf{S_{dev}} = \mathsf{G_{dev}} \cdot \mathsf{c_{p,vol}} \cdot (\mathsf{T_s} - \mathsf{T_o}) \qquad \frac{\mathsf{W}}{\mathsf{m^3}} \tag{6.57}$$

where:

$c_{p,vol}$ - thermal capacity of volatiles, $\frac{J}{kgK}$.

The source/sink terms associated with heterogeneous reactions 6.45 and 6.46 are calculated as follows:

- for the solid phase energy balance equation:

$$\begin{aligned} S_{char} &= \Delta H^a_{CO_2}\left(\frac{2}{\Theta}-1\right)\frac{M_c}{M_{O_2}}\frac{\Theta}{1}G^a + \Delta H^a_{CO}2\left(1-\frac{1}{\Theta}\right)\frac{M_c}{M_{O_2}}\frac{\Theta}{1}G^a + \\ &+ \Delta H^b\frac{M_c}{M_{CO_2}}G^b \qquad \frac{W}{m^3} \end{aligned} \tag{6.58}$$

where:
$\Delta H^a_{CO_2} = 32791.67\frac{kJ}{kg}$, $\Delta H^a_{CO} = 9208.33\frac{kJ}{kg}$, $\Delta H^b = -14375.00\frac{kJ}{kg}$,

are heats of reactions (char combustion - Equation 6.45 and gasification - Equation 6.46).
The source term of the solid-phase energy balance, which is associated with physical enthalpy of reactants and products of reactions 6.45 and 6.46, is calculated as:

$$\begin{aligned} S_{fs} &= G^a \cdot c_{p,O_2} \cdot (T_g - T_o) - G^a_{CO_2} \cdot c_{p,CO_2} \cdot (T_s - T_o) \\ &+ G^b_{CO_2} \cdot c_{p,CO_2} \cdot (T_g - T_o) - G_{CO} \cdot c_{p,CO} \cdot (T_s - T_o) \qquad \frac{W}{m^3} \end{aligned} \tag{6.59}$$

- for gaseous phase energy balance equation:

$$\begin{aligned} S_{fg} &= -G^a \cdot c_{p,O_2} \cdot (T_g - T_o) + G^a_{CO_2} \cdot c_{p,CO_2} \cdot (T_s - T_o) \\ &- G^b_{CO_2} \cdot c_{p,CO_2} \cdot (T_g - T_o) + G_{CO} \cdot c_{p,CO} \cdot (T_s - T_o) \\ &+ G_{vap} \cdot c_{p,w,g} \cdot (T_s - T_o) + G_{dev} \cdot c_{p,vol} \cdot (T_s - T_o) \qquad \frac{W}{m^3} \end{aligned} \tag{6.60}$$

The temperature difference between the solid fuel and the gas that flows through the fuel bed results in heat exchange between the two phases. The term:

$$S_{conv} = \alpha_{eff} \cdot A_s\,(T_g - T_s) \qquad \frac{W}{m^3} \tag{6.61}$$

describes the convective heat transfer rate. To determine the amount of transported heat one has to know the value of the heat transfer coefficient α_{eff} and the contact surface area per unit of volume of solid (A_s).

The contact surface area

To calculate rates of heterogeneous reactions it is necessary to determine the contact surfaces area between the two phases (see Figure 6.7).

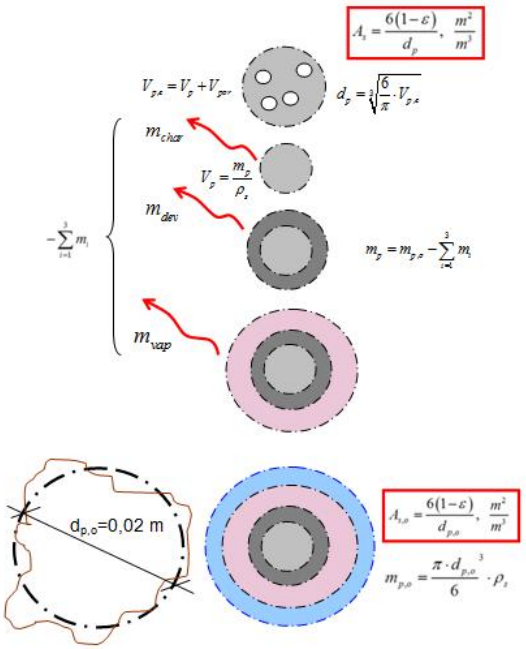

Figure 6.7: Determination of the contact surface area between solid fuel and the gaseous phase

The initial ratio of the contact surface area to the particle volume is calculated by means of the following formula [95]:

$$A_{s,o} = \frac{6\,(1-e)}{d_{p,o}} \qquad \frac{m^2}{m^3} \tag{6.62}$$

The newly developed model assumes that a particle with its initial diameter $d_{p,o}$ reduces its volume during the combustion process. The particle initial mass can be calculated as:

$$m_{p,o} = \frac{\pi \cdot {d_{p,o}}^3}{6} \cdot \rho_s \qquad kg \tag{6.63}$$

while its mass change during the combustion process is:

$$m_p = m_{p,o} - \sum_{i=1}^{3} m_i \qquad kg \tag{6.64}$$

where:
$\sum_{i=1}^{3} m_i = m_{vap} + m_{dev} + m_{char}$.

When the mass m_p is known, it is possible to calculate the volume of non-porous solid particle:

$$V_p = \frac{m_p}{\rho_s} \qquad m^3 \tag{6.65}$$

Actually, solid particles have a certain internal porosity that is subject to variations during

combustion, and the volume of a porous particle is:

$$\mathsf{V_{p,e}} = \mathsf{V_p} + \mathsf{V_{por}} \qquad \mathsf{m^3} \tag{6.66}$$

where:

$V_{p,e}$ - volume of a porous particle, m^3,
V_{por} - volume of pores inside the particle, m^3.

Knowing the volume of the porous particle its diameter is calculated as :

$$\mathsf{d_p} = \sqrt[3]{\frac{6}{\pi} \cdot V_{p,e}} \qquad \mathsf{m} \tag{6.67}$$

that can be subsequently used to calculate the actual area of the contact surface between the phases:

$$\mathsf{A_s} = \frac{6\,(1-\mathsf{e})}{\mathsf{d_p}} \qquad \frac{\mathsf{m^2}}{\mathsf{m^3}} \tag{6.68}$$

The just calculated contact area is the external surface area of a sphere with a diameter of d_p.

During the combustion process the structure of pores located inside coal particles is a subject to alterations. Such alterations may lead to variations (increase or decrease) of reactions surface area. For this study the assumption is made that the total area of internal pores S_{in}, where the chemical reactions between the solid and gaseous phases can take place, is calculated in accordance with the "random pore model„ [33, 58, 59, 60]. Variations of the pore surface are related to a parameter known as the degree of char conversion. The latter is defined as the ratio of the reacted char to its initial amount:

$$\mathsf{X_c} = \frac{\mathsf{G_{char,o}} - \mathsf{G_{char}}}{\mathsf{G_{char,o}}} \qquad \frac{\mathsf{kg}}{\mathsf{kg_o}} \tag{6.69}$$

where:

G_{char} - instantaneous mass of char, kg,
$G_{char,o}$ - initial mass of char, kg.

The total surface area of internal pores, where heterogeneous reactions take place, is calculated by means of the formula:

$$\mathsf{S_{in}} = \mathsf{S_{in,o}}(1-\mathsf{X_c})\sqrt{1-\psi\ln(1-\mathsf{X_c})} \qquad \mathsf{m^2} \tag{6.70}$$

where:

$S_{in,o}$ - initial surface area, m^2,
Ψ - structural parameter of pores,
X_c - degree of char conversion.

To calculate the instantaneous surface area it is necessary to know the initial contact surface area S_o between phases, the degree of char conversion X_c and the ψ parameter that defines the structure of pores. This parameter is determined for the primary (non-combusted) fuel samples and is defined in the following way [62, 130]:

$$\psi = (-\mathsf{ln}(1 - \mathsf{e_o}))^{-1} \tag{6.71}$$

where:

$e_o = 0.2$ - initial porosity of particle, $\frac{m_f^3}{m^3}$.

In turn, the initial surface area of internal pores $S_{in,o}$ is calculated using the following formula:

$$\mathsf{S_{in,o}} = \mathsf{A_w} \cdot \mathsf{m_p} \qquad \mathsf{m^2} \tag{6.72}$$

where:

m_p	- particle mass,	kg,
$A_w = 1.5$	- specific surface area of particle internal pores,	$\frac{m^2}{g}$,
$S_{in,o}$	- initial surface area of internal pores,	m^2.

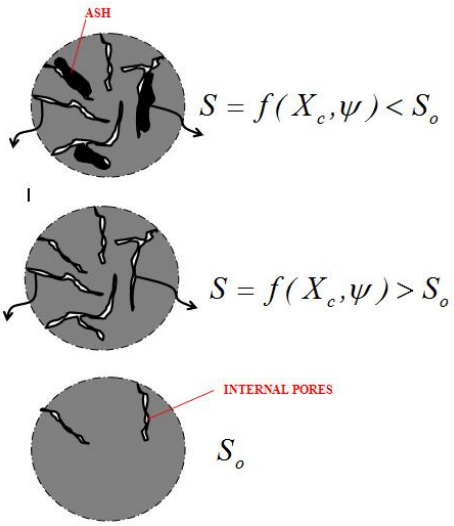

Figure 6.8: Determination of the surface area for internal pores

The value for specific surface area A_w and initial porosity of particle ε_o is calculated following reference [22]. The method for calculation of the surface area for internal pores is shown in Figure 6.8. The relationship that describes variations in the surface area as a function of the char conversion degree is not a monotonous function. Figure 6.9 shows that the maximum surface area of reaction occurs when 40% of char is subject to combustion. Further combustion leads to gradual reduction of the surface area. Figure

6.9 also demonstrates that the surface area S_{in} is strongly depended on ψ parameter that describes the structure of pores.

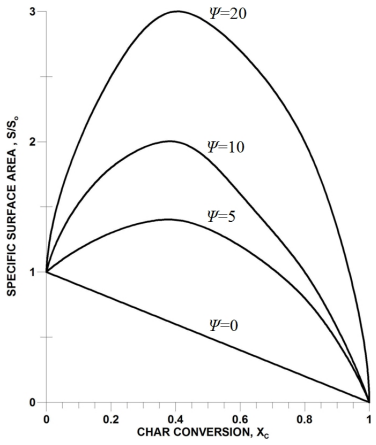

Figure 6.9: Specific surface area as a function of char conversion degree [33]

In order to find out the volume of internal pores V_{por} it is assumed that sizes of pores encapsulated inside the particle increase as a result of mass decrease. When one knows the total mass of matter $\sum_{i=1}^{3} m_i$ reacted at the moment of τ and assumes that the combustion rate is proportional to the contact area between the gaseous and solid phases, the volume of pores can be calculated by means of the following relationship:

$$\mathsf{V_{por}} = \frac{\frac{\mathsf{S_{in}}}{\mathsf{S_{in}}+\mathsf{S_{ex}}} \sum_{i=1}^{3} \mathsf{m_i}}{\rho_\mathsf{s}} + \mathsf{V_{por,o}} \qquad \mathsf{m^3} \tag{6.73}$$

where:

$V_{por,o}$	- initial volume of pores,	m^3,
V_{por}	- total volume of internal pores,	m^3,
S_{in}	- surface area of internal pores,	m^2,
S_{ex}	- external surface area of particle,	m^2.

The total contact area between the gaseous phase and the solid phase (Figure 6.10) is the sum of the surface area for internal pores S_{in} and the external particle surface area S_{ex}:

$$\mathsf{S} = \mathsf{S_{in}} + \mathsf{S_{ex}} \qquad \mathsf{m^2} \tag{6.74}$$

The external particle surface area is just the surface area of a sphere with the diameter d_p.

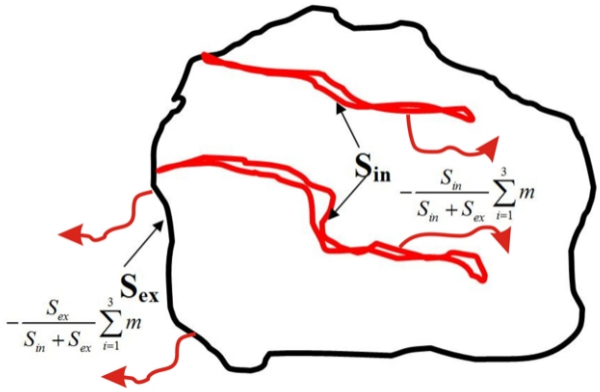

Figure 6.10: Total area of the contact surface between particles and gaseous phase

6.2.4 Diffusion of gaseous species

The diffusion of gaseous species into surface of solid particles where the heterogeneous reactions take place (Figure 6.11) is the matter of substantial importance in calculating the overall rates of oxidation and gasification reactions. To determine the impact of the diffusion, it is a common practice to introduce the effective rate constant of chemical reactions, that for the needs of this study is calculated in the following way:

$$\frac{1}{\mathsf{k}_{\mathsf{eff}}} = \frac{1}{\mathsf{k}} + \frac{1}{\beta} \tag{6.75}$$

where:

β - mass transfer coefficient, $\frac{m}{s}$.

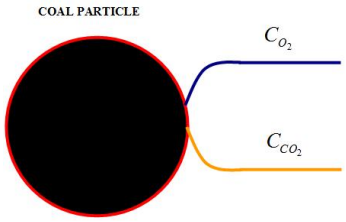

Figure 6.11: Concentration of gaseous substrates at surfaces of solid particles

The mass transfer coefficient β is calculated using the Sherwood number defined as:

$$\mathsf{Sh} = \frac{\beta \mathsf{d_z}}{\mathsf{D}} \tag{6.76}$$

where:

β - mass transfer coefficient, $\frac{m}{s}$,
d_z - linear characteristic dimension, m,
D - binary diffusion coefficient, $\frac{m^2}{s}$.

The Sherwood number is calculated using [22, 23, 131] the following correlation:

$$\mathsf{Sh} = 2 + 0.16\mathrm{Re}^{\frac{2}{3}} \tag{6.77}$$

The dependence of the diffusion coefficient on both temperature and pressure is accounted for using:

$$\mathsf{D} = \mathsf{D_o}\left(\frac{\mathsf{T}}{\mathsf{T_o}}\right)^{1.75}\frac{\mathsf{p_o}}{\mathsf{p}} \qquad \frac{\mathsf{m}^2}{\mathsf{s}} \tag{6.78}$$

where:

D_o	- mas diffusivity at reference parameters T_o, p_o,	$\frac{m^2}{s}$,
T	- temperature,	K,
p	- pressure,	Pa.

6.2.5 Structure of fuel bed

According to Atkinson & Merrick [27] the fixed - bed of solid fuel during the combustion process may achieve one of the three final structures: particulate, plastic or coke stage. In each of the three stages the heat transfer inside the bed, as well as the heat exchange with the surrounding gas, proceed differently. This is due to different pores (size, shape) characteristic for each of the three final stages.

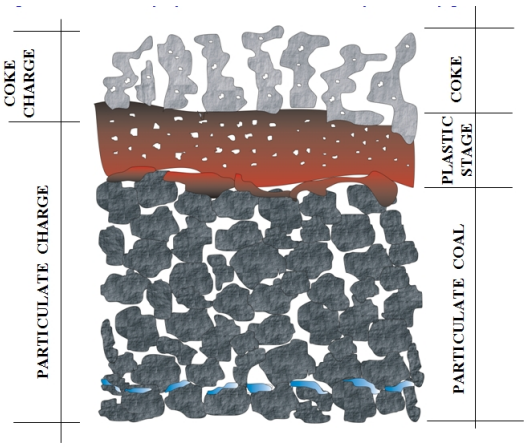

Figure 6.12: Porosity variation within the fixed-bed [54]

In this thesis the bed is split into two parts (particulate charge and coke charge) which are shown at Figure 6.12. In particulate charge only inter- particle porosity exists (external porosity) while in the coke charge two types of porosities occur namely the internal and external one.

In order to describe the heat transfer process in the fixed - bed one has to take account of substantial variations in thermal properties of the bed. The specific heat and the ther-

mal conductivity strongly depend on temperature of the material as well as on the fuel composition and structure that vary during the combustion process.

6.2.6 Thermal conductivity

The developed model calculates the effective coefficient of thermal conductivity in accordance with the work of Atkinson and Merrick [27]. It takes account of the most important mechanisms, see Figure 6.13, that are associated with heat transfer and take place inside a fixed - bed.

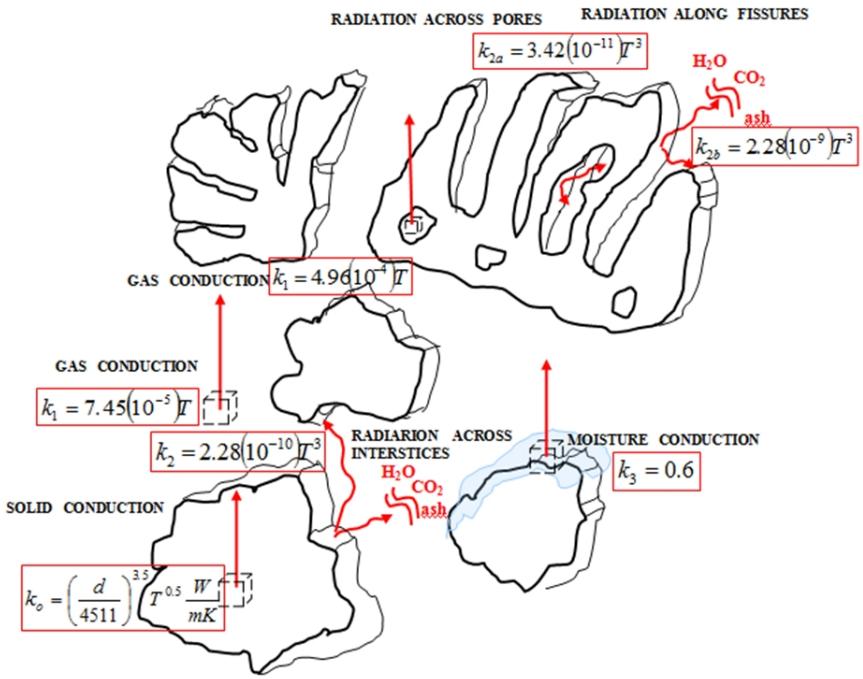

Figure 6.13: Thermal conductivity in the bed of solid fuel (k in $\frac{W}{mK}$)

The particulate charge has the structure of fixed-bed of solid particles with interpartical porosity. It is assumed that the overall heat conduction can be represented by three parallel processes namely: by heat conduction through moisture, heat conduction through solid particles and gas filling up the interparticle space, and the heat conduction through solid particles which is enhanced by contribution of radiation, as shown in 6.14. To find out the effective thermal conductivity k_{eff} it is mandatory to know the effective porosity e' [27]:

$$e' = 1 - (1 - e)^{\frac{1}{3}} \tag{6.79}$$

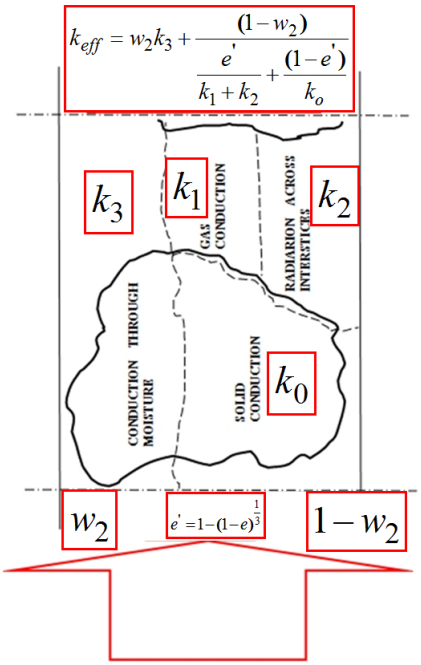

Figure 6.14: Effective thermal conductivity (particulate charge) [27]

Following Atkinson & Merrick [27] thermal conductivity of solid fuel is determined using the formula that brings together the temperature and the fuel density.

$$\mathsf{k_o} = \left(\frac{\rho_\mathsf{s}}{4511}\right)^{3.5} \mathsf{T_s^{0.5}} \qquad \frac{\mathsf{W}}{\mathsf{mK}} \tag{6.80}$$

where:

ρ_s - true density of coal, $\frac{kg}{m^3}$,
T - coal temperature, K.

For the particulate charge considered it is necessary to take into account the effect of moisture trapped in the fuel. Due to the fact that moisture evaporates rather quickly at the temperature of about 100^oC, the value of the thermal conductivity coefficient can be assumed constant and equal to:

$$\mathsf{k_3} = 0.6 \qquad \frac{\mathsf{W}}{\mathsf{mK}} \tag{6.81}$$

Any bed of solid fuel comprises also pores filled with air. Within the particulate charge these are the gaps between particles. The coefficient of thermal conductivity via pores is determined by means of the following relationship:

$$\mathsf{k_1} = 7.45\left(10^{-5}\right)\mathsf{T_g} \qquad \frac{\mathsf{W}}{\mathsf{mK}} \tag{6.82}$$

According to [27], the radiative thermal conductivity expressed as a function of particle surface temperature takes the following form:

$$k_2 = 2.28\left(10^{-10}\right) T_s^3 \qquad \frac{W}{mK} \tag{6.83}$$

Finally, to find out the effective coefficient of thermal conductivity in the particulate charge, the following formula is used:

$$k_{eff} = w_2 k_3 + \frac{(1-w_2)}{\frac{e'}{k_1+k_2} + \frac{(1-e')}{k_o}} \qquad \frac{W}{mK} \tag{6.84}$$

where:

w_2 - mass fraction of moisture in coal, $\frac{kg_w}{kg_{pal}}$,

e - porosity of coal, $\frac{m^3_{pores}}{m^3_{coal}}$.

The solid fuel reaches the form that is referred to as the coke charge after exceeding the specific temperature that is the threshold for re-solidification after passing the softening zone. In case of the coke charge (Figure 6.15) the method to determine the effective coefficient of thermal conductivity is slightly different as compared to the particulate charge. It is caused by presence of two porosity types (internal and external ones) as well as different shapes of pores, unlike the gaps between coal particles that exist within the particulate charge.

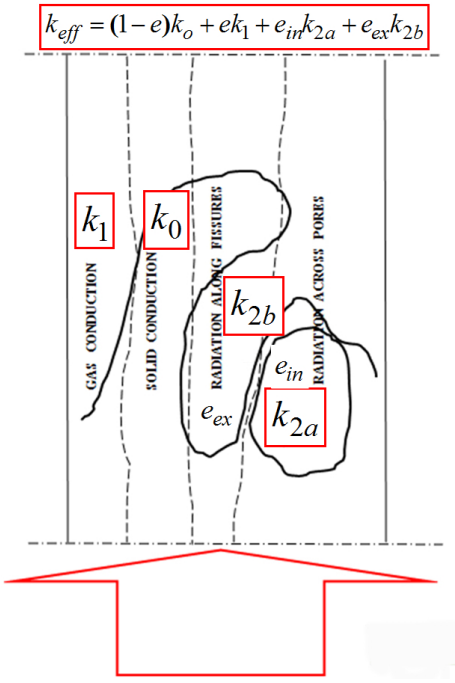

Figure 6.15: Effective thermal conductivity (coke charge) [27]

.

Within the coke charge, beside the already mentioned radiation mechanism, heat is transferred by means of conduction through a solid body, conduction through gas that fills internal pores as well as conduction along fissures. Thus, the overall heat conduction is represented by four parallel contributions as shown in Figure 6.15.

For gases filling the pores the coefficient of thermal conductivity depends on temperature in the following way [27]:

$$k_1 = 4.96\left(10^{-4}\right) T_g \qquad \frac{W}{mK} \tag{6.85}$$

The importance of the radiative transfer in cavities increases with the temperature ($\lambda \sim T_s^3$) as exemplified in Figure 6.16.

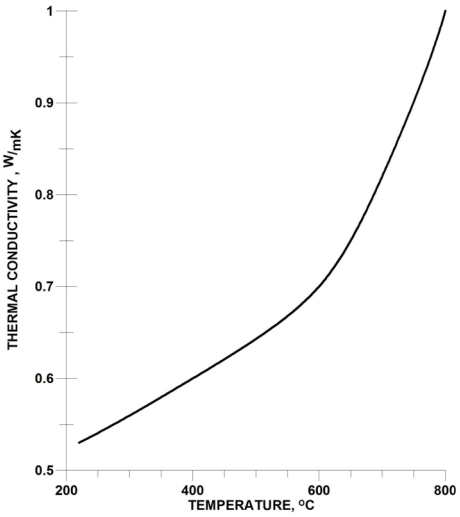

Figure 6.16: Effective thermal conductivity vs. temperature [55]

The above relationship is developed under the assumption that pores encapsulate substantial amounts of hydrogen that is emitted during the final stage of the carbonization process. The radiation in internal pores and along fissures has been defined by means of the following equations:
for internal pores (the characteristic dimension is assumed to be 0.15 mm):

$$k_{2a} = 3.42\left(10^{-11}\right) T_s^3 \qquad \frac{W}{mK} \tag{6.86}$$

for fissures (with the characteristic dimension from 5 to 20 mm):

$$k_{2b} = 2.28\left(10^{-9}\right) T_s^3 \qquad \frac{W}{mK} \tag{6.87}$$

Finally, the effective thermal conductivity for the coke charge is determined using the following formula:

$$k_{eff} = (1-e)k_o + ek_1 + e_{in}k_{2a} + e_{ex}k_{2b} \qquad \frac{W}{mK} \tag{6.88}$$

where:

e_{in}	- internal porosity within the coal bed,	$\frac{m_{in}^3}{m_c^3}$,
e_{ex}	- external porosity within the coal bed,	$\frac{m_{ex}^3}{,m_c^3}$,
e	- porosity of coal,	$\frac{m_p^3}{,m_c^3}$.

6.2.7 Specific heat of the fuel bed

The coal specific heat demonstrates significant variations with temperature and composition. The specific heat of solid fuel that is continuously heated to high temperatures is not a monotonic function of the bed temperature. This is so, since the bed is subject to various physical and chemical alterations associated with vaporisation of moisture, devolatilization and char oxidation (Figure 6.17). The highest value of the specific heat is attributed to moisture, then volatile matter and char. Giving off substances with high values of specific heat results in lowering of the specific heat of the solids remaining in the bed. The values of specific heat for a fixed - bed of coal as a function of temperature are shown in Figure 6.18. The diagram shows a clear maximum that results from the fact that components with high values of specific heat have already been released.

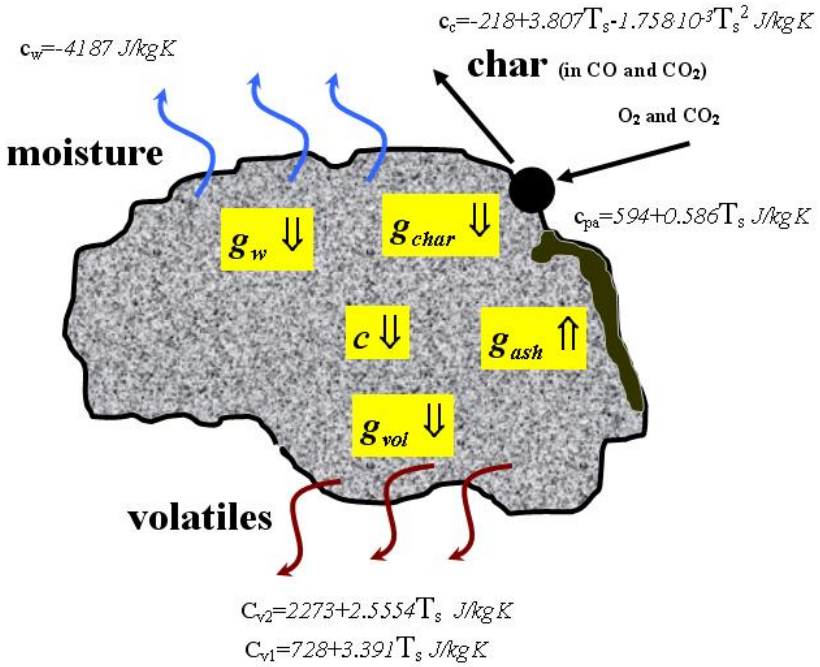

Figure 6.17: Specific heat for coal components (see Equation 6.89)

.

For calculating the equivalent specific heat for a fixed - bed the following formula is used:

$$\mathsf{c} = \mathsf{g_w c_w} + \mathsf{g_{pz} c_{pz}} \qquad \frac{\mathsf{J}}{\mathsf{kgK}} \tag{6.89}$$

where:

g_w	- mass fraction of moisture,	$\frac{kg_i}{kg_{coal}}$,
g_{pz}	- mass fraction of dry coal,	$\frac{kg_i}{kg_{coal}}$,
c_w	- specific heat of moisture,	$\frac{J_i}{kg_{coal}K}$,
c_{pz}	- specific heat of dry coal,	$\frac{J_i}{kg_{coal}K}$,
c	- equivalent specific heat,	$\frac{J}{kgK}$.

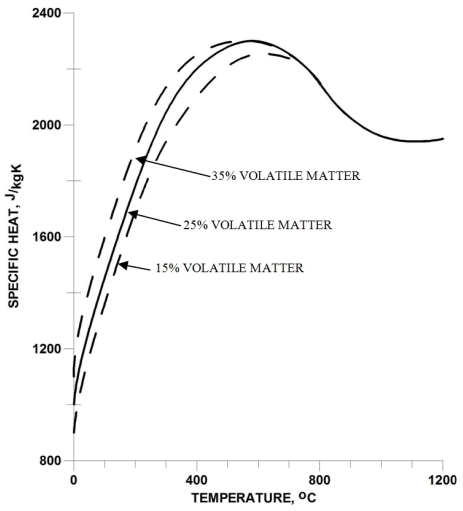

Figure 6.18: Predicted variations of specific heat within the fixed - bed versus temperature. The heating rate 3 $\frac{K}{min.}$ [30]

The formulas for specific heats for char, ash, volatile matter and moisture have been sourced from [30] and [23]. The newly developed model assumes that the specific heat of moisture takes a constant value of $c_w = 4187 \frac{J}{kgK}$. The specific heat of dry coal is calculated by means of the Kirov formula [109]:

$$\mathsf{c_{pz}} = (1 - \mathsf{a^d})\mathsf{c_{pp}} + \mathsf{a^d c_{pa}}, \qquad \frac{\mathsf{J}}{\mathsf{kgK}} \tag{6.90}$$

where:

a_d	- mass fraction of ash in dry coal,	$\frac{kg_a}{kg^d_{coal}}$,
c_{pa}	- specific heat of ash,	$\frac{J}{kg_{ash}K}$,
c_{pp}	- specific heat of combustible part of coal,	$\frac{J}{kg^{comb}_{coal}K}$.

The specific heat for ash (c_{pa}) is calculated from the equation:

$$\mathsf{c_{pa} = 594 + 0.586 T_s} \qquad \frac{\mathsf{J}}{\mathsf{kgK}} \tag{6.91}$$

The specific heat for the combustible part of coal (c_{pp}) depends on the content of volatiles in dry, ash-free coal V_{daf}. The formulas that are used adopt the following forms:

for $V_{daf} > 0.1$:

$$\mathsf{c_{pp} = (1 - V^{daf})c_c + (V^{daf} - 0.1)c_{v1} + 0.1 c_{v2}} \qquad \frac{\mathsf{J}}{\mathsf{kgK}} \tag{6.92}$$

for $V_{daf} < 0.1$:

$$\mathsf{c_{pp} = (1 - V^{daf})c_c + V^{daf} c_{v2}} \qquad \frac{\mathsf{J}}{\mathsf{kgK}} \tag{6.93}$$

where:

V_{daf} - mass fraction of volatiles in the dry and ash - free coal, $\frac{kg_{volatiles}}{kg_{daf}}$.

The above equations are accompanied by:

$$\mathsf{c_c = -218 + 3.807 T_s - 1.758 \cdot 10^{-3} T_s^2} \qquad \frac{\mathsf{J}}{\mathsf{kgK}} \tag{6.94}$$

$$\mathsf{c_{v1} = 728 + 3.391 T_s} \qquad \frac{\mathsf{J}}{\mathsf{kgK}} \tag{6.95}$$

$$\mathsf{c_{v2} = 2273 + 2.554 T_s} \qquad \frac{\mathsf{J}}{\mathsf{kgK}} \tag{6.96}$$

where:

c_c - specific heat of char, $\frac{J}{kg_{char}K}$,

c_{v1} - specific heat of low temperature volatile matter, $\frac{J}{kg_{vol_1}K}$,

c_{v2} - specific heat of high temperature volatile matter, $\frac{J}{kg_{vol_2}K}$.

6.2.8 Heat transfer coefficient

Temperature difference between gaseous phase and solid fuel results in a flow of heat between gas that fills pores in the fixed - bed and solid particles. The heat transfer rate is taken into account in the energy balances of both solid and gaseous phases (see Equations 6.31 and 6.34) by means of the source term:

$$\mathsf{S_{conv} = \frac{dS}{dV} \cdot \alpha_{eff} \cdot \Delta T_{g-s}} \qquad \frac{\mathsf{W}}{\mathsf{m^3}} \tag{6.97}$$

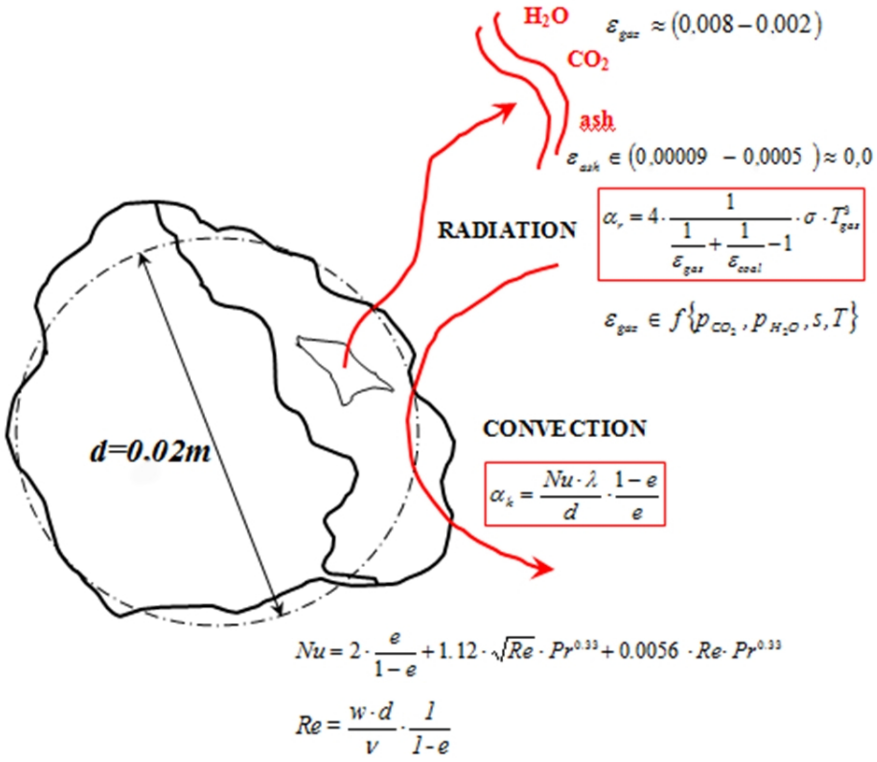

Figure 6.19: Effective heat transfer coefficient

where:

dS	- contact surface between phases within a volume dV,	m^2,
α_{eff}	- effective heat transfer coefficient,	$\frac{W}{m^2K}$,
ΔT_{g-s}	- temperature difference between the phases,	K.

The effective heat transfer coefficient α_{eff} is made up of the convective part α_k and the radiative part α_r (Figure 6.19) and can be calculated using the formula:

$$\alpha_{\mathsf{eff}} = \alpha_{\mathsf{k}} + \alpha_{\mathsf{r}} \qquad \frac{\mathsf{W}}{\mathsf{m^2K}} \tag{6.98}$$

The convective heat transfer coefficient is calculated using the Nusselt number:

$$\alpha_{\mathsf{k}} = \frac{\mathsf{Nu} \cdot \mathsf{k_g}}{\mathsf{d_s}} \cdot \frac{1-\mathsf{e}}{\mathsf{e}} \qquad \frac{\mathsf{W}}{\mathsf{m^2K}} \tag{6.99}$$

where:

k_g	- thermal conductivity of gas,	$\frac{W}{mK}$.

while the Nusselt number is calculated using the following Nusselt function [40]:

$$\mathrm{Nu} = 2 \cdot \frac{\mathrm{e}}{1-\mathrm{e}} + 1.12 \cdot \sqrt{\mathrm{Re}} \cdot \mathrm{Pr}^{0.33} + 0.0056 \cdot \mathrm{Re} \cdot \mathrm{Pr}^{0.33} \tag{6.100}$$

The Reynolds number for a porous bed is calculated as follows:

$$\mathrm{Re} = \frac{\mathrm{w} \cdot \mathrm{d_s}}{\nu} \cdot \frac{1}{1-\mathrm{e}} \tag{6.101}$$

where:

ν	- kinematic viscosity,	m^2/s,
d_s	- particle diameter,	m,
w	- gas velocity,	m/s,
e	- porosity of coal bed,	$\frac{m^3_{pores}}{m^3_{bed}}$.

while the Prandtl number is evaluated as:

$$\mathrm{Pr} = \frac{\mathrm{c_{p,g}} \cdot \mu}{\mathrm{k}} \tag{6.102}$$

where:

μ	- dynamic viscosity,	$Pa \cdot s$,
k	- thermal conductivity,	$\frac{W}{mK}$,
$c_{p,g}$	- specific heat of gas in the fixed - bed,	$\frac{J}{kgK}$.

The heat transfer coefficient increases with the temperature of the gaseous phase. The heat exchange is intensified when dimensions of fuel particles are reduced. In the model presented in this thesis, the coal particles are represented as spheres of an initial diameter of d_s=0.02m. The determined effective heat transfer coefficient (Figure 6.19) takes account for the effect of such compounds as CO_2, H_2O, that inhibit heat conveyed by radiation from a solid body surface. The influence of fly ash (dust) is neglected due to its low concentration. The radiative heat transfer coefficient is calculated by means of the relationship [40]:

$$\alpha_\mathrm{r} = 4 \cdot \frac{1}{\frac{1}{\varepsilon_\mathrm{g}} + \frac{1}{\varepsilon_\mathrm{s}} - 1} \cdot \sigma \cdot \mathrm{T_g^3} \qquad \frac{\mathrm{W}}{\mathrm{m^2K}} \tag{6.103}$$

where:

ε_g	- emissivity of gas,
ε_s	- emissivity of solid particles,
T_g	- gas temperature, K.

To calculate the gas phase emissivity the following formula is applied [32] :

$$\varepsilon_{\mathsf{g}} = \mathsf{A} \cdot \mathsf{e}^{-\mathsf{BT}} \tag{6.104}$$

The coefficients A, B for CO_2 and H_2O are determined using Hottel's diagrams for a specified partial pressure of CO_2 and H_2O and for an average path length of ray within the gaseous space:

$$\mathsf{A}, \mathsf{B} = \mathsf{f}\left(\mathsf{p} \cdot \mathsf{s}\right) \tag{6.105}$$

where:

A, B	- dimensionless coefficients, typical for any specific gas,	
T	- gas temperature,	K,
p	- partial pressure of gas,	Pa.

7 Validation of the fixed-bed model

The newly developed model has to be validated against experimental data. The primary objective of the validation is to determine degree of consistency between the model predictions and the real processes. The algorithm of the fixed - bed model created in this work simplifies composition of fuel into four species: char, volatile matter, moisture and ash. As pointed out before, the initial diameter of coal particle is 0.02 m.

7.1 Composition and calorific value of the EKORET fuel

The composition of the EKORET fuel and its calorific value have been measured, see Table 7.1. Using proximate and ultimate analysis of EKORET coal it is possible to calculate the composition of the volatile matter. The assumption is made that:

- char is represented by pure carbon,
- molecular weight of volatiles is equal to M_{coal}=30 $\frac{kg}{kmol}$,
- volatiles molecule has a form: $C_xH_yO_zN_t$.

EKORET fuel (as delivered)				
PROXIMATE ANALYSIS				
		a	d	daf
Total moisture(ar). %	7	6.1	-	-
Air dried moisture(ad). %	6	6.1	-	-
Ash. %	5.3	5.3	5.7	-
Combustisble substance. %	87.8	88.6	94.3	-
Volatile matter. %	31.5	31.9	31.9	35.9
HCV. kJ/kg	29 359	29 655	31 565	33 456
LCV. kJ/kg	28 235	28 545	30 540	32 370
ULTIMATE ANALYSIS				
carbon. %	73.64	74.38	79.17	83.91
hydrogen. %	4.37	4.41	4.69	4.98
oxygen. %	7.94	8.02	8.54	9.05
nitrogen. %	1.39	1.4	1.49	1.58
sulphur. %	0.43	0.43	0.46	0.49
chlorine. %	0.22	0.22	0.24	-
fluorine. %	0.002	0.003	0.003	0.003

Table 7.1: Proximate and ultimate analysis of raw coal - EKORET and substitute coal

The proximate analysis on dry-ash-free basis (daf) is:

$$g_{char}^{daf} = \frac{g_{char}}{1 - g_{ash} - g_{moist}} \tag{7.1}$$

$$g_{vol}^{daf} = \frac{g_{vol}}{1 - g_{ash} - g_{moist}} \tag{7.2}$$

Using the char and volatiles mass fractions and ultimate analysis of coal (in mass % daf) it is possible to formulate the following mass balances of species:

$$CARBON : c^{daf} = g_{char}^{daf} \cdot c_{char}^{daf} + g_{vol}^{daf} \cdot c_{vol}^{daf} \tag{7.3}$$

$$HYDROGEN : h^{daf} = g_{vol}^{daf} \cdot h_{vol}^{daf} \tag{7.4}$$

$$OXYGEN : o^{daf} = g_{vol}^{daf} \cdot o_{vol}^{daf} \tag{7.5}$$

$$NITROGEN : n^{daf} = g_{vol}^{daf} \cdot n_{vol}^{daf} \tag{7.6}$$

where:

$c_{char}^{daf}, h^{daf}, o^{daf}, n^{daf}$	- carbon, hydrogen, oxygen, nitrogen content in daf coal,	$\frac{kg_i}{kg^{daf}}$,
c_{char}^{daf}=1	- carbon content in daf char,	$\frac{kg_c}{kg_{char}^{daf}}$,
$c_{vol}^{daf}, h_{vol}^{daf}, o_{vol}^{daf}, n_{vol}^{daf}$	- carbon, hydrogen, oxygen, nitrogen content in daf volatiles,	$\frac{kg_i}{kg_{vol}^{daf}}$.

In the above equations there are four unknows which have to be calculated ($c_{vol}^{daf}, h_{vol}^{daf}, o_{vol}^{daf}$, n_{vol}^{daf}). In order to calculate stoichiometric coefficients x, y, z, t of volatiles molecule ($C_xH_yO_zN_t$) the following equations are used:

$$x = \frac{c_{vol}^{daf} \cdot M_{coal}}{12} \tag{7.7}$$

$$y = \frac{h_{vol}^{daf} \cdot M_{coal}}{1} \tag{7.8}$$

$$z = \frac{o_{vol}^{daf} \cdot M_{coal}}{16} \tag{7.9}$$

$$t = \frac{n_{vol}^{daf} \cdot M_{coal}}{14} \tag{7.10}$$

Finally, the volatile matter molecule is represented by:

$$[volatiles] - C_{1.05}H_{4.22}O_{0.74}N_{0.0761} \tag{7.11}$$

When the calorific value of coal and the ultimate analysis are known it is possible to estimate the amount of heat that is released during combustion of volatile matter $Q_{r,vol}$.

On the basis of the following reactions:

$$[\mathrm{volatiles}] + 1.74 \cdot O_2 \rightarrow 1.05 \cdot CO_2 + 2.11 \cdot H_2O + 0.038 \cdot N_2 - Q_{r,vol.} \tag{7.12}$$

$$C + O_2 \rightarrow CO_2 - 393.8\mathrm{kJ/mol} \tag{7.13}$$

one can develop a relationship that enables determination of $Q_{r,vol}$ since:

$$LCV = \frac{g_{vol.} \cdot MQ_{r,vol.}}{M_{vol.}} + \frac{g_{char.} \cdot MQ_{r,char.}}{M_{char.}} - g_{moist.} \cdot Q_{vapour.} \qquad \frac{J}{kg} \tag{7.14}$$

where:

$g_{vol.}$	- mass fraction of volatile matter in coal,	$\frac{kg_{vol.}}{kg_{coal}}$,
$MQ_{r,vol.}$	- amount of heat generated during combustion reactions of volatiles,	$\frac{kJ}{kmol}$,
$M_{vol.}$= 30	- molecular weight of volatile matter (assumed),	$\frac{kg}{kmol}$,
g_{char}·	- mass fraction of char in coal,	$\frac{kg_{char.}}{kg_{coal}}$,
$MQ_{r,char.}$= 393.8	- amount of heat generated during combustion reactions of char,	$\frac{kJ}{mol}$,
$M_{char.}$= 12	- molecular weight of char,	$\frac{kg}{kmol}$,
$g_{mist.}$	- mass fraction of moisture in coal,	$\frac{kg}{kmol}$,
$Q_{vapour.}$= 2.440	- evaporation heat of moisture (latent heat),	$\frac{kJ}{kg}$,
LCV	- lower calorific value of fuel,	$\frac{kJ}{kg}$.

The heat of combustion of volatiles for the EKORET coal has been calculated to be $Q_{r,vol}$=980 $\frac{kJ}{mol}$.

7.2 Measurements for validation of the fixed-bed model

A reactor, shown in Figures 7.1 and 7.2, has been used to carry out measurements [56] which are used in this thesis for validation of the fixed-bed model. The reactor of 0.28m height and 0.06m diameter is filled up with the particles of EKORET fuel. The fuel bed rests on a grate located at the bottom of the reactor. The fuel is ignited at the reactor top, nearby the exhaust port of the flue gas.

The combustion front of the fuel travels from the place of ignition (at the reactor top) downwards to the reactor grate. Four thermocouples equally spaced along the reactor length, see Figure 7.1, are to determine the rate in which the combustion zone moves downwards. The distance between adjacent thermocouples is 0.05 m. The flue gas has

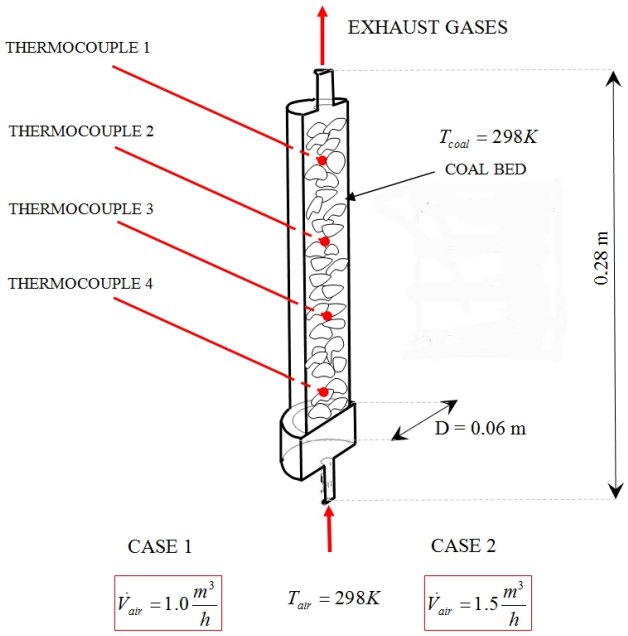

Figure 7.1: Geometry of the reactor

been sampled and analyzed for three gaseous components: CO, O_2 and CO_2. The gas composition as well as the bed temperatures have been logged into a recorder that stored data within 30 seconds intervals.

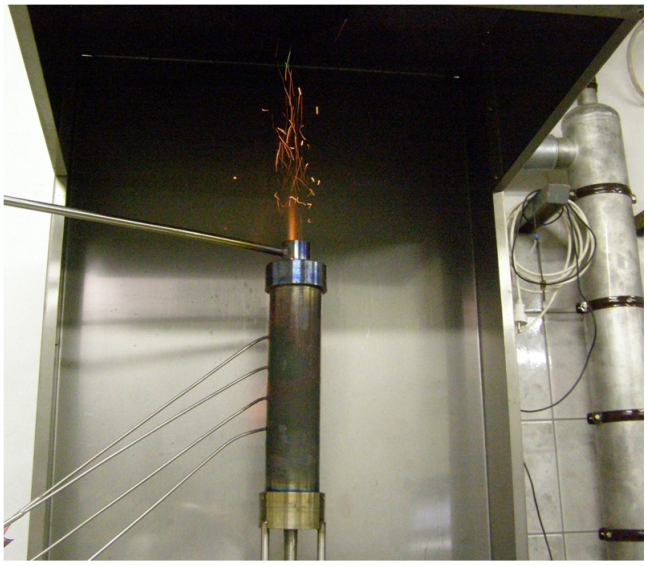

Figure 7.2: Photo of the reactor

The air necessary to sustain the combustion process is supplied at the reactor bottom. The stream of the supplied oxidizer is controlled using valves and measured by means of a rotameter. Two measured cases, shown in Table 7.2, are considered in this thesis. They correspond to air flow rates of: $1.0\frac{m^3}{h}$ and $1.5\frac{m^3}{h}$ which correspond to the values of super-

ficial air velocity of $0.17\frac{m}{s}$ and $0.26\frac{m}{s}$, respectively. The initial temperature of air and fuel is $298K$. Detailed description of both the measurement equipment and the measured data can be found in PhD thesis of R. Nosek [56].

	Numerical calculations	
	CASE 1	CASE 2
SOLID PHASE		
Fuel	EKORET	EKORET
Density. kg/m^3	1300	1300
Specific heat	**f**(Temperature)^2	**f**(Temperature)^2
Thermal conductivity	**f**(Temperature)^2	**f**(Temperature)^2
Heat transfer coefficient (between phases). W/m^{2}K	**f**(Temperature)^2	**f**(Temperature)^2
Initial porosity of fixed-bed	ε =0.35	ε =0.35
Fuel initial temperature	298	298
GAS PHASE		
Air flow rate. m^3/h	1.0	1.5
Inlet air velocity. m/s	3.54	5.31
Inlet air temperature. K	298	298
Initial gas temperature. K	298	298
External air temperature. K	298	298
Heat transfer coefficient (wall-external air). W/m^{2}K	α=7.9+0.053(T-273)^1	α=7.9+0.053(T-273)^1
Emmisivity of internal wall (rusty steel)	ε_r= 0.8	ε_r= 0.8
Emmisivity of external wall	ε_r= 0.8	ε_r= 0.8

Table 7.2: Initial and boundary conditions for numerical calculations. [1] - [22], [2] -see Paragraph 6.2.5

7.3 Numerical simulations of the fixed-bed reactor

The fixed - bed model developed and described in Chapter 6, has been implemented into the Fluent CFD package. The $\frac{1}{8}$ sector (45^o) of the reactor (Figure 7.3) has been modeled using the 3 - dimensional model. Time dependent calculations have been performed for the two cases (Table 7.2) that differed in the flow rates of supplied air.

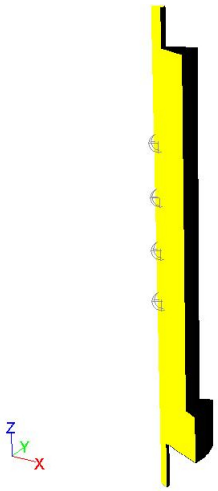

Figure 7.3: Geometry of the numerical model

The initial temperature of coal and air is equal to 298 K. The free convection heat transfer coefficient between reactor walls and ambient air is calculated by means of the relationship taken from [132] (see Table 7.2). The emissivity of the reactor walls is assumed to be 0.8. It is also assumed that the initial coal density is equal to $1300\frac{kg}{m^3}$. The initial value of the coal specific heat is $0.9\frac{kJ}{kgK}$ which during the process varies and reaches value up to $2.3\frac{kJ}{kgK}$. Similarly, the coefficient of thermal conductivity within the coal bed takes values from 0.1 to $3.0\frac{W}{mK}$. The specific heat and thermal conductivity are calculated using relationships described in Section 6.2.7 (specific heat) and Section 6.2.6 (thermal conductivity).

Figures 7.5, 7.4 and 7.6 show example results obtained from the numerical simulations of Case 1 at time of 1800 sec. The diagrams show variations of many parameters, including the properties of coal along central lines of the coal bed. The analysis of the profiles shows that the combustion front is roughly at the bed height of 0.1 m. It means that after τ =1800 sec the combustion zone traveled by a half of the total coal bed height of 0.2m and the temperature at that position is about $1400K$.

The values of thermal conductivity and heat transfer coefficient rapidly increase within the combustion zone, mostly due to increasing role of radiation in the process of heat transfer both inside the bed and between fuel phases. As far as the specific heat of the bed is concerned, its highest value occurs just in front of the zone where the highest values of temperature are reached. The volatiles, with high values of their specific heat, are given off, which is associated with a decrease of the bed specific heat.

The next results, which are closely associated with the newly developed model, refer to values of coal particle diameters and porosity. The diagrams clearly show that particle diameter diminishes rapidly within the combustion zone with simultaneous growth of the porosity. This is due to both devolatilization and heterogeneous reactions. Consequently, the bed loses a part of its weight. The diagrams show also thermal effects that take place inside the bed of burning fuel. It is clearly visible that a part of energy (in the model

considered as a source component) just nearby the reactor grate (at the bottom of the reactor) is consumed for evaporation of moisture. The main source of energy for the solid phase is the reaction of char combustion. The energy released during the combustion reaction provides heat for endothermic reaction that cool down the solid fuel pilled in the bed. The diagrams show also the values of mass source terms for individual gaseous substances, where these source terms simulate heterogeneous reactions and the devolatilization process. One can notice that the highest values for the mentioned source components occur nearby or inside zones of high temperatures.

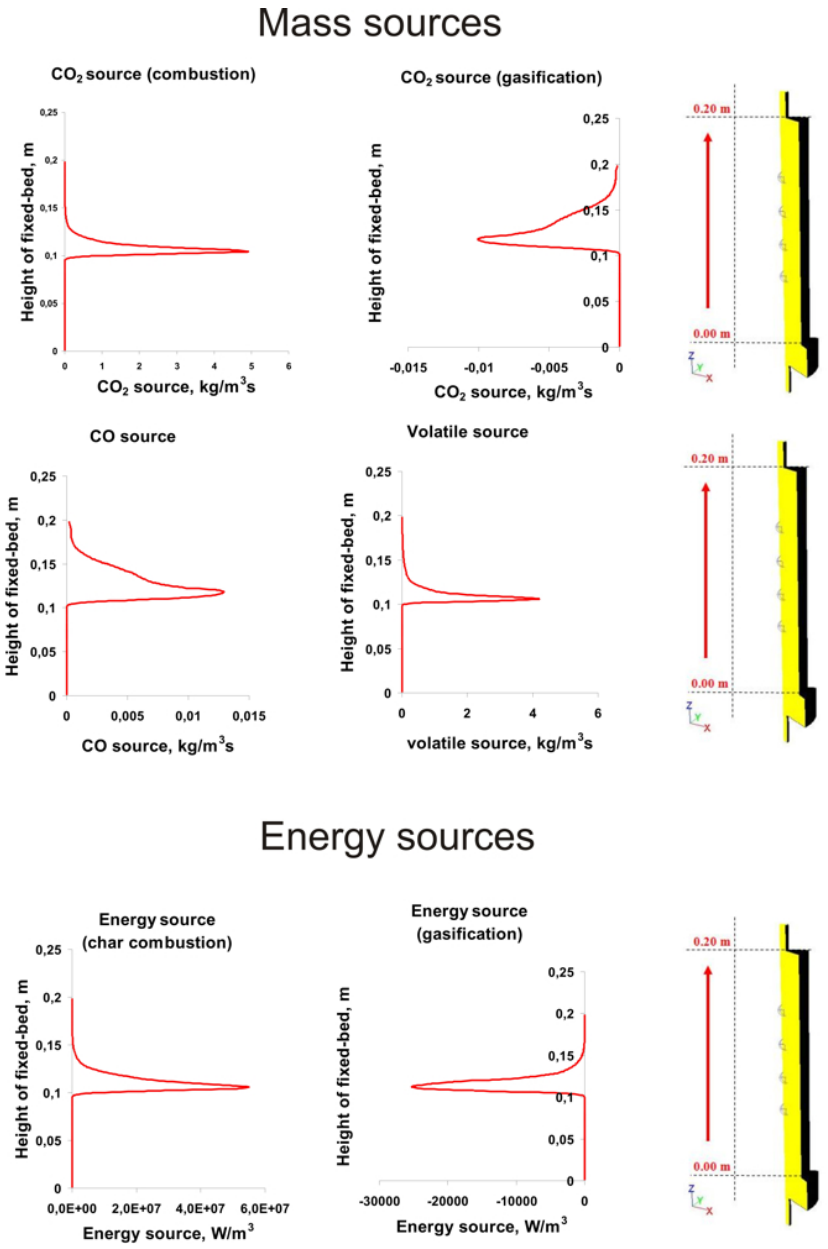

Figure 7.4: Model predictions along the center-line of the fixed-bed - A (τ =1800 sec.) (Case 1 see Table 7.2)

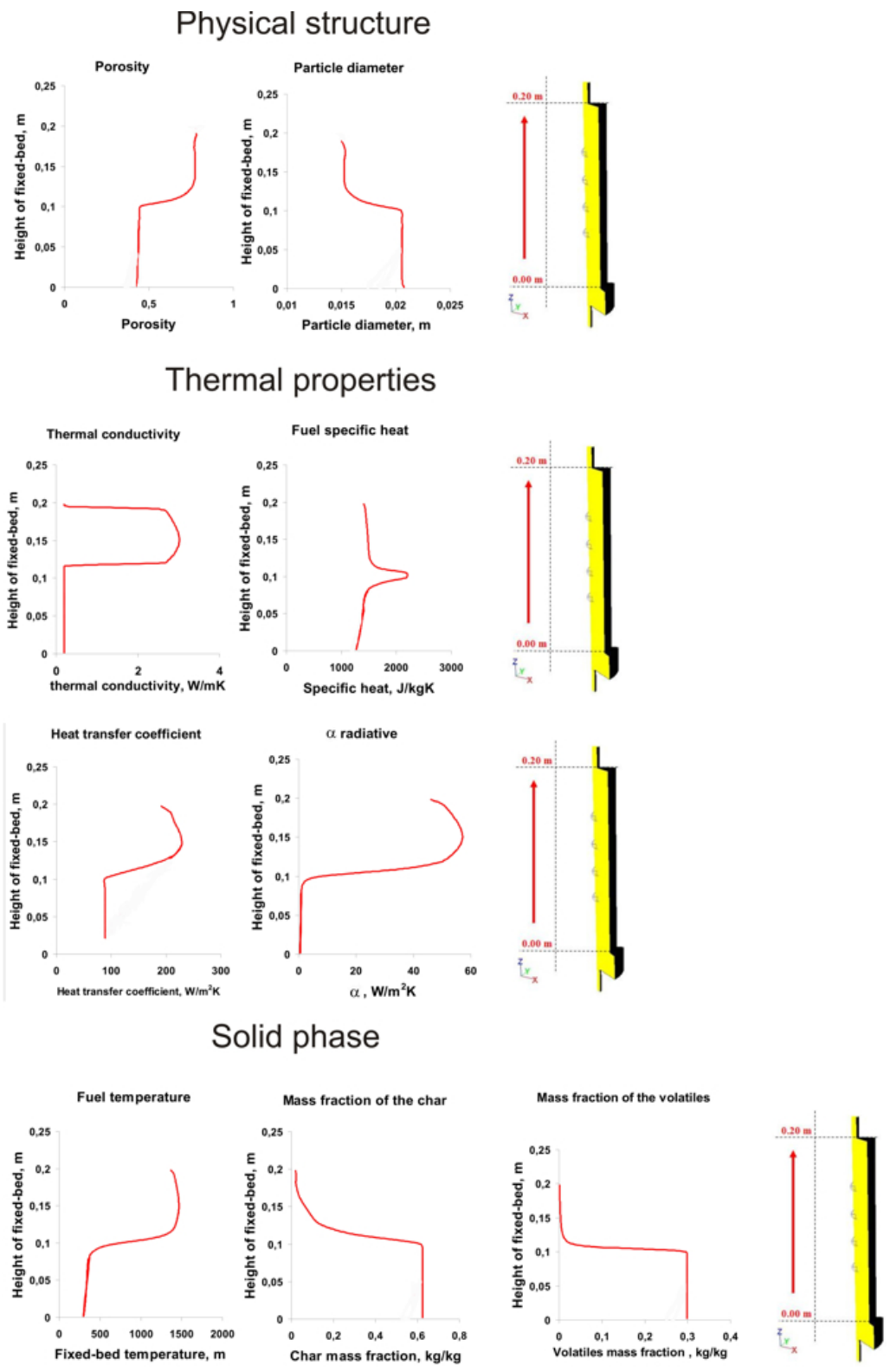

Figure 7.5: Model predictions along the center-line of the fixed-bed - B (τ =1800 sec.) (Case 1 see Table 7.2)

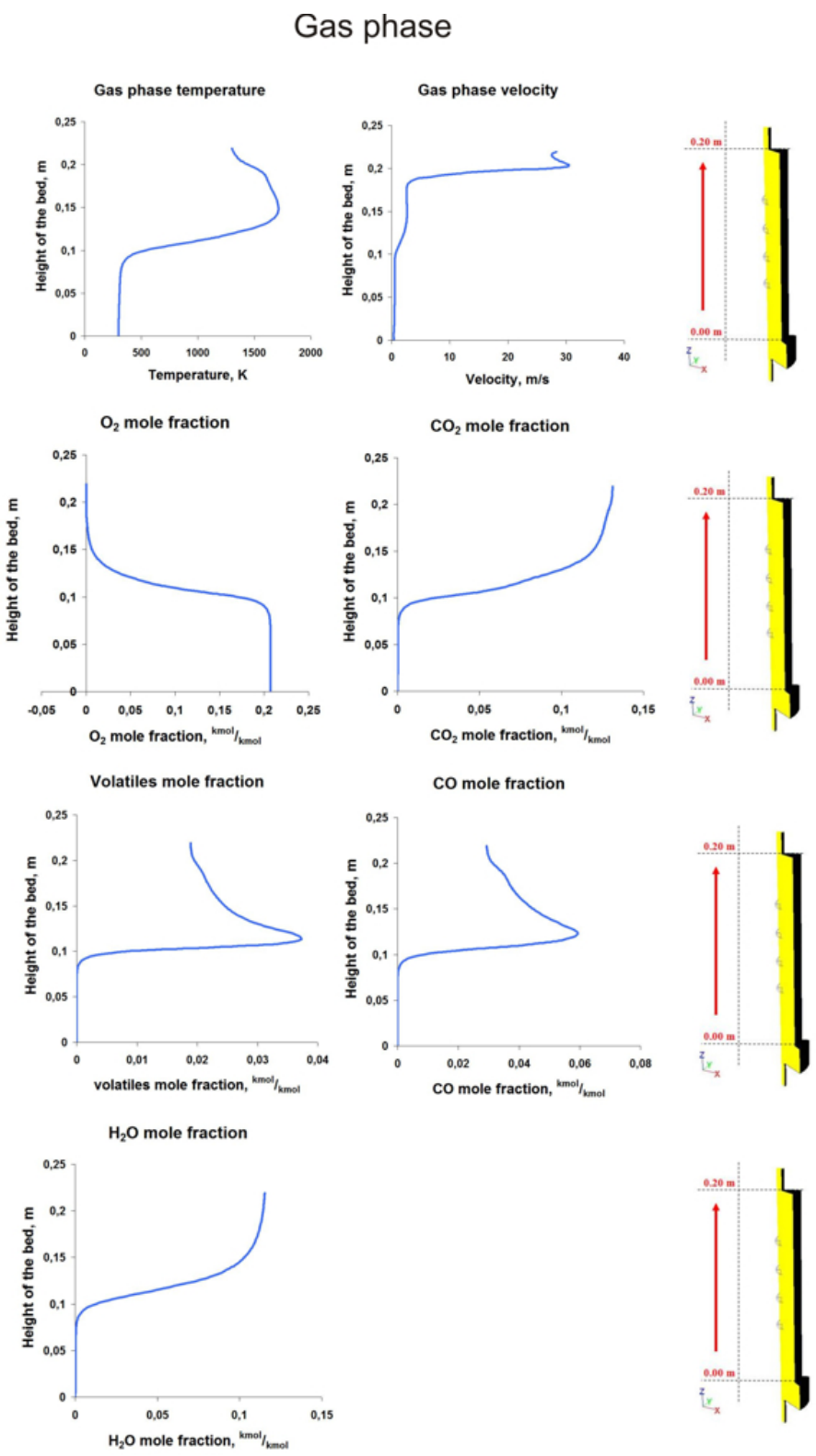

Figure 7.6: Model predictions along the center-line of the fixed-bed - C (τ =1800 sec.) (Case 1 see Table 7.2)

7.4 Comparison of the model predictions against the measured data

The comparison of the model predictions and the experimental data concerns the temperature values inside the fuel bed and the flue gas composition (CO, CO_2, O_2) measured at the reactor outlet.

As mentioned before, two cases corresponding to the air flow rates of $\dot{V}_{air} = 1.0\frac{m^3}{h}$ and $\dot{V}_{air} = 1.5\frac{m^3}{h}$ (see Table 7.2) are considered.

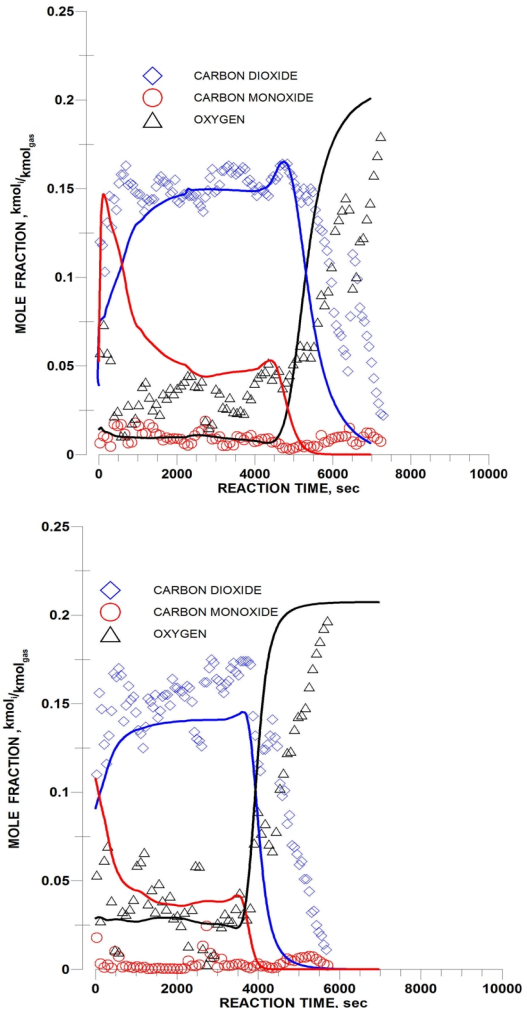

Figure 7.7: Flue gas composition ($V_a = 1.0\frac{m^3}{h}$ and $V_a = 1.5\frac{m^3}{h}, T_a = 298K, p_a = 0.1MPa$) (lines - predicted data, symbols - measured data)

Figure 7.7 shows the measured and model predicted composition of the reactor exhaust gases for Case 1 and Case 2 while Figure 7.8 shows the variations of the bed temperature with time. The above mentioned figures show that the model represents fairly the measured data. Figure 7.7 clearly shows that for the $\dot{V}_{air} = 1.0\frac{m^3}{h}$ air flow rate the combustion process ends after about 6000 seconds. This is the moment when the oxygen molar fraction in exhaust gases reaches 21% and concentrations of other monitored gases (CO_2, CO) rapidly

drops to zero. When the air flow rate increases to $\dot{V}_{air} = 1.5\frac{m^3}{h}$ the fuel consumption rate also increases and the retorting is complete after 5000 seconds.

At the initial phase, the measured CO concentration in the flue gas substantially deviates from calculation results which is related to the initial temperature which has to be specified to initiate the time dependent calculations of the fixed-bed model.

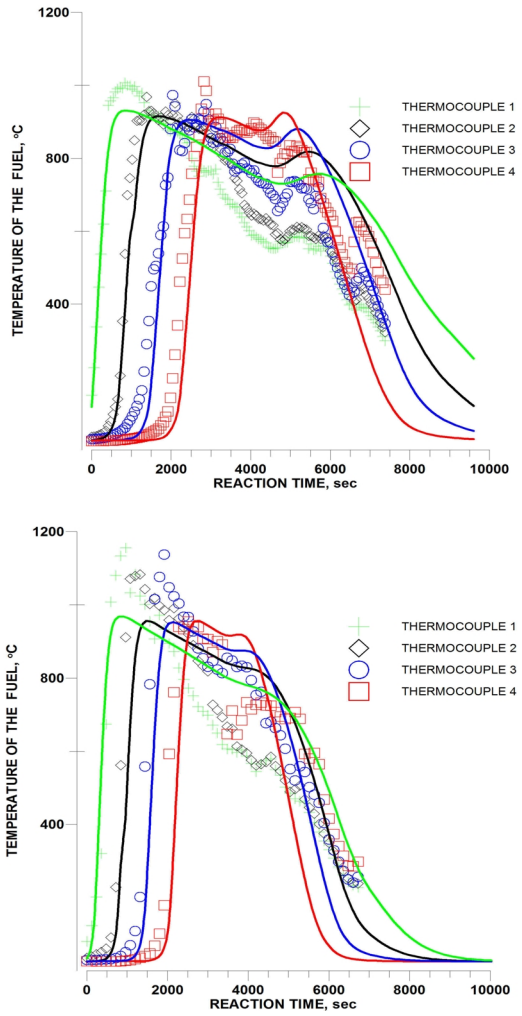

Figure 7.8: Coal bed temperature ($V_a = 1.0\frac{m^3}{h}$ and $V_a = 1.5\frac{m^3}{h}, T_a = 298K, p_a = 0.1MPa$) (lines - predicted data, symbols - measured data)

The graphs shown in Figure 7.8 present both the predicted and measured fixed - bed temperatures. The results that illustrate variation of the bed temperature during the process indicate no effect of the high fuel temperature assigned to the ignition zone since the thermocouples are located downstream of the ignition point, thus the ignition area only insignificantly affects results presented in Figure 7.8.

7.5 Correlation between model predictions and measured data

To establish whether the mode predictions are in accord with measured data, several correlation coefficients are calculated (see Tables 7.3 and 7.4). The coefficients are defined as:

$$\rho_{x,y} = \frac{\mathrm{Cov}(X,Y)}{\sigma_x \cdot \sigma_y} \tag{7.15}$$

where:

$cov(X,Y)$	- covariance between variables x and y,
σ_x, σ_y	- standard deviations for variables x and y,
x	- series of calculation data,
y	- series of measurement results.

Table 7.3 presents the correlation coefficients related to the fixed-bed temperatures measured at four locations along the reactor.

Temperature	Corrlelation coefficient V_a=1.0 m^3/h	Corrlelation coefficient V_a=1.5 m^3/h
Thermocouple 1	0.858	0.914
Thermocouple 2	0.884	0.895
Thermocouple 3	0.952	0.957
Thermocouple 4	0.946	0.872

Table 7.3: Correlation coefficients - Temperatures

The correlation coefficients reach values ranging from 0.858 to 0.957 indicating that the developed model is capable to predict temperatures of the fixed - bed in line with the measured data.

In turn, Table 7.4 contains the correlation coefficients calculated for the flue gas composition. The values of correlation coefficients for O_2 and CO_2 fall into 0.871 to 0.906 interval which means that cohesion between the calculations and the measurements is sufficient. The correlation coefficients related to determination of CO concentration range between 0.52 and 0.53, which is surprisingly low. The reason for such poor correlation of measurement results and calculation data for CO is the fact that a too high initial temperature of the coal bed has been entered for the ignition zone. This results in formation of large amount of CO originating from the gasification process. The CO concentration values after about 4000 seconds start to resemble values that have been obtained from measurements.

Temperature	Corrlelation coefficient V_a=1.0 m^3/h	Corrlelation coefficient V_a=1.5 m^3/h
O_2	0.906	0.893
CO_2	0.890	0.871
CO	0.531	0.524

Table 7.4: Correlation coefficients - Gas composition

7.6 Sensitivity analysis of the fixed - bed model

The developed fixed-bed model requires a number of input parameters. This section is meant to check how variations in parameters adopted for the model (i.e. thermal properties and kinetics) may affect the obtained results. This shall enable finding the parameters that must be determined with the topmost accuracy.

Figure 7.9 comprises diagrams that show how temperature of the fuel bed calculated using the developed model may vary when the value of the selected parameters is increased by 20%. Two diagrams, for energy activation (E_a) and pre-exponential factor (k_{comb}) of char combustion reaction ($C + O_2 \rightarrow CO_2$), show the influence of variations in the kinetic parameters. When the activation energy k_{comb} is increased by 20%, its value is so high that the combustion process does not begin. The ignition temperature assigned to the upper part of the reactor fails to initiate the reaction of combustion. On the contrary, the increase of the pre-exponential factor of the reaction results in acceleration of the combustion process.

The three subsequent diagrams show how the 20% increases of coal density, effective thermal conductivity and effective heat transfer coefficient affect the model predictions. The presented diagrams indicate that higher values of density and the intensification of heat transfer between the solid and the gas phases result in slowdown of the process. The burning front travels at a lower velocity from the ignition place (top of the reactor) to the reactor grate (bottom of the reactor). It is because a higher density results in an increase of the fuel mass for a given flow rate of air. It results in a drop of the excess air ratio as well as the fuel conversion rate. On the other hand, an increase of the heat transfer coefficient intensifies the transfer of energy between the solid and gaseous phases. Consequently, coal is more intensely cooled down by the surrounding gas which, to some extent, slows down the combustion. As it can be seen in Figure 7.5, the thermal conductivity value increases only within the combustion zone and it remains low otherwise. The sensitivity analysis indicates that an increase of the thermal conductivity coefficient by 20%, insignificantly affects the rate of the process inside the reactor.

The model parameters have been merely estimated or evaluated with a various degree of accuracy. The above analysis shows that some parameters should be determined or adjusted with exceptional care. The reaction of char oxidation (Equation 6.45) seems to be exceptionally important for the whole process, and particular attention should be paid

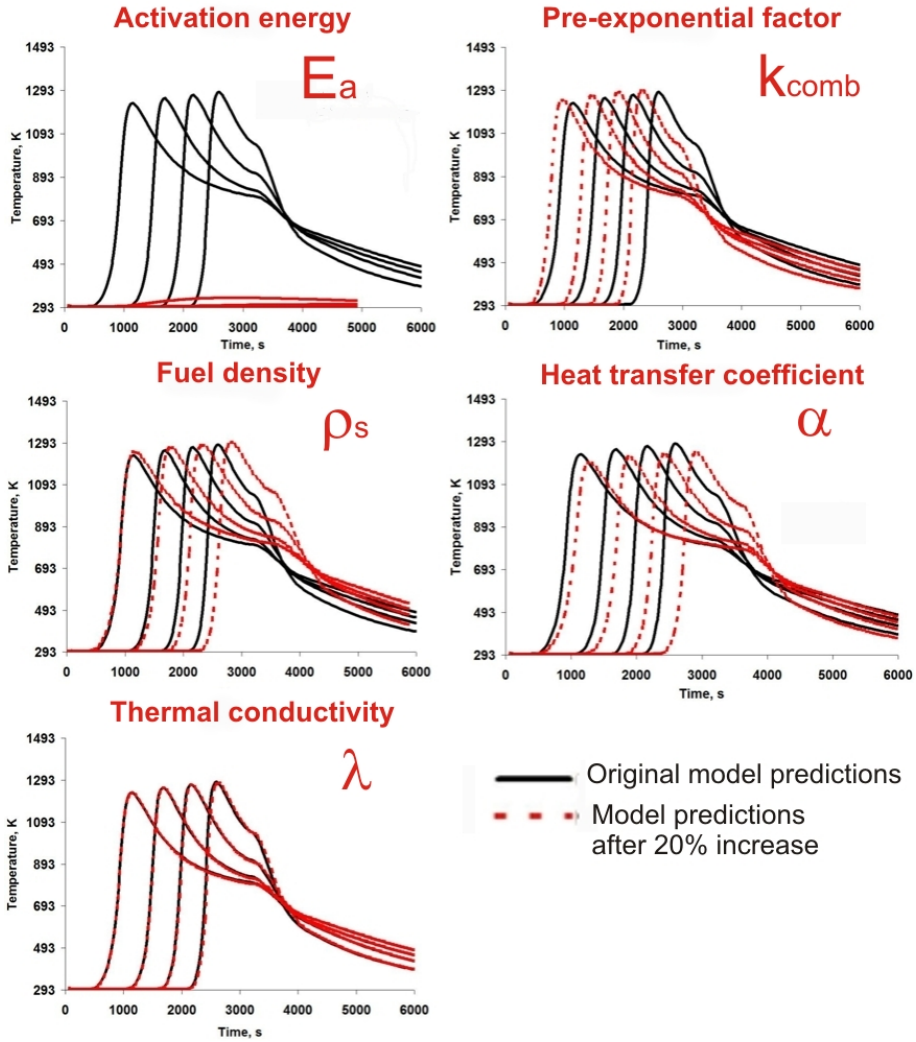

Figure 7.9: Sensitive analysis - fuel temperature (parameters increased by 20%), E_a - activation energy, k_{comb} - pre-exponential factor, ρ_s - fuel density, α - heat transfer coefficient (between phases), λ - thermal conductivity.

to the pre-exponential factor and the activation energy. A pretty large effect on the obtainable results (temperature profile) is observed for the density of solid fuel. On the other hand, the accuracy associated with measurements (calculations) of the thermal conductivity coefficient seems to be of much less importance. The assessment of the sensitivity of the five model parameters listed in Table 7.5 on the calculated temperatures is carried out by calculation of the logarithmic sensitivity factor LSF:

$$\mathsf{LSF} = \frac{\partial \ln \mathsf{y}}{\partial \ln \mathsf{p}} = \frac{\partial \mathsf{y}}{\partial \mathsf{p}} \cdot \frac{\mathsf{p}}{\mathsf{y}} \tag{7.16}$$

To assess global parametric sensitivity within the analyzed time interval $t_1 - t_k$, the average logarithmic sensitivity factor $ALSF$ is used:

$$ALSF = \frac{\sum_{i=1}^{k-1} |LSF(t_i) \cdot (t_{i+1} - t_i)|}{t_k - t_1} \tag{7.17}$$

Results of the completed calculations are summarized in Table 7.5. The calculations show that variation of the pre-exponential factor for the reaction of char combustion as well as of its activation energy (Equation 7.9) has the largest impact on the model results. Much less importance is recorded for the heat transfer coefficient, whilst variations of the thermal conductivity remain nearly negligible for the model predictions.

SENSITIVITY ANALYSIS				
Parameter p	Thermocouple 1	Thermocouple 2	Thermocouple 3	Thermocouple 4
α	0.205	0.317	0.383	0.462
E_a	2.517	2.247	1.938	1.591
k_{comb}	0.401	0.566	0.721	0.837
λ	0.020	0.022	0.033	0.066
ρ_s	0.458	0.566	0.664	0.782

Table 7.5: Average logarithmic sensitivity factor for the fixed -bed model

7.7 Overall assessment of the fixed - bed model

The results presented in Chapter 7 demonstrate a good consistency between the measurements and the calculations. The correlation coefficients presented in Tables 7.3 - 7.4 show a satisfying agreement between the predictions and the experimental data. The sensitivity analysis shows that the parameters such as pre-exponential factor and activation energy of char oxidation reaction (see Equation 6.45) have significant influence on fixed-bed model predictions and should be estimated as accurately as possible.

It is worth stressing again that the literature data have been used to calculate the kinetics of both combustion and gasification reactions. Such data are in general applicable to the EKORET coal, as demonstrated in this Chapter, however their accuracy remains unknown. A better approach would be to measure the kinetic data for the EKORET coal in a separate experiment. However such an experiment is not easy to carry out and often the determination of the pre-exponential factor and the activation energy is unbiques [146].

8 Simulations of the combustion process in a small - scale retort boiler.

Completion of the fixed-bed model development initiates modeling of the whole retort boiler for which the fixed-bed model constitutes a part only. The numerical calculations of the combustion process in a retort boiler of 25 kW nominal power are carried out under steady-state conditions. The boiler unit is fired with the peas-sized EKORET coal, that is the same fuel grade for which the fixed-bed model has been developed. The fixed-bed model has been implemented into the FLUENT software package and enables simultaneous calculations of the fuel bed (retort) as well as combustion of combustibles above the retort. Figure 8.1 shows the retort for which the fixed-bed model described in Paragraph 6.2 is used. The coal is continuously fed into the retort.

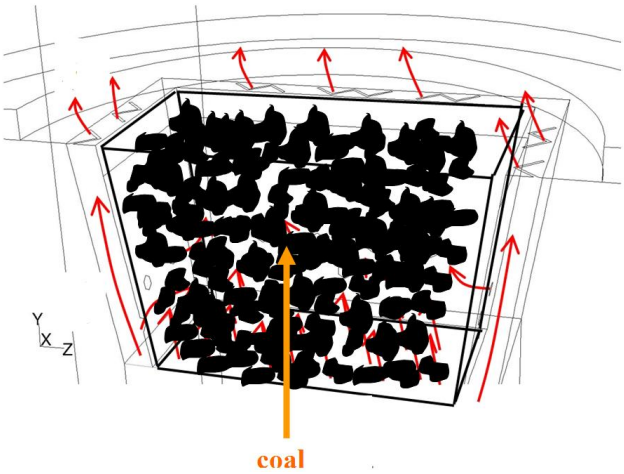

Figure 8.1: Coal in the retort

8.1 Boiler geometry and dimensions

The boiler, shown in Figure 8.2 is made up of a fuel reservoir, a screw feeder that transport fuel to the combustion chamber, a retort where the actual combustion takes place and a fan that supplies air to the combustion chamber.

Figure 8.2: The retort boiler considered in this work

The whole boiler unit is contained within a water jacket that receives heat generated in the boiler. The boiler operation is controlled by a microprocessor that regulates the amount of air and fuel supplied to the combustion chamber.

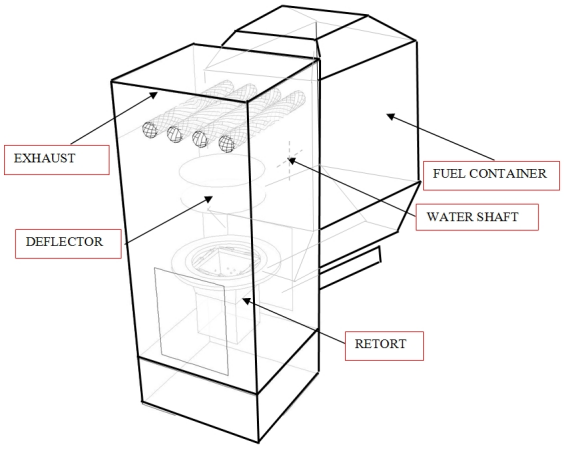

Figure 8.3: The sketch of the whole boiler

As pointed out in Paragraph 2, the boiler consists of the radiative and convective sections. Only the radiative section is considered in this Chapter for which the most important elements are: the retort, the free-board space above the retort and the space below it. The geometry of the numerical model is shown in Figure 8.4. To reduce the computing time only half of the boiler is simulated since the boiler is symmetrical. Major

dimensions of the combustion chamber are shown in Figure 8.5.

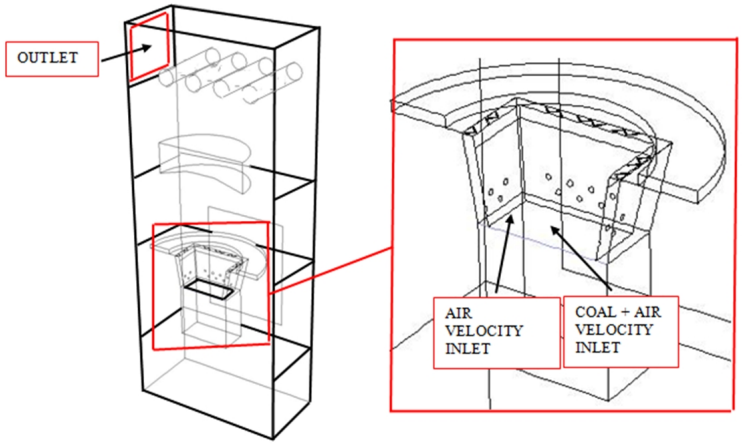

Figure 8.4: Geometry of the model

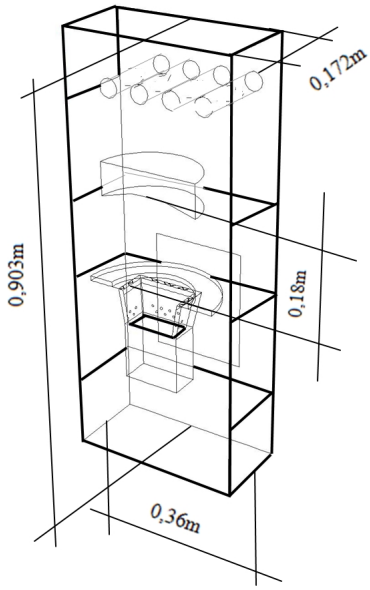

Figure 8.5: Dimensions of the geometry of radiation section

Figure 8.6 shows a sketch of the upper part of a retort. The air is provided into the boiler by means of a fan and is delivered to the combustion chamber through a channel that embraces the retort. In that channel the supplied air (oxidizer) is split into the primary and the secondary air streams. The primary air is delivered through holes (d = 5 mm) that are located on the side wall of the retort (2). The holes deliver the incoming air directly to the fuel bed. Narrow slots of 0.5 mm width guide the secondary air (3) around the retort. Thus, the secondary air does not mix with the solid fuel. A small amount of air enters into the combustion chamber together with the fuel particles (1).

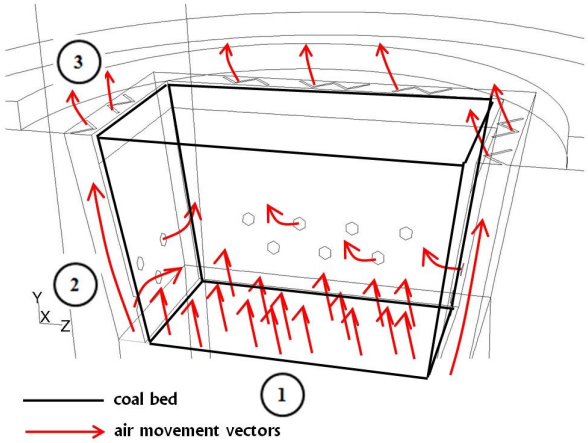

Figure 8.6: The air distribution to the combustion chamber

8.2 Material properties

The gaseous phase comprises six chemical species: nitrogen, oxygen, carbon monoxide, carbon dioxide, water vapor and volatile matter (as a single chemical compound). Properties of all mentioned gases have been copied from FLUENT database.

STEEL PROPERTIES			
Density, kg/m^3	Specific heat, J/kgK	Thermal conductivity, W/mK	Emissivity (rusted+sooty) material
8030	502.48	16.27	1

Table 8.1: Properties of steel

The boiler walls are made out of steel of the properties listed in Table 8.1. The deflector is made out of a ceramic material with thermal properties as listed in Table 8.2

CERAMICS PROPERTIES			
Density, kg/m^3	Specific heat, J/kgK	Thermal conductivity, W/mK	Emissivity (rusted+sooty) material
3720	880	25	1

Table 8.2: Properties of the ceramics of the deflector

It has been assumed that emissivity of boiler walls and the deflector equals $\varepsilon = 1.0$ since the inner surface of the combustion chamber are covered with soot formed during the combustion process. For comparison purposes another simulation has been carried out where the emissivity takes a value of $\varepsilon = 0.8$.

It is also assumed that combustion chamber gas is fully transparent for thermal radiation. Despite the presence of CO_2, H_2O and some soot and particulates such an assumption is justified as the optical thickness is small so that the mentioned species absorb and emit

not too much of thermal radiation. Similarly, additional comparative calculations have been carried out using Discrete Ordinate model with gas emissivity calculated by weighted sum of gray gases model (wsggm).

8.3 Boundary conditions

Formulation of boundary conditions is an important part of the numerical simulations. Inappropriate boundary conditions may lead to discrepancies of numerical calculations or results that contradict the reality. In the boiler considered, the combustion process is carried out at relatively high excess air ratio at the level of $\lambda = 2$. The combustion chamber of the boiler considered is contained in a water jacket. Typically, the water reaches the temperature of $(70 - 80)^oC$. Following the measurements, the temperature of 373 K has been specified as heat transfer boundary conditions at the combustion chamber walls.

The diagram of the boiler geometry along with the major boundary conditions is shown in Figure 8.7 and they are listed in Table 8.3. The amount of air delivered to the boiler unambiguously results from the boiler power and the excess air ratio. It is assumed that both the fuel and air are delivered to the combustion chamber at $T = 298K$ temperature.

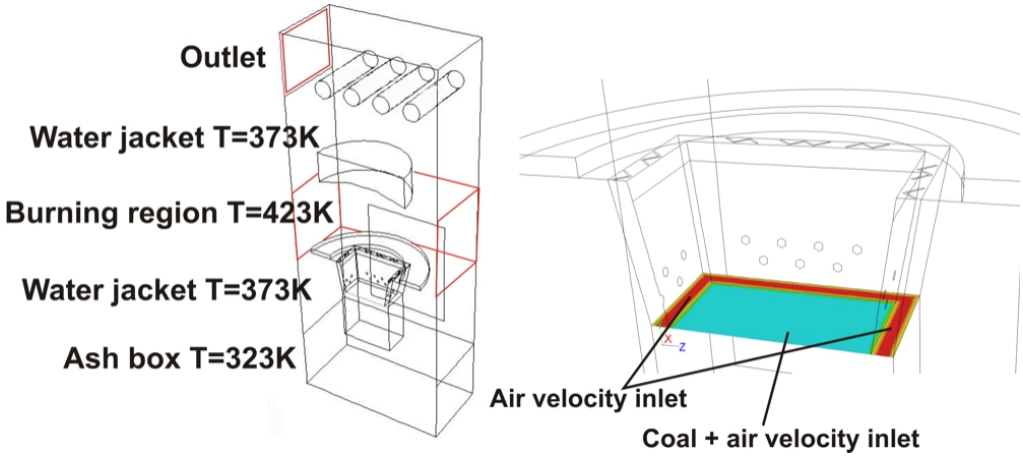

Figure 8.7: Boundary conditions

8.4 Results of the calculations

After setting up the boiler geometry, entering the materials properties and inlet conditions and specifying the boundary conditions as described in the previous section, a non-structural mesh consisting of around 1,000,000 tetrahedral elements is generated.

BOUNDARY CONDITIONS RADIATIVE SECTION OF THE BOILER	
General	
[1]fuel flow rate, kg/h	3.83
[1]rated power, kW	25
[1]flue gas temeprature, K	523
Inlets	
air velocity, m/s	3.04
fuel velocity, m/s	0.0001342
air temeprature, K	298
fuel temeprature, K	298
Walls	
[1]water jacket temperature	373
[1]burner region temperature	423
[1]ash box temperature	323
emissivity	1.0

Table 8.3: Boundary conditions [1] - experimental data (25kW nominal power, 30kW fuel input)

8.4.1 Fixed-bed results

Figures 8.8 and 8.9 refer to the combustion process in the retort. In Figure 8.8 one can see the retort and temperature distribution for the fuel placed therein. The solid fuel moves from the bottom to the top of the retort and the combustion zone is located in the upper part of the bed. The fuel bed temperature never exceeds $1400K$ owing to the mechanism of temperature stabilization typical for coal combustion in fixed-beds. This mechanism is based on chemical reactions associated with the combustion and gasification processes. When the fuel bed temperature is high the gasification reactions tend to dominate and the heat is taken away from the reacting particles.

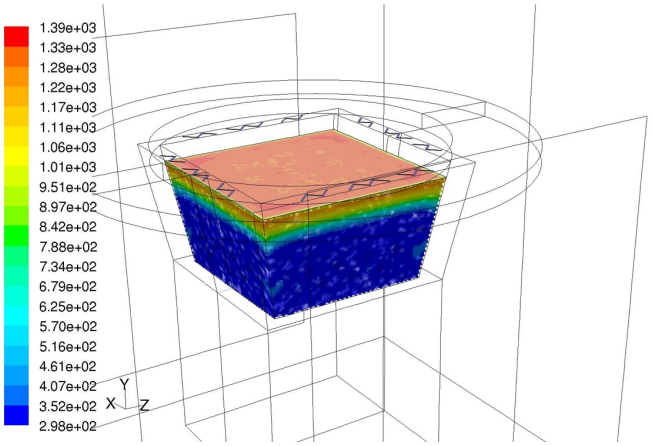

Figure 8.8: Solid bed temperature inside the retort (in Kelvin)

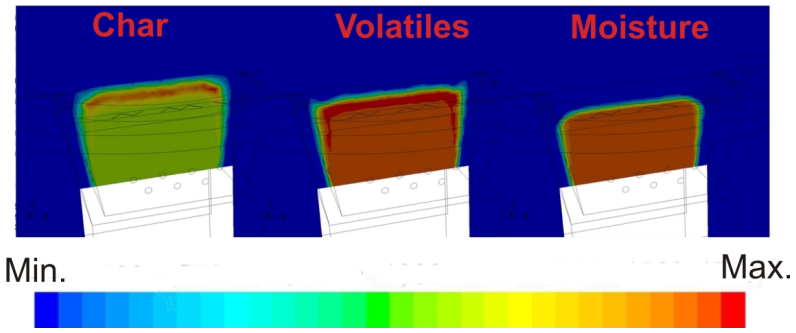

Figure 8.9: Mass fraction of char, volatiles and moisture in the coal bed

Figure 8.9 shows mass fractions of coal components during combustion. Here one has to emphasize the role of the deflector positioned just above the retort. Beside the obvious effect of distribution (baffle) of combustion products leaving the retort, there is one more valuable benefit of the deflector. A substantial portion of energy leaves the bed by thermal radiation and is reflected by the deflector back toward the retort. Such a design definitely improves the combustion, resulting in an improve fuel ignition and burnout.

8.4.2 Free-board results

Figure 8.10 shows the temperature field inside the boiler. In the plane that intersects the boiler into symmetric halves, the highest temperature ($1700K$) is below the deflector. Outside the flame located just above the retort, the combustion products are subject to very fast cooling even as much as by several hundreds centigrades. Such a substantial temperature gradient may lead to an incomplete combustion of combustibles. The deflector surface temperature is worth considering. As compared to the temperature of combustion products that flow around the deflector, the deflector surface temperature is rather low at the level of $800K$. Such a low temperature results from intensive radiation (emission) from the deflector surface to cold walls $(373-425)K$ of the combustion chamber that are cooled by the water. Contact of the flue gas with such a cold solid body may worsen combustion conditions and, in consequence, its efficiency. The temperature profile as shown in Figure 8.10 discloses one more significant fact. The bottom part of the combustion chamber (located below the retort) has temperature as low as (400 - 500)K, so the combustibles reaching that area have no chance to undergo complete combustion.

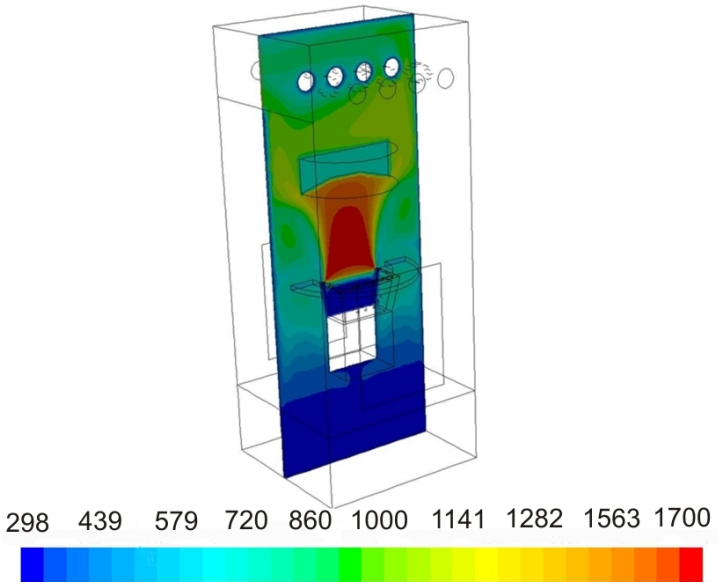

Figure 8.10: Temperature profile (in Kelvin)

Figures 8.11 and 8.13 show the path lines indicating the gas flow pattern in the combustion chamber. The pictures show how the flue gas flows round the deflector and then, nearly immediately, leaves the combustion zone being discharged at the exit of the radiative section. Such organization of the combustion process can be described as „poor mixing", which eventually results in incomplete combustion of the fuel.

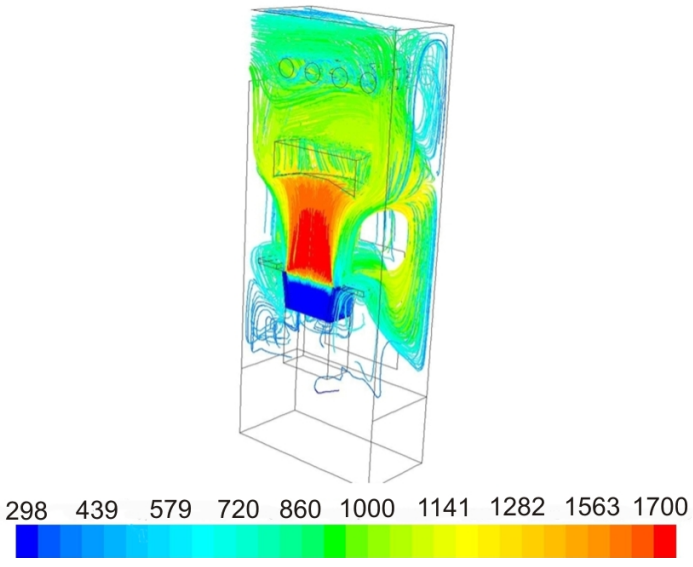

Figure 8.11: Path lines colored by temperature (in Kelvin)

Figure 8.12 shows the oxygen molar fraction inside the combustion chamber. The oxidizer is fed to the combustion chamber via appropriately designed nozzles. The calculations show that a substantial portion of air escapes from the combustion chamber not

participating in the combustion process. It is easy to see that the oxidizer is insufficiently distributed inside the combustion chamber hence the oxygen concentration is non - uniform in the radiative part of the boiler. The calculation results also reveal that supplying of cold air directly to the combustion zone substantially cools down the area nearby the secondary air nozzles.

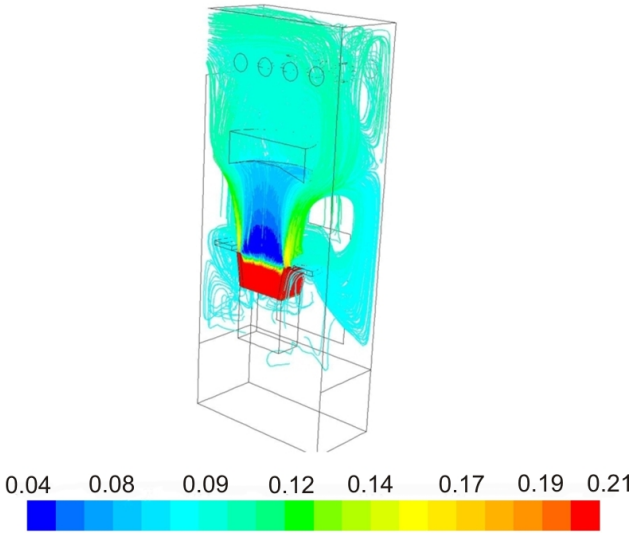

Figure 8.12: Path lines colored by oxygen mole fraction (in $\frac{kmol_{O_2}}{kmol}$)

Figure 8.13 shows the CO molar fractions inside the combustion chamber. The results reveal that the coal gasification is one of the major mechanisms that lead to CO formation. One can clearly see how important function is performed by the deflector inside the boiler. The deflector retains gas within the combustion area before the gas is discharged to the relatively cold convective zone.

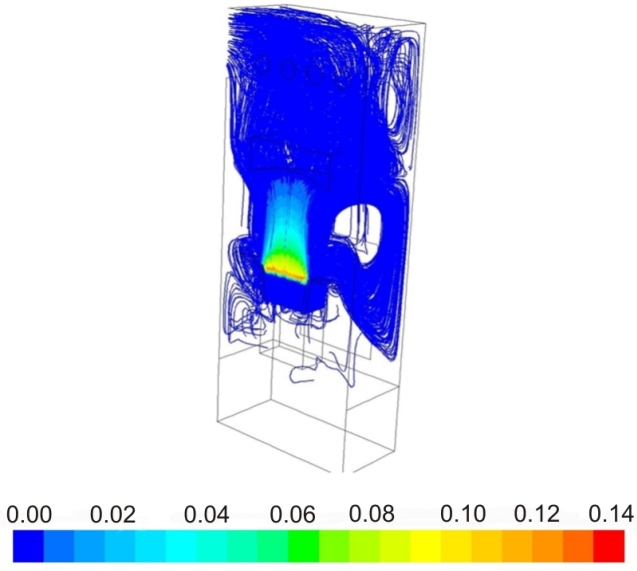

Figure 8.13: Path lines colored by CO mole fraction (in $\frac{kmol_{CO}}{kmol}$)

8.5 Sensitivity analysis

In this Paragraph, sensitivity analysis is conducted using the Logarithmic Sensitivity Factor (LSF) defined by the relationship 7.16. The factor has been calculated for the entire part of the combustion chamber (see Figures 8.14 - 8.17).

8.5.1 Sensitivity to mesh density

In any numerical simulations it is imperative to examine how the mesh size affects the predictions. Tetrahedral elements are used. During the process of the mesh generation the particular attention has been paid to the following features of the mesh:

- Smoothness – changes in dimensions of the mesh elements should be smooth so that the volumetric ratio of the adjacent elements shall be low.
- Skewness - shapes of mesh elements should be as close as possible to equilateral tetrahedrons. Apex angles of the solid should be about 60^o.
- Aspect ratio - this is the parameter that serves as a measure how much the mesh is stretched. The parameter value should never exceed 5. It is defined as a halved ratio of the element length to its width.

Two meshes consisting of 800,000 and 1,000,000 nodes have been used. In both meshes for which the above rules applied, the volume of individual element range from 10^{-6} to 10^{-10} m^3. The numerical mesh is denser inside and nearby the retort as well as within the area between the deflector and the retort. Dimensions of the mesh elements gradually increase towards the bottom part of the boiler.

Figure 8.14 shows the map of sensitivity factors for the temperature profile against variations of the mesh density. The picture demonstrates that modifications of the mesh density within the range from $800,000$ to $1,000,000$ of cells affect the obtained results exclusively for areas nearby the walls of the deflector and the water jacket. For nearly entire volume of the model under analysis the denser mesh has no substantial impact on the predictions. Thus, one can assume that the mesh density adopted for calculations is sufficient. Owing to correctly designed numerical mesh, the results that are obtained during simulations depend only marginally on numerical errors.

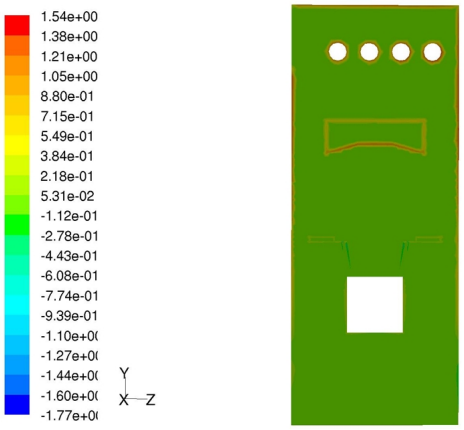

Figure 8.14: Sensitivity factor for temperature with a respect to mesh size

8.5.2 Sensitivity to physical parameters

The mathematical model describing the processes that take place in the combustion chamber requires a number of parameters, such as the amount of supplied air (the excess air ratio), wall temperature or wall emissivity. Therefore the Logarithmic Sensitivity Factor (LSF), already defined in the former parts of this study, has been calculated for some of the parameters. The results, in the form of a map that presents sensitivity factors on the symmetry plane of the combustion chamber, are shown in Figures 8.15 - 8.17. Variations of all the analyzed parameters amounts to 10% of the initial parameter value. The excess air ratio has been reduced from the initial value of $\lambda = 2.0$ to 1.8, and emissivity of the combustion chamber from $\varepsilon = 1.0$ to 0.9. Similarly, the wall temperatures have been decreased.

The impact of such alterations on the predicted temperature inside the combustion chamber is the most significant within the closest vicinity of the chamber walls. The highest values (10.9) of logarithmic sensitivity factors near the walls are obtained for wall emissivity (Figure 8.17). Even if distance from walls is very short the values of logarithmic sensitivity factors rapidly decrease. For wall emissivity these values are always less than 0.02 and for wall temperatures they never exceed 0.07 (Figure 8.16). The largest impact onto the temperature profile inside the combustion chamber is recorded for the excess air ratio. The logarithmic sensitivity factors calculated for that parameter may even exceed the level of 0.23.

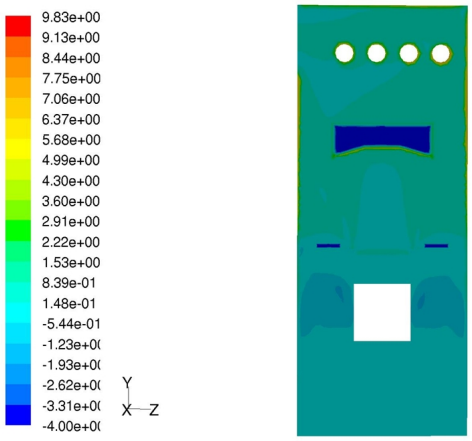

Figure 8.15: Temperature sensitivity factor with a respect to excess air ratio

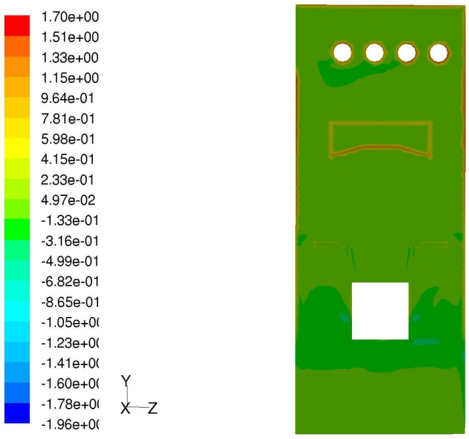

Figure 8.16: Temperature sensitivity factor with a respect to walls temperature

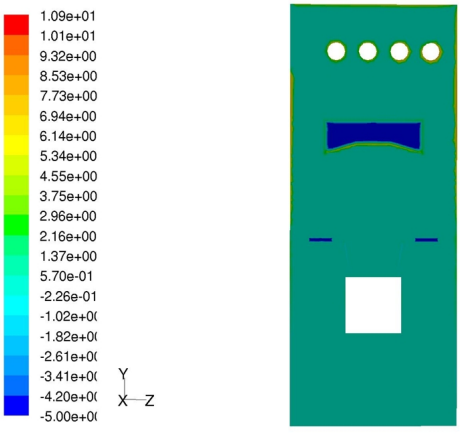

Figure 8.17: Temperature sensitivity factor with a respect to walls emissivity

The averaged, over the entire chamber volume, logarithmic sensitivity factors have also been computed using the following formula:

$$\mathsf{ALSF} = \frac{\sum_{i=1}^{k-1} |\mathsf{LSF}(V_i) \cdot V_i|}{V_m} \tag{8.1}$$

where:

V_m	- total volume of the combustion chamber,	m^3,
V_i	- volume of mesh element "i",	m^3,
$LSF(V_i)$	- logarithmic sensitivity factor calculated for the i-th mesh element,	
k	- number of mesh elements inside the combustion chamber.	

Table 8.4 shows the calculated values of the sensitivity factors for predictions of both, the temperature and the oxygen molar fraction.

Parameter	Logarythmic Sensitivity Factor	
	Temeprature	O_2 mole fraction
Wall temperature	0.0720	0.0559
Wall emissivity	0.0197	0.0568
Mesh density	0.0020	0.0032
Excess air ratio	0.2825	0.7011

Table 8.4: Average logarithmic sensitivity factors

One can unambiguously state that the model predictions are the most sensitive to variations of the excess air ratio. The temperature and emissivity of walls are only important within a very small volume. Thus, particular attention must be paid to correct, as accurate as possible, determination of the excess air ratio. Due to a very probable effect of air in-leakage, particularly in the boiler bottom parts, the actual value of the excess air ratio may deviate from the value entered in the calculations.

The wall temperatures of the water jacket demonstrate quite narrow variations that never exceed 10%, since the water cooling is rapid. The average logarithmic sensitivity factor for temperature is equal to $ALSF = 0.072$ (Table 8.4), so that the assumption of the constant wall temperature value shall lead to variation of computation results at the level of 0.72% since:

$$\frac{\partial \mathsf{T_g}}{\mathsf{T_g}} = \mathsf{LSF} \cdot \frac{\partial \mathsf{T_w}}{\mathsf{T_w}} \tag{8.2}$$

$$\frac{\partial \mathsf{T_g}}{\mathsf{T_g}} = 0.072 \cdot 0,1 = 0.0072 \tag{8.3}$$

where:

T_w	- temperature of walls,	K,
T_g	- temperature of gas inside the combustion chamber,	K,
LSF	- logarithmic sensitivity factor.	

Wall emissivity values are subject to variations only within an insignificant range and the assumption that the emissivity is nearly one is a good approximation, which is confirmed by the value for the calculated average sensitivity factor of $ALSF = 0.0197$ (Table 9.3).

In summary, the predicted profiles of temperature and oxygen concentration are the most significantly affected by variations of the excess air ratio. Other parameters that have been also considered, such as the temperature or the emissivity of the combustion chamber walls have only minor impact on the calculation results.

9 Validation of the numerical model

In this Chapter the overall boiler model is validated against the measurements of temperature, O_2, CO_2 and CO concentrations which have been taken in the free board (radiative section) of the boiler. Thus, this validation is limited to the radiative section only.

9.1 Procedure of experimental measurements

The boiler has been modified, as shown in Figure 9.1, to provide access for temperature and gas composition measurements.

Figure 9.1: Measurement ports located on the side wall of the boiler

Figure 9.2 and Figure 9.3 show the location of the measurement ports which have been selected so that the most crucial areas inside the combustion chamber could be examined. These areas include the space above the deflector, between the deflector and the retort as well as below the retort. The inner temperature of walls have been measured at the side of the combustion chamber using flat thermocouples. The temperature and gas composition inside the combustion chamber have been measured using a purposefully designed water-cooled probe. Traversing the probes allow for measurements in tree vertical planes: at two side walls and along the central plane of the unit.

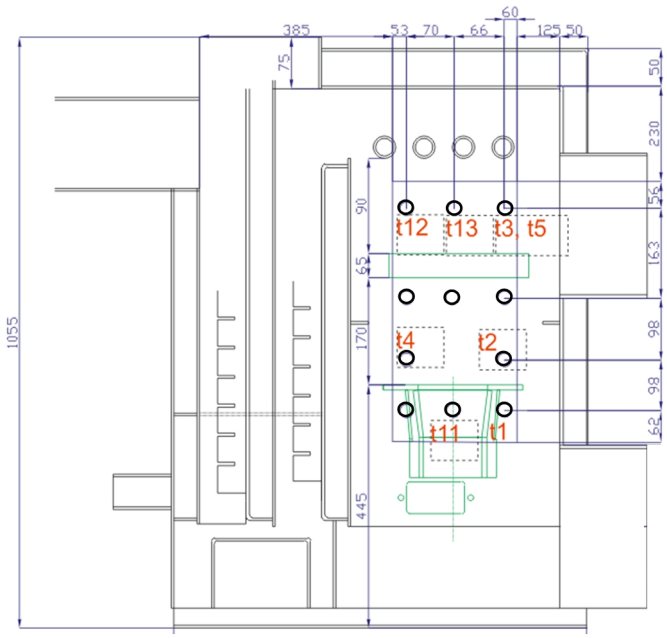

Figure 9.2: Location of the measurement ports in the boiler – side view

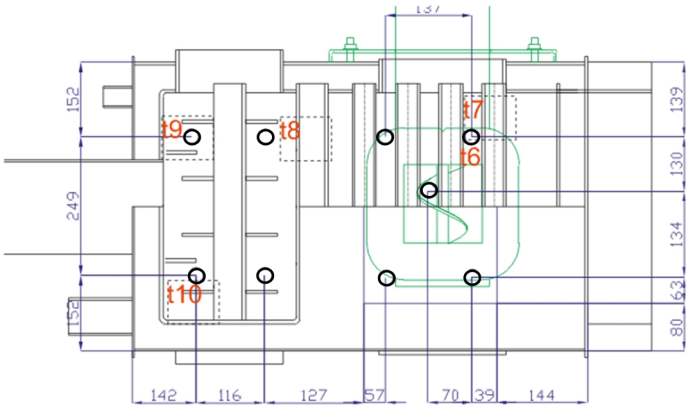

Figure 9.3: Location at the measurement ports in the boiler

During the measurements the boiler has been operated at rated power of $25kW$ with the excess air ratio of $\lambda = 2.0$. The measurements have been taken under steady-state conditions of the boiler. The unit under tests achieved its steady-state conditions after about 30 minutes from the moment when tests are commenced. Details related to measurements, such as description and technical characteristic of the applied equipment can be found in the PhD thesis of R. Nosek [56].

9.2 Comparison of calculations with experimental results

The measurements have been carried out along two planes, marked in Figure 9.4 as 'a' and 'b' planes. Plane „a" is the symmetry plane at the boiler while plane „b" is located in

the vicinity of the side wall.

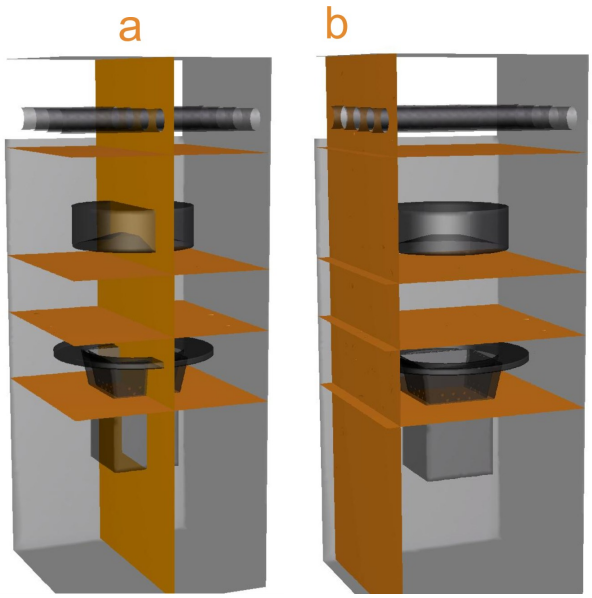

Figure 9.4: Measuring planes inside the combustion chamber

Locations of the measurement points are shown in Tables 9.1 and Table 9.2.

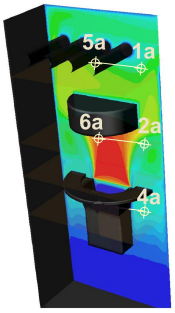

SLOT		[CO], %	[CO_2], %	[O_2], %	T, K
1a	CALCULATIONS	0.000	10.9	10.5	1016
	MEASUREMENTS	0.010	11.8	8.2	812
2a	CALCULATIONS	0.221	12.7	8.4	1481
	MEASUREMENTS	1.120	12.7	6.8	1354
4a	CALCULATIONS	0.004	10.5	9.9	603
	MEASUREMENTS	0.280	2.3	18.5	515
5a	CALCULATIONS	0.000	10.9	10.2	1049
	MEASUREMENTS	0.060	14.1	5.2	755
6a	CALCULATIONS	1.043	13.5	7.2	1589
	MEASUREMENTS	7.290	13.9	0.1	1605

Table 9.1: VALIDATION of the model - plane a

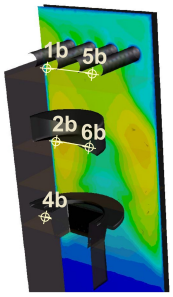

SLOT		[CO], %	[CO_2], %	[O_2], %	T, K
1b	CALCULATIONS	0.001	10.9	10.3	1088
	MEASUREMENTS	0.010	13.3	6.5	949
2b	CALCULATIONS	0.031	10.4	10.7	1001
	MEASUREMENTS	0.060	7.6	13.0	820
4b	CALCULATIONS	0.003	10.4	9.9	430
	MEASUREMENTS	0.070	0.07	20.1	455
5b	CALCULATIONS	0.010	10.4	10.7	1065
	MEASUREMENTS	0.200	12.4	7.0	834
6b	CALCULATIONS	0.160	9.0	11.9	917
	MEASUREMENTS	0.110	7.4	0.1	959

Table 9.2: VALIDATION of the model - plane b

The measurements along the symmetry plane „a" (Table 9.1) that passes through the combustion chamber center are to determine the temperature and gas composition inside the combustion chamber close to the flame (point 2a), in the flame center (point 6a), below the retort (4a) and near the water cooled pipes (5a, 1a). Measurement in plane „b" (Table 9.2) provide information about the near walls region.

Experimental and predicted data summarized in Table 9.1 and Table 9.2 demonstrate deviations ranging from 9% to 30%, as compared to numerical calculations. The largest discrepancy is seen at the location below the retort. The measurement results indicate that the gas composition at this location is very close to the atmospheric air whilst the calculations show combustion products of composition very similar to the one above the retort. The described discrepancy is associated with design features of the boiler. The sampling point below the retort (point 4a) is located nearby the ash-pan and service doors, so additional air is entrained to the considered area from outside via any untight slots and this is clearly seen in the gas composition measured. Leaks via unsealed joints of the boiler alter the excess air ratio. The amount of uncontrolled air and locations where it is entrained into the combustion chamber are hard to detect and evaluate. It is the reason that reliable and accurate reproduction of conditions inside the combustion chamber of a real boiler is difficult.

The calculated correlation coefficients (see Table 9.3) indicate that the developed model is capable to predict, with satisfying reliability, alterations in gas temperature and concen-

tration.

[CO]	[CO_2]	[O_2]	T
0.99	0.70	0.82	0.94

Table 9.3: Correlation coefficient between measurements and calculations

In summary of this Paragraph one observes that the predicted carbon monoxide concentration differs substantially from the measured value, as shown in Tables 9.1 and Table 9.2. However, the high value of the CO correlation coefficient indicates a strong correlation between the model predictions and measurements. Thus, the model is good enough to predict trends in CO concentration changes although the absolute values may depart from reality.

10 Improvements to the boiler design

The model predictions allow for an analysis of the combustion process inside the boiler. In this Chapter, such an analysis is performed with a twofold objective to identify deficiencies and to propose improvements.

Figure 10.1 shows the predicted temperature inside the radiative section at the symmetry plane of the boiler. The predictions are for steady-state operation at 25 kW rated power (30 kW thermal input) and excess air ratio of 2.0. The deflector is positioned 0.18 cm above the retort. This boiler configuration and inputs is named as Baseline Case.

Figure 10.1 indicates substantial gas temperature gradients inside the combustion chamber. The flue gas leaving the flame zone is rapidly cooled down by several hundreds of centigrades. Such a rapid temperature drop inhibits combustion reactions indicated in the flame zone and results in an increase of unburned species. The temperature drop is caused by the cold air that is supplied as the secondary air. In other words, the secondary combustion air forms a curtain of cold air flowing upwards along the flame zone. Both the walls temperature and the deflector temperature inside the combustion chamber are also disadvantageous in terms of the combustion process efficiency.

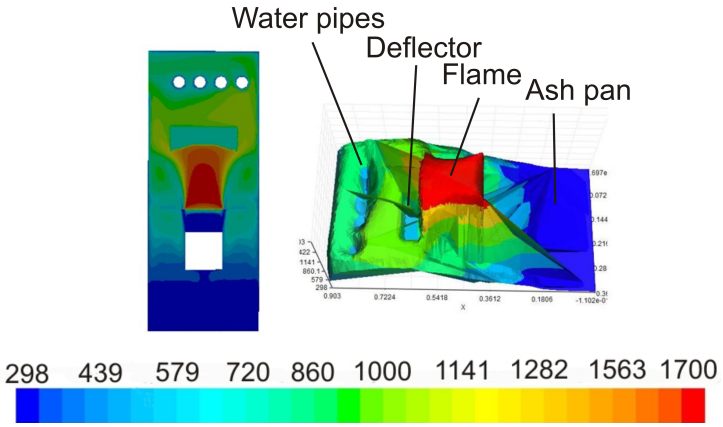

Figure 10.1: Temperature distribution inside the combustion chamber (in Kelvin) (Baseline Case)

The combustion chamber walls are cooled down by water that circulates in the water jacket that embraces nearly the whole combustion chamber. The flue gas that resides nearby the water cooled chamber walls is relatively cold and, in the cold near wall region, the combustion reactions are terminated.

The deflector, situated inside the combustion chamber above the retort and secondary air nozzles, is to improve the combustion process as it prolongs the residence time inside the boiler and improves mixing of substrates. The deflector also retains a portion of energy that is released (lost) from the fixed-bed by radiation and reflects it back up towards the retort, which improves the combustion process for solid fuel. However, such a deflector has got also some disadvantages.

The modeling results show that the deflector temperature of 800K is much lower than the gas temperature of 1600K. The deflector emits thermal radiation to the boiler side walls that are relatively cold. The deflector, placed just above the retort, improves mixing of gas but also cools the gas that hits its relatively cold surface. However, the mixing process is still insufficiently intense (Figure 10.2) and the retention time of incompletely combusted flue gas in the radiative part of the boiler is still too short. The combustion process takes place exclusively in the upper part of the combustion chamber, it means in the space above the retort, and the temperature in the area below the retort is as low as 400K. Incompletely combusted gas that penetrates into this area has no chance to be oxidized to completion. A great deal of gas remains in „corners" of the combustion chamber (Figure 10.3). These are the areas that are much colder than the remaining space where conditions for combustion are unfavorable.

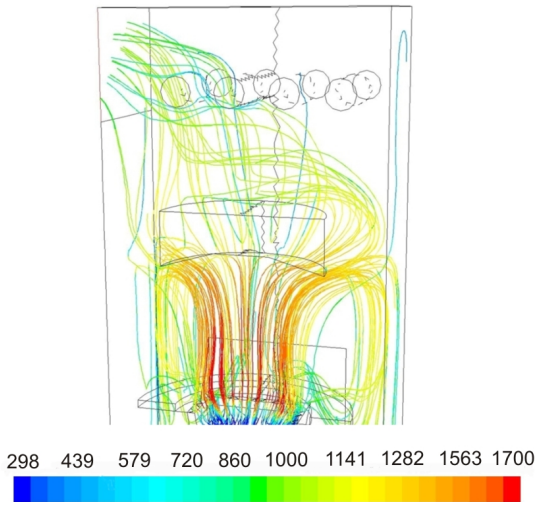

Figure 10.2: Path lines colored by temperature (temperatures in Kelvin) (Baseline Case)

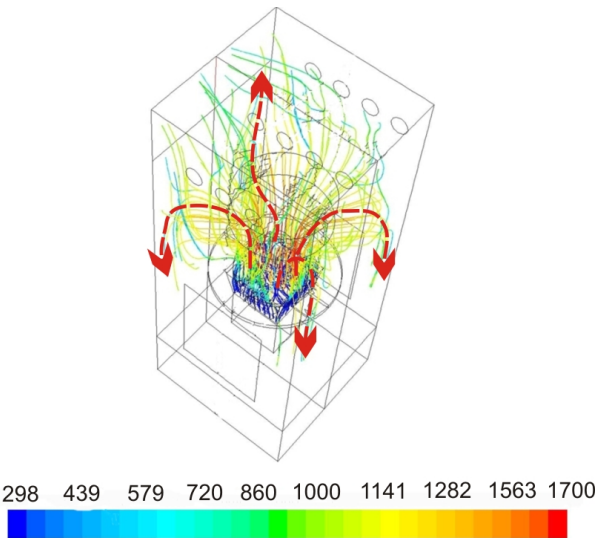

Figure 10.3: Distribution of gases in the combustion chamber (temperature in Kelvin) (Baseline Case)

Combustion in the retort and in the boilers proceeds with a substantial (2.0) excess of air so as to provide sufficient amount of oxygen inside the boiler to decrease the content of combustible matter in flue gas. Such a large flow of the oxidizer leads to substantial pressure losses in air channels and in bed itself. An excessively high velocity of gas inside the combustion chamber reduces the residence time of substrates in the combustion zone and it may lead to incomplete combustion. To summarize all the foregoing remarks, one has to conclude that the combustion process in the retort boiler can be improved by modification of the deflector, redirection of air flows and alterations to shape and design of the combustion chamber.

In the subsequent paragraphs one considers a number of boiler modifications which are named as follows:

- Cases A - J - modifications concerning the deflector,
- Cases K - O - modifications concerning the air supply,
- Case P, R - modifications concerning the shape of combustion chamber.

10.1 Influence of deflector on flue gas composition

To improve the substrates mixing the deflector is lowered by 0.065 m and is suspended at a distance of 0.115 m above the retort. Figure 10.4 shows the path lines colored with temperature which correspond to this modification, named as Case A. Figure 10.4 should be compared with Figure 10.2 showing the same informations for the original deflector position. Lowering of the deflector leads to higher velocities of gas that hits the deflector surface, which leads to a better mixing. As the deflector is closer to the retort it directly affects a larger portion of gas leaving the retort. One should realize that the deflector should be optimized, it means there is an optimum position of the deflector above the retort. Positioning too close to the retort may even deteriorate the combustion efficiency and result in combustion instabilities caused by accumulation of excessive amount of cold air (from air nozzles) within the flame zone.

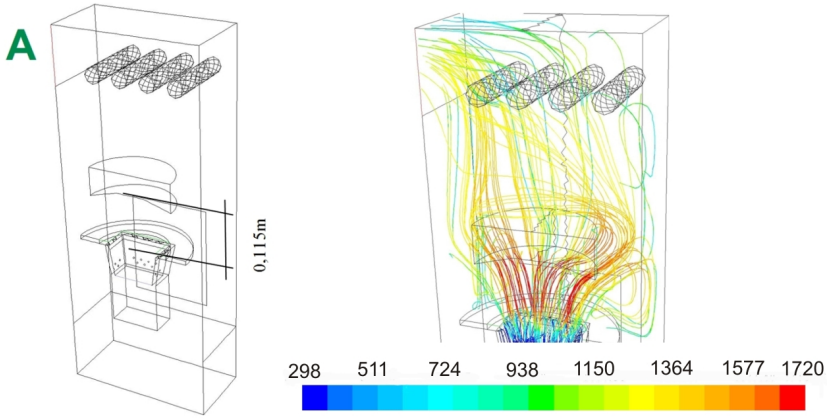

Figure 10.4: Case A (temperature in Kelvin)

The next case that is considered (Case B) includes modifications to the deflector shape and size. The new deflector is of 0.12m diameter so that its surface area is smaller than the surface area of the original deflector (d=0.21). The new deflector is suspended at 0.18m distance above the retort. Flow path lines in Figure 10.5 show that flue gas escapes from the combustion chamber along the shortest possible path. Consequently, the modification B deteriorates the degree of combustion. In case of CO, the combustion completeness is nearly threefold worse that in the Baseline Case.

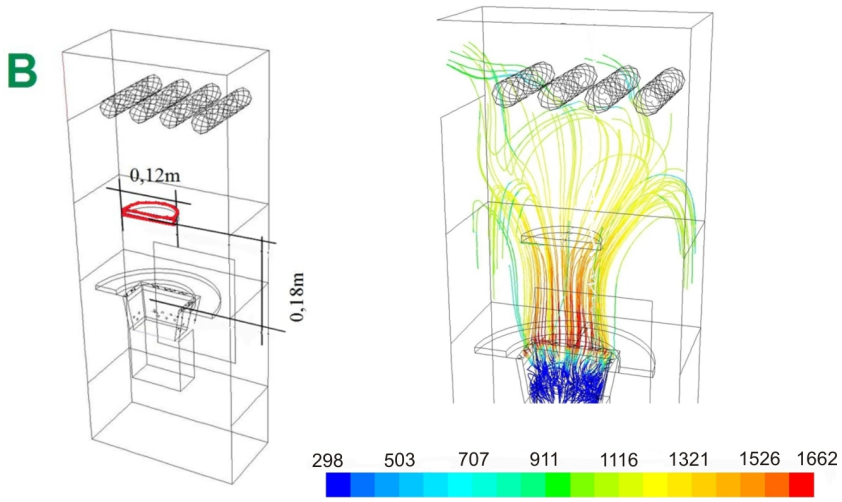

Figure 10.5: Case B (temperature in Kelvin)

The Case C (Figure 10.6) is actually a modification of Case B. The deflector is identical as in the Case B but is lowered by 0.1 m. The mathematical modeling demonstrates that lowering of this small deflector does not improves the combustion conditions.

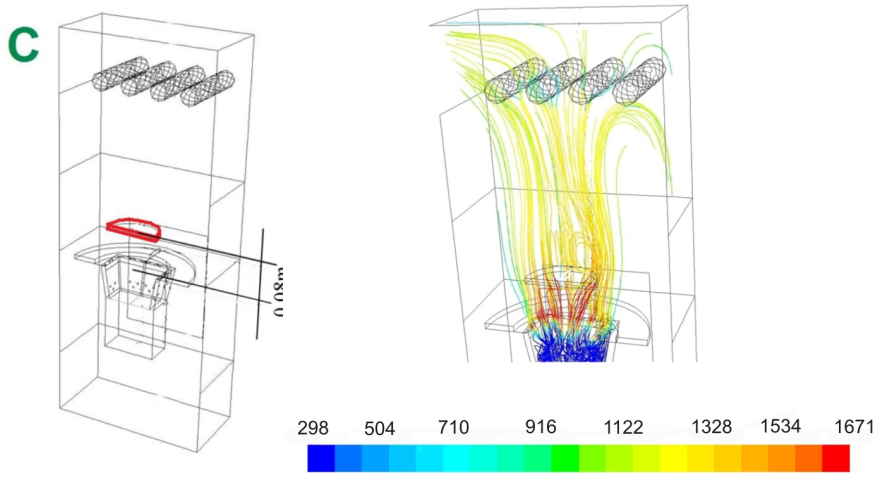

Figure 10.6: Case C (temperature in Kelvin)

For Case D (Figure 10.7) a deflector of 0.24m diameter is suspended 0.08m above the retort. In order to reduce loss of heat, a screen is used as shown in Figure 10.7. The analysis of calculation results clearly shows that gas in the combustion chamber is redirected towards cold walls. As flue gas flows via the coldest area of the combustion chamber chemical reactions are inhibited. It results in a deterioration of flue gas purity with more than twice higher emission of CO, as compared to Baseline Case (see Figures 10.2-10.3).

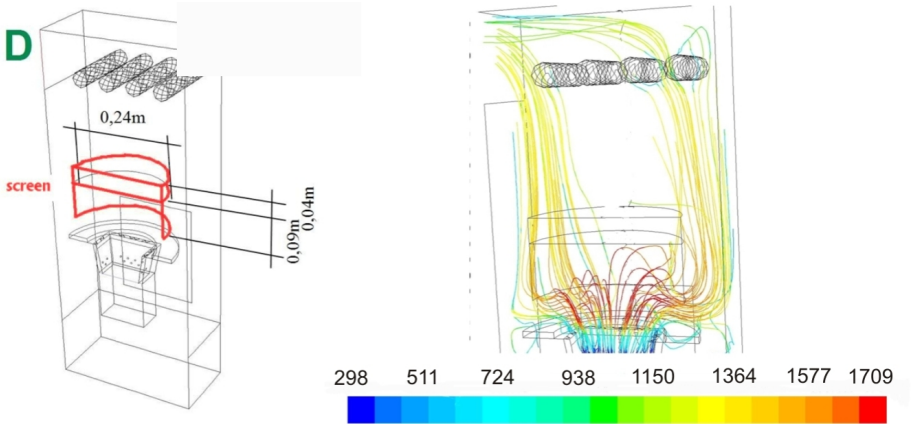

Figure 10.7: Case D (temperature in Kelvin)

Case E (Figure 10.8) refers to the identical geometrical design as Case D, the only difference is in slots present in the screen. The slots enable a portion of the flue gas to pass from the flame zone to the free board zone. This solution improves completeness of CO combustions by nearly 70 %, as compared to Baseline Case.

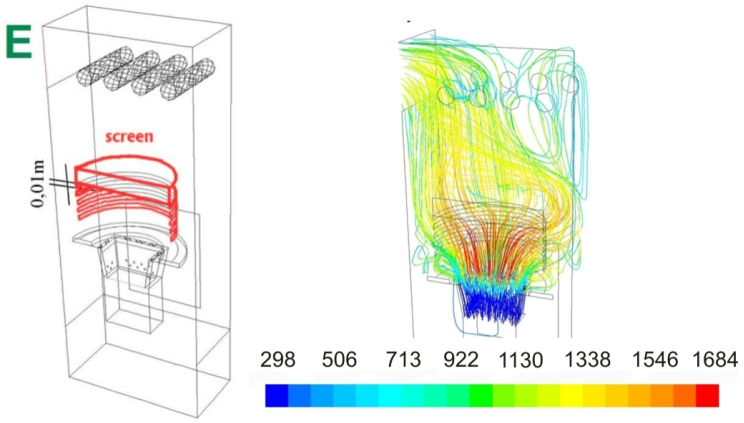

Figure 10.8: Case E (temperature in Kelvin)

A totally different solution is presented as Case F. The deflector, that covers almost the whole cross-section of the boiler (see Figure 10.9), is perforated by drilling boreholes with the diameter of 0.02m. The inside surfaces of the holes are hotter than external walls of the deflector. Such surfaces irradiate each other, which prevents the deflector from loss of heat to the combustion chamber walls. As one can clearly see in Figure 10.9, the gas flows through the holes and immediately escapes to cold areas of the boiler. Thus, it can be observed that too large dimensions of holes as well as of the deflector itself result in an increase of CO concentration in the flue gas by fourteen times, if compared to the Baseline Case.

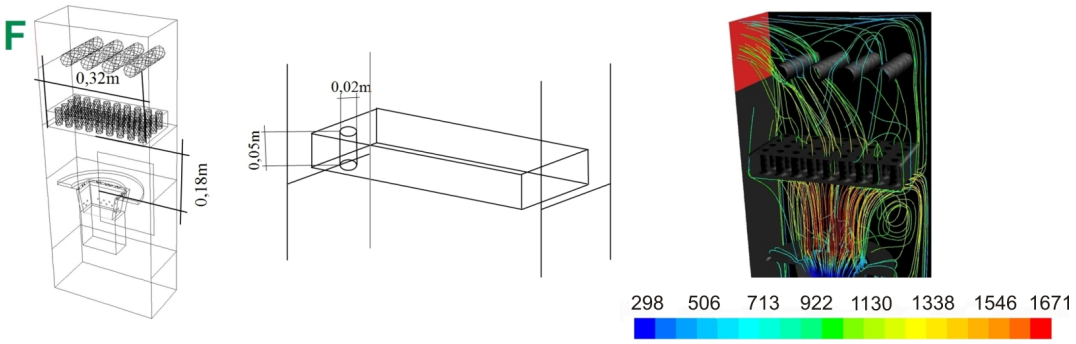

Figure 10.9: Case F (temperature in Kelvin)

Option G (Figure 10.10) takes advantage of the idea comprised in Case F. The deflector is substituted with a number of perforated plates. The plates with drilled boreholes are mutually displaced and form a chessboard pattern to enforce mixing of flowing flue gas and air. The subsequent analysis of flue gas composition performed using the numerical calculations demonstrated an increase of CO concentration in flue gas by four times, if compared to Baseline Case. Despite the improved mixing the set of plates inhibits chemical reactions in the gaseous phase.

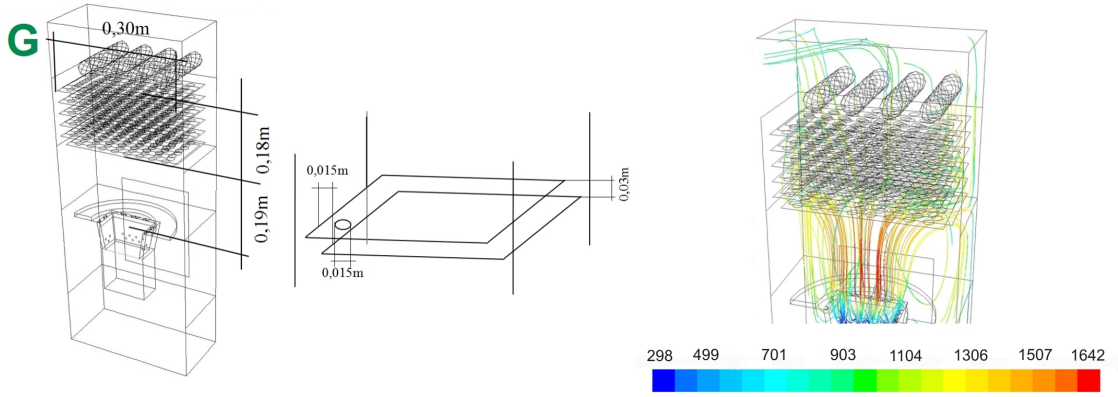

Figure 10.10: Case G (temperature in Kelvin)

For Case H (Figure 10.11) the combustion chamber has been divided by means of a partitioning plate to prevent gas from premature escape from the radiative part to the convective part of the boiler. Such a partitioning plate substantially increases the residence time in the boiler. In Case H the hot combustion products leaving the flame are directed towards a cold side wall and remain in cold bottom part of the boiler for long. With respect to CO concentration, Case H presents the worst solution among all that have already been presented in this study.

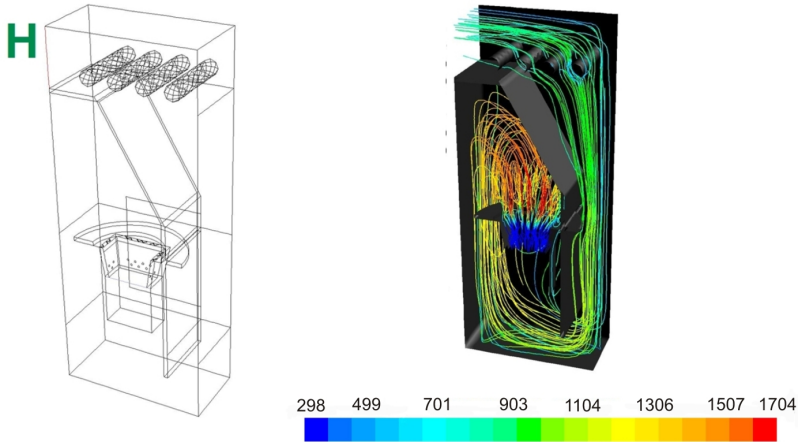

Figure 10.11: Case H (temperature in Kelvin)

Cases I and J (Figure 10.12) present deflectors with very sophisticated shapes that are hard in manufacturing. They are designed to improve mixing. However, the simulations have shown that these designs are also associated with high CO emission, if compared to Baseline Case.

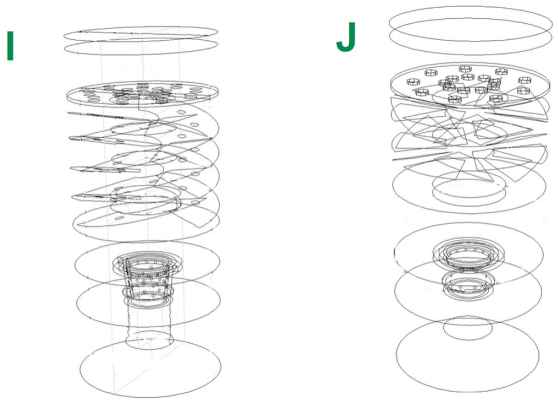

Figure 10.12: Case I and Case J

Example results for the option J (Figure 10.13) demonstrate that gas, owing to the appropriate shape of the deflector has favourable conditions for mixing. Unfortunately, intensive gas circulation occurs in the space between deflector plates so that the gas is cooled and this is the reason for rather poor results obtained for the two last cases.

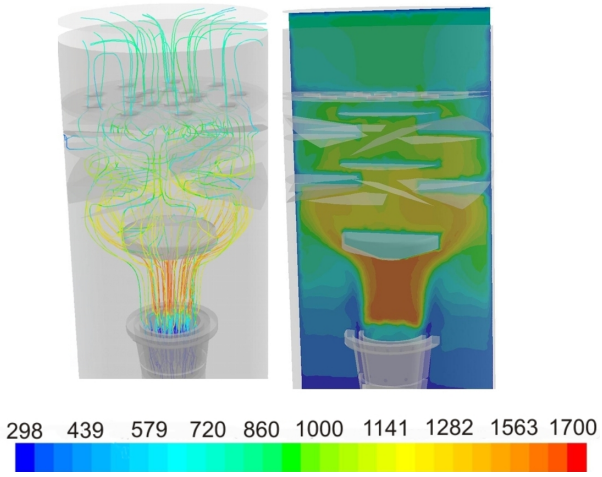

Figure 10.13: Case J

Table 10.1 summarizes the calculation results for all the options associated with modifications of the deflector design. The results indicate that the best solution enabling a decrease of CO and unburned hydrocarbons concentration in discharged flue gas consists of a screen that "shields off" the combustion zone from the water jacket walls (Case E). Similar improvements can also be achieved by lowering of the deflector position (Case A).

Comparison - deflector modifications			
Case	Flue gas Temperature K	CO molar fraction ppm	Hydrocarbons molar fraction ppm
Baseline	938	19	0
A	1082	7	0
B	925	55	0
C	1015	88	0
D	1019	47	0
E	1072	6	0
F	859	273	0
G	852	79	0
H	769	1184	0
I	733	311	5
J	772	510	6

Table 10.1: Comparison of the deflector modifications. Predictions of the mathematical model at the exit of the radiative section.

10.2 Influence of the air distribution

In this paragraph several modifications to the air distribution are considered. In Case K additional air holes, marked in Figure 10.14 as „new openings", are added. The total cross-section area of nozzles suppling the primary air to the retort is increased twofold. The intention is to achieve a lower pressure loss across air channels and a more uniform air supply into the retort. This is also the solution that may reduce hazard of coal sintering. A uniform air distribution may minimize the high temperatures peaks that are responsible for sintering effects. The solution proposed in Case K improves also behavior of flue gas above the bed as shown in Figure 10.14. The gas leaving the bed stays away from the combustion chamber walls. The new air distribution reduce emission of CO by nearly 70% if compared to Baseline Case.

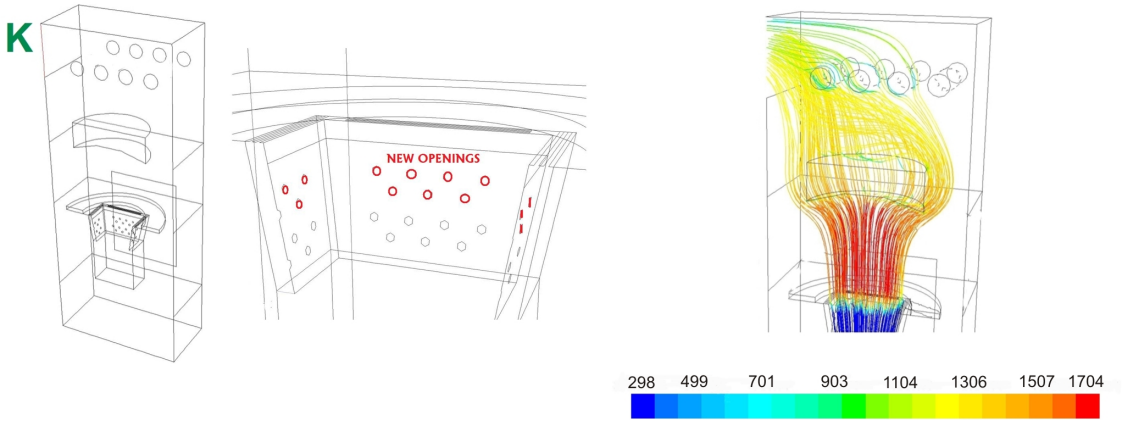

Figure 10.14: Case K (temperature in Kelvin)

In Case L (Figure 10.15) the combustion air is divided into three streams. The first two streams are delivered in the same way as in the Baseline Case. The third ambient temperature air is injected to the combustion chamber at the height of the deflector. Unfortunately, such a solution fails to improve efficiency of combustion. The temperature of the third air is definitely too low which results in fast cooling of the entire chamber.

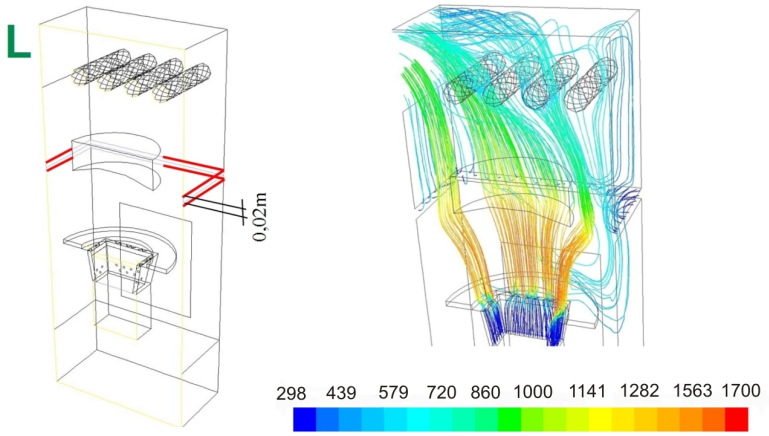

Figure 10.15: Case L (temperature in Kelvin)

In Case M (Figure 10.16) the attempt is made to recirculate some of the combustion products containing about 10% of oxygen back to the flame zone. The additional channel in the retort, shown in Figure 10.16, allows to obtain such an effect by using air stream injected into the combustion chamber. The calculations demonstrate that such a method allows for recirculation of about 10% (by mass) of the flue gas back to the combustion zone. However, calculations demonstrate a deterioration of exit flue gas purity. Concentration of combustible substances in discharged gas substantially increased, as compared to Baseline Case. The recirculation of the flue gas leads to a temperature decrease in the flame zone, which is the main reason for an increased emission of products of incomplete combustion.

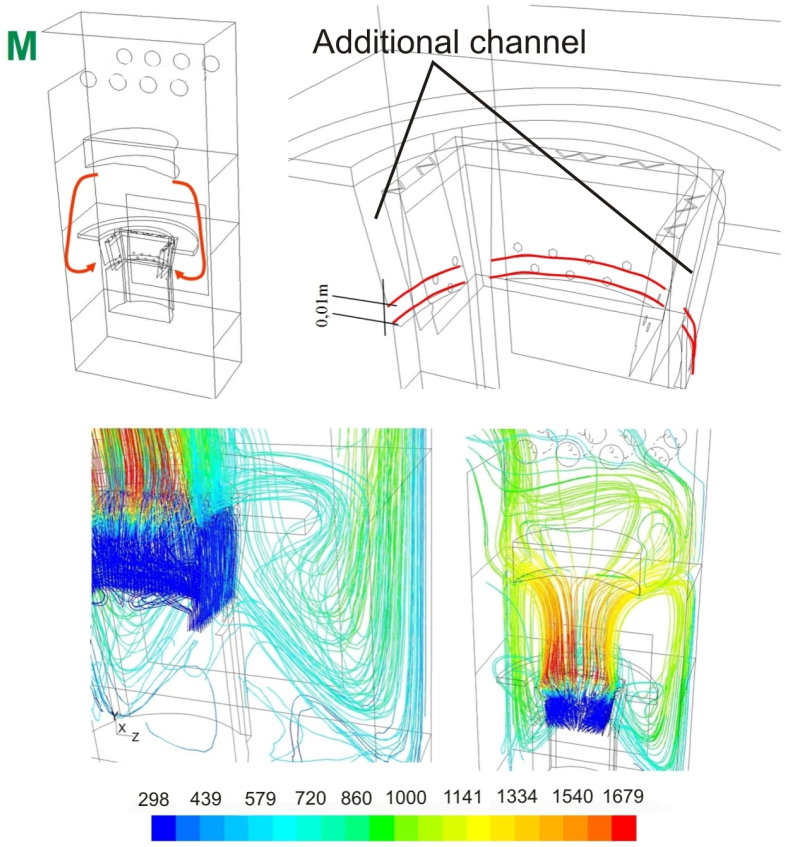

Figure 10.16: Case M (temperature in Kelvin)

One of the major design issues of the commercial 25kW boiler is the method of air supply system. Figure 8.6 shows the layout of orifices (original design) that supply air to the retort and to the combustion zone above. The cold air supplied above the retort to the flame results in cooling of combustibles leaving the retort. Case N (Figure 10.17) is an attempt to reduce the detrimental effect of the cold air. The air is divided into several streams and therefore is gradually mixing with the gas leaving the retort. The calculation results demonstrate that the high temperature zone is spread over much a large area of the boiler and, what is also a beneficial factor, the high temperature gradients exist no more inside the combustion chamber. All these factors lead to substantial improvements of the fuel gas purity, as compared to the Baseline Case. Carbon monoxide emissions are reduced by almost 50%.

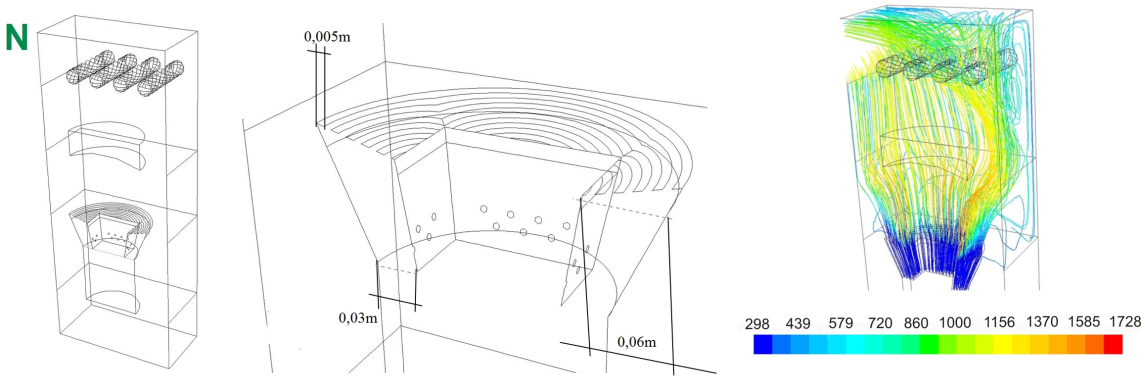

Figure 10.17: Case N (temperature in Kelvin)

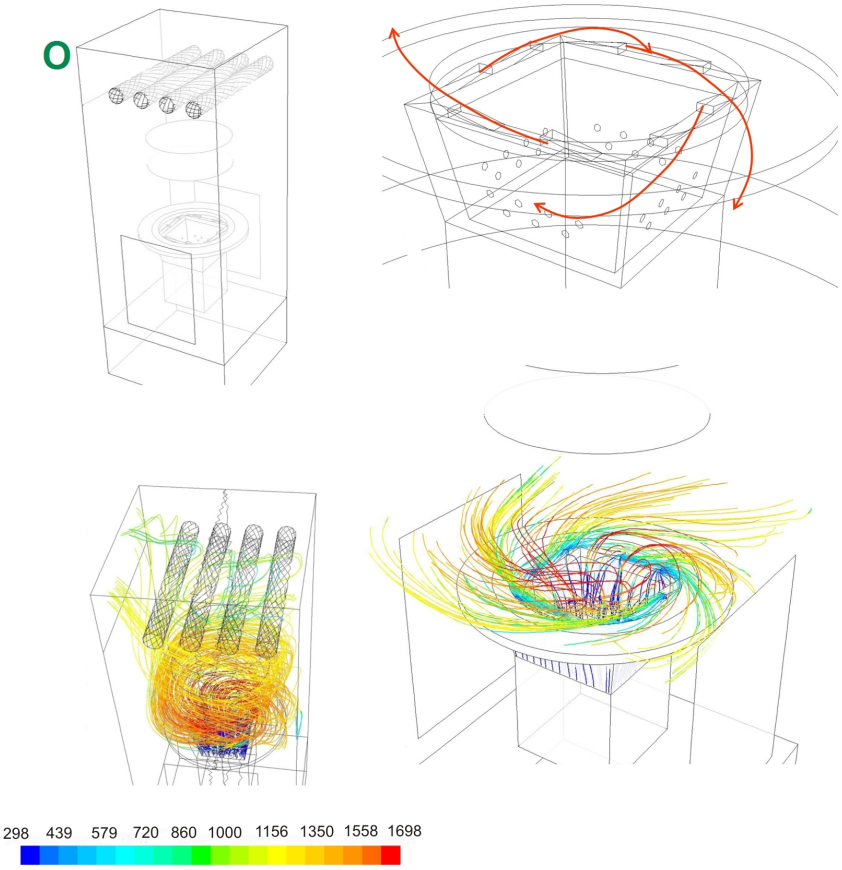

Figure 10.18: Case O (temperature in Kelvin)

The next idea is to improve the mixing by adding a swirling component to the combustion air stream, see Case O shown in Figure 10.18. By redesigning the secondary air nozzles one can easily introduce a swirling velocity component. The calculation results demonstrate that such a mixing pattern leads to an improved uniformity of temperature

inside the combustion chamber. If the solution proposed for this option were applied, the CO concentration in flue gas would be reduced by more than 70% (see Table 10.2) as compared to the Baseline Case.

Table 10.2 shows a comparison of the K - O designs. The best solution, in terms of flue gas purity, is swirling of a portion of the combustion air inside the combustion chamber (Case O).

Comparison - air distribution modifications			
Case	Flue gas Temperature K	CO molar fraction ppm	Hydrocarbons molar fraction ppm
Baseline	938	19	0
K	1099	6	0
L	793	65	0
M	880	70	0
N	1100	10	0
O	1012	6	0

Table 10.2: Comparison of air distribution modifications. Predictions of the mathematical model at the exit of the radiative section.

10.3 Influence of the combustion chamber shape

This part of the study deals with the effect of the combustion chamber shape on the combustion process. The combustion chamber of a commercial 25 kW unit has a shape of a cuboid. That cuboid is embraced by a water jacket. The coldest volumes of that cuboid are located in corners. When gas parcels enter such volumes the combustion reactions are significantly inhibited, which results in an increased emission of unburned combustibles. For Case P (Figure 10.19) the combustion chamber is cylindrical while the other parts remained unaltered, as compared to Baseline Case.

The results obtained by the numerical modeling indicate that the combustion chamber of a circular cross-section, without overcooled corners, substantially improves combustion conditions with a decrease of CO emissions by more than 80%, if compared to CO concentration in flue gas discharged from the combustion chamber of Baseline Case.

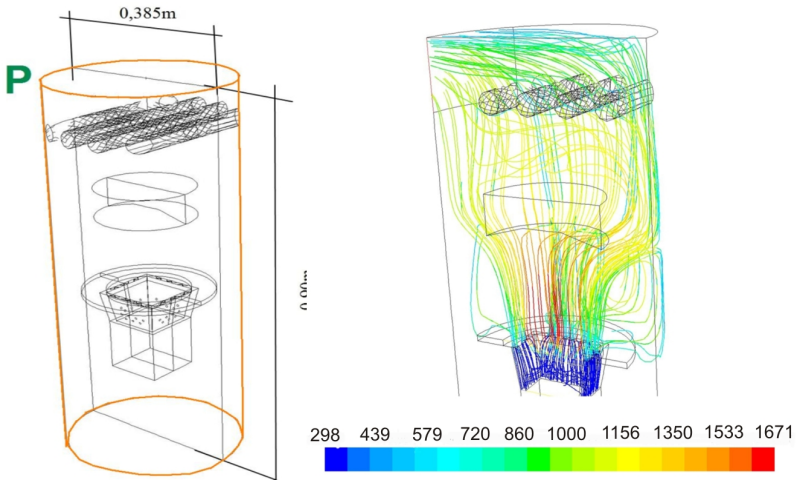

Figure 10.19: Case P (temperature in Kelvin)

Reshaping of the combustion chamber improves the combustion process but at the same time the surface area of walls that separate the combustion chamber and the water jacket is reduced and it deteriorates the heat exchange between these two sub-assemblies of the boiler. To improve the heat transfer rate while keeping the combustion chamber cylindrical Case R is considered (see Figure 10.20). In Case R the gases leaving the retort flow downwards and enter an annular channel flowing then upwards along the boiler walls. The swirling at the combustion air stream has been retained. The calculations demonstrate that Case R seems to be the best design option in terms of the flue gas purity as well as the exchange of heat with water circulating inside the water jacket. The model predictions show 90% CO emission reduction, if compared to Baseline Case.

In summary of this paragraph Table 10.3 is presented. The analysis of CO concentration in the flue gas provides the evidence that the combustion chamber shape affects the combustion process more than modifications associated with redesigning of the deflector shape or redistribution of air inside the boiler. Therefore, the best solution, in terms of flue gas purity, is Case R that consists of a cylindrical combustion chamber, a screen (annular channel) to separate the flame zone from walls of the water jacket, and nozzles that impart swirl to the combustion air stream.

Comparison - boiler construction modifications			
Case	Flue gas Temperature K	CO molar fraction ppm	Hydrocarbons molar fraction ppm
Baseline	938	19	0
P	961	3	0
R	689	0	0

Table 10.3: Comparison of the boiler construction modifications. Predictions of the mathematical model at the exit of the radiative section.

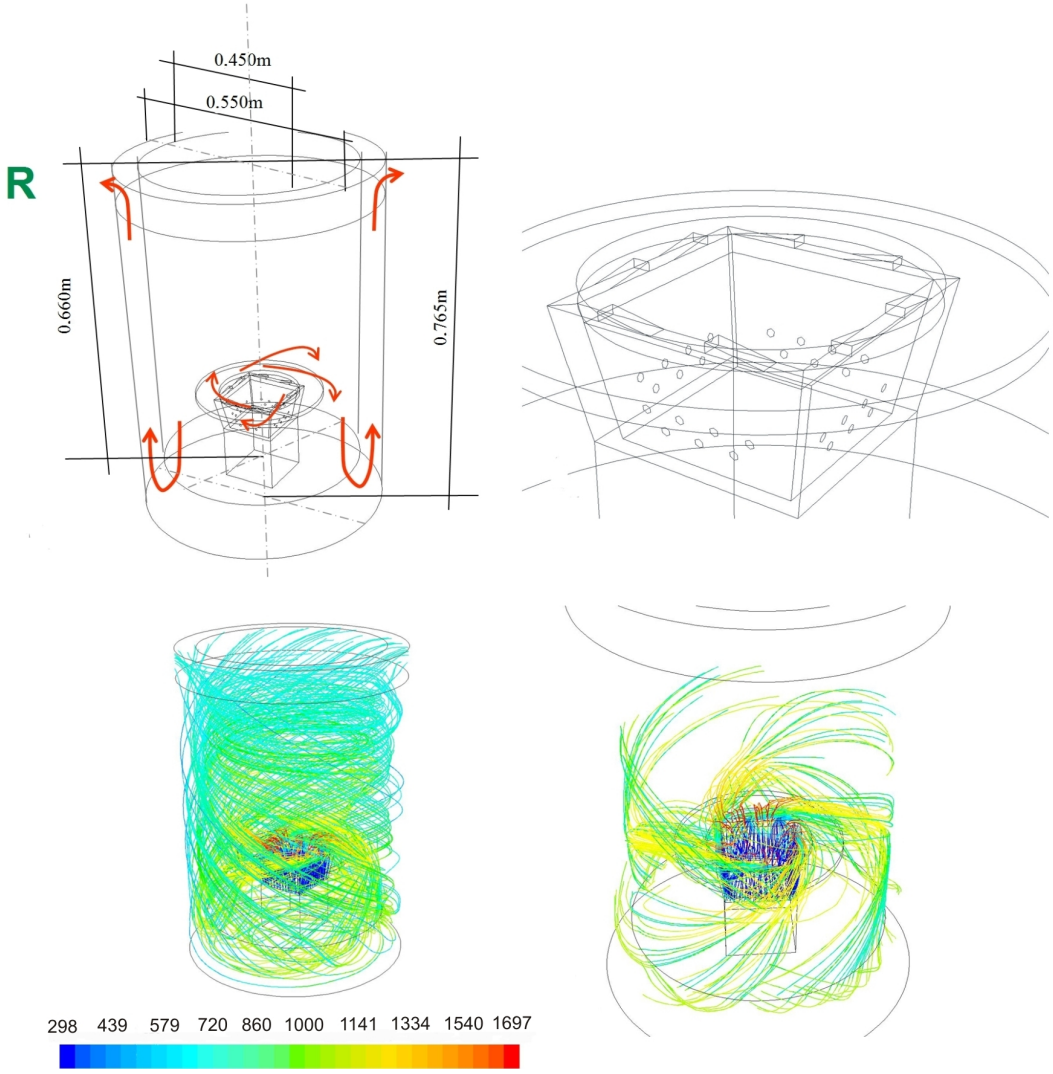

Figure 10.20: Case R - The best design (temperature in Kelvin)

10.4 Improvements related to emission of solid particles

The excess air ratio affects the dust emissions. The air stream delivered to the boiler picks up and conveys small particles (dust) from the bed to the outlet. The larger air flow, the more solid particles reach the boiler outlet. The combustion process with the excess air ratio as high as $\lambda = 2$, which is typical for low-power retort boilers, is known for extensive emission of dust. Table 10.4 presents calculation results related to emissions of solid particles. The analysis is carried out for two design solutions: Baseline Case and Case R. For each of the options the simulations are carried out for two values of the excess air ratio $\lambda = 1.5$ (N1, R2) and $\lambda = 2.0$ (N, R). The assumption is made that 0.05% of the fuel flow rate forms the dust. The dust particle diameters range from 10^{-3} to 10^{-6} m as former investigations demonstrated. Details related to the size distribution of the dust particles are summarized in Table 10.5.

The results, that are summarized in Table 10.4, demonstrate that the reduction of the excess air ratio results in solid particles emissions reduction. The best results are achieved for Case R2. The appropriate design of the combustion chamber combined with reduction of the excess air ratio brings about more than 80% reduction in particulates emission, if compared to Baseline Case. Figure 10.21 shows behavior of solid particles inside the boiler. One can clearly see that for Case R2 dust particles accumulate at the boiler bottom.

Comparison - particles emissions			
Case	Initial mass of the particles released from coal bed, kg/s	Mass of the particles escaped from the chamber, kg/s	Percentage of particles remaining in the chamber, %
Baseline	0.00001298	0.00001199	7.6
N2	0.00001298	0.00001046	19.4
R	0.00001298	0.00001288	0.8
R2	0.00001298	0.00000257	80.2

Table 10.4: Comparison of the cases-particles emissions

Diameter distribution	Rosin-Rammler
Min. Diameter	1.0e-6
Max diameter	1.0e-3
Mean diameter	1.0e-5
Spread parameter	3.5

Table 10.5: Size distribution

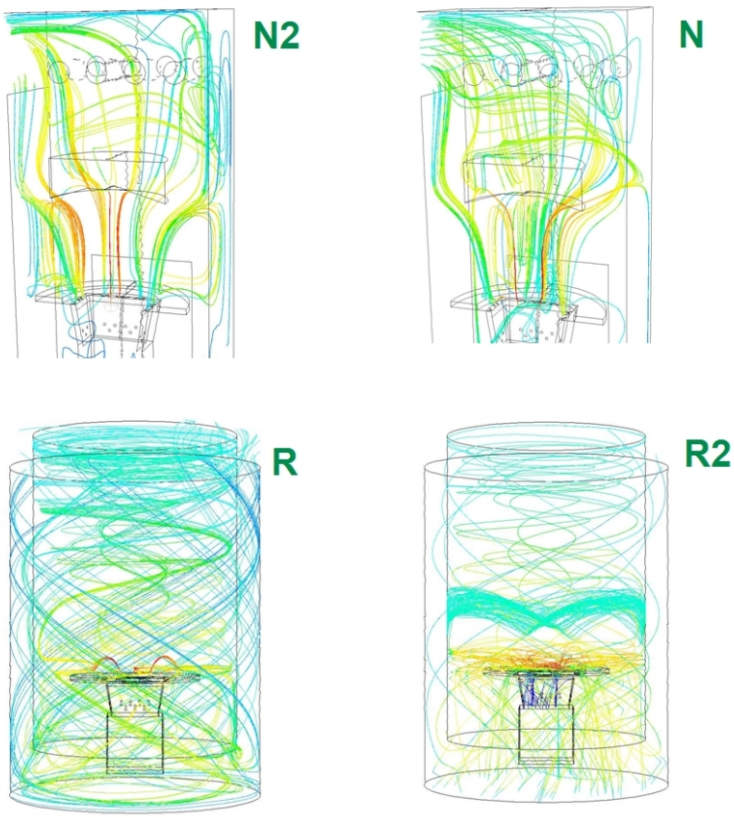

Figure 10.21: Comparison of the cases - particles tracks

10.5 Comparison of the modifications

All modifications considered in Chapter 10 have been intended to improve the combustion process inside the boiler. An overall comparison is shown in Table 10.6 which is accompanied by Figure 10.22. The first part of the table facilities a comparison between boiler design options concerning the deflector shape and position, redistribution of air flow, and reshaping of the combustion chamber. The second part is dedicated to the effect of the excess air ratio on the combustion process for the best design option, namely Case R. The third part of the table brings together the results of calculations carried out to examine alterations to boiler shape and construction.

Comparison - deflector modifications				
Case	Flue gas Temperature, K	CO molar fraction, ppm	hydrocarbons molar fraction, ppm	Percentage of fuel input extracted in radiative section
Baseline	938	19	0	49.2
A	1082	7	0	36.7
B	925	55	0	50.3
C	1015	88	0	42.5
D	1019	47	0	42.2
E	1072	6	0	37.6
F	859	273	0	55.9
G	852	79	0	56.5
H	769	1184	0	63.4
I	733	311	5	66.3
J	772	510	6	63.1
Comparison - air distribution modifications				
Case	Flue gas Temperature, K	CO molar fraction, ppm	hydrocarbons molar fraction, ppm	Percentage of fuel input extracted in radiative section
K	1099	6	0	35.2
L	793	65	0	61.4
M	880	71	0	54.1
N	1100	10	0	35.1
O	1012	6	0	42.8
Comparison - boiler construction modifications				
Case	Flue gas Temperature, K	CO molar fraction, ppm	hydrocarbons molar fraction, ppm	Percentage of fuel input extracted in radiative section
P	961	3	0	47.2
R	689	0	0	69.9
R1	682	0	0	73.3
R2	676	0	0	77.8
N1	994	27	0	58.1
N2	989	1	0	57.8
$N_{em.}$	940	18	0	49.0
$N_{cold.}$	919	32	0	50.8
$N_{hot.}$	973	3	0	46.2

Table 10.6: Comparison of the cases considered in this study

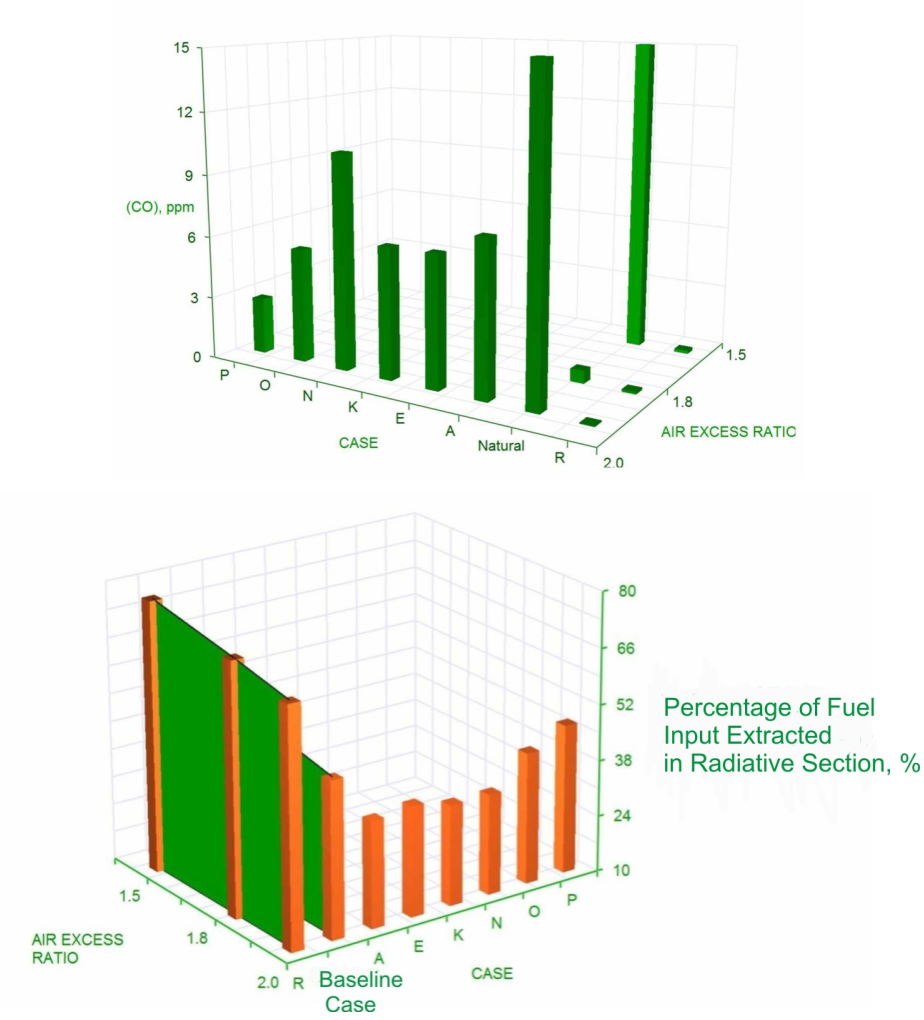

Figure 10.22: Comparison of the best cases

The best solution, in terms of combustion efficiency and exchange of heat inside the radiative part is represented by Case R. This is the option that facilities the improvement of the air distribution and reshaping of the combustion chamber. Additionally, the deflector is removed and the annular channel has been added.

The large number of numerical simulations performed in this thesis allow to identify clear trends in the boiler performance depending on the design/modification implemented. The first notable beneficial change is the modification examined for Case A. The lowering of the deflector may result in a decrease of CO emission even by 60%, as compared to the emission of Baseline Case (25 kW commercial boiler). The next advantageous alteration consists of application of a screen that protects the deflector from excessive loss of heat by radiation to cold walls. Such a screen is proposed for the Case E and results in reduction of CO emission by more than 60%. The subsequent promising modification is associated with the air supply to the retort. The solution proposed for Case K assumes that the number of air orifices is increased. This is the solution that cuts down emission of CO

by nearly 70%. The next favourable solutions are represented by Cases N, O and P that brings about reduction of CO emission by 46%, 72% and 86% respectively. For the Case N the air staging is applied, Case O is associated with swirling of the combustion air whilst Case P assumes the cylindrical shape of the radiative part in the boiler.

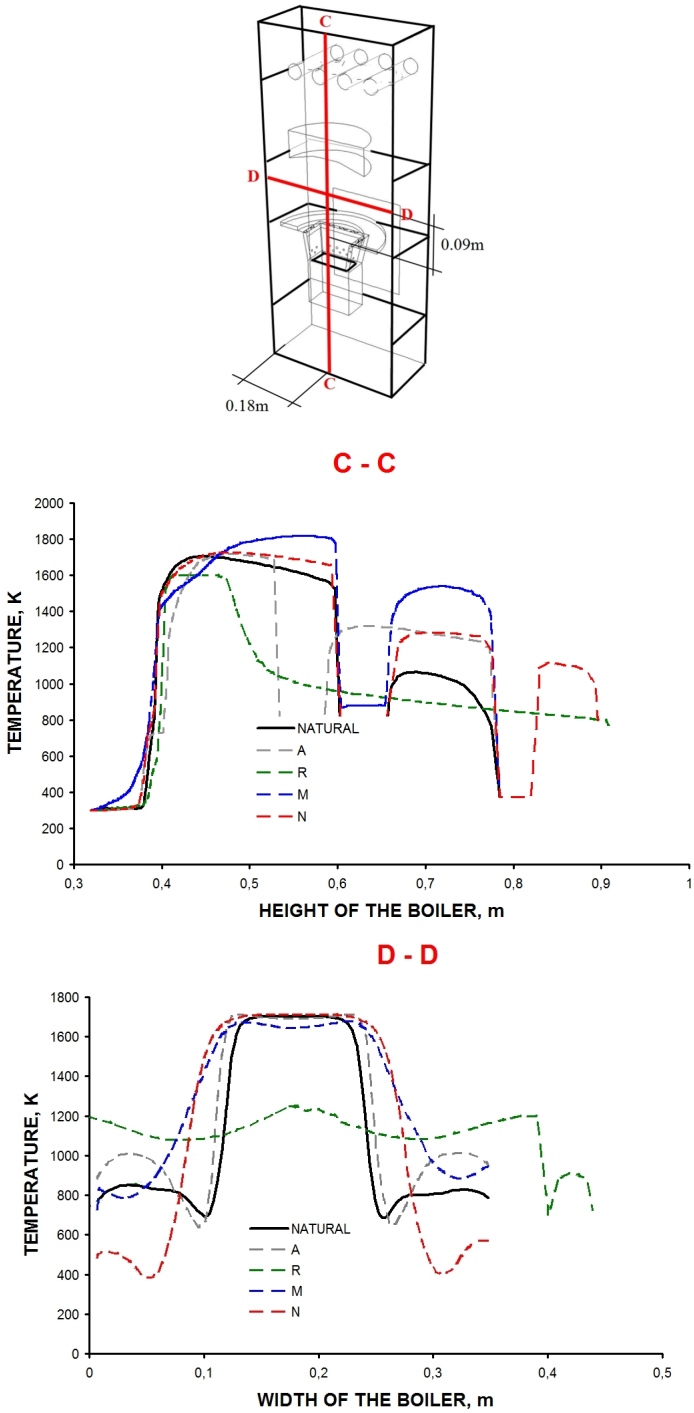

Figure 10.23: Temperature profiles (cross-section C and D)

Figure 10.23 shows a comparison between the most interesting modifications. The two

lower diagrams show temperature profiles across two traverses. The $C-C$ traverse, that presents distribution of the gas temperatures along the boiler height, shows the cooling effect of both the deflector and components of the water jacket. On the other hand, the $D-D$ traverse demonstrates that substantial temperature difference may occur between the combustion chamber centre and the areas nearby the water jacket walls. The diagrams show that the application of air swirling as well as the screen prevent the rapid decrease of temperature inside the combustion chamber.

A prolonged residence time of flue gas within high temperature zones is beneficial for completing the gas phase combustion reactions. Table 10.7 shows the calculated residence time of the gas parcels in the boiler. The table demonstrates that for Case R the resident time is the longest. In such a case the combustibles remain inside the combustion chamber for 1.6 to 3.0 seconds whilst the residence time for the initial design of the combustion chamber (Baseline Case) is never longer than 1.0 second.

Comparison - residence time	
Case	Residence time, sec.
Baseline	0.4 - 1.0
A	0.7 - 0.9
N	0.5 - 1.5
M	0.8 - 1.8
R	1.6 - 3.0

Table 10.7: Residence time - comparison of the cases

A certain improvement of combustion conditions can be achieved even without alterations to the boiler design. An appropriate organization of the combustion process in 25 kW commercial unit may lead to a pretty high improvement of the flue gas purity. Cases N2 and N1 refer to examinations of the relationship between the excess air ratio and emissions of products of uncompleted combustion. For Case N2 it is assumed that the excess air ratio inside the combustion chamber is $\lambda = 1.8$, whilst for Case N1, $\lambda = 1.5$. One can see that the excess air ratio in the 25 kW commercial unit should be reduced to the value of $\lambda = 1.8$ (N2). The excess air ratio of $\lambda = 2$ results in overcooling of the combustion chamber interior and excessive loss of heat. The reduction of the excess air ratio results in a reduction of CO by 90% as well as a reduced chimney loss.

Finally, for N_{cold} and N_{hot} Cases one examines how temperature of water jacket walls affects the discharged flue gas. In Case N_{cold} the temperature of the water jacket walls is $303K$ while in N_{hot} Case it is $453K$. The results summarized in Table 10.6 demonstrate a relationship between the temperature of the water jacket walls and pollutants emission. The higher temperature of combustion chamber walls, the lower is the emission of products from incomplete combustion.

Table 10.6 shows the effect caused by the excess air ratio for the (best) Case R; two

values of the excess air ratio, namely R2- $\lambda = 1.5$ and R1- $\lambda = 1.8$ have been considered. The effect of λ parameter onto emission of undesired substances is insignificant. One can conclude that the combustion process for the 'R' design option is less sensitive to variations of the excess air ratio, if compared to Baseline Case.

The analyses related to behavior of solid particles (fly ash) inside the combustion chamber have demonstrated that operation of boilers with low values of the excess air ratio results in reduced emissions of solid particles. Figure 10.21 indicates that the best solution corresponds to Case R2. The cylindrical shape of the combustion chamber as well as reduced air ratio result in more than 80% reduction of solid particles discharge.

10.6 Efficiency of the retort boiler

The efficiency of retort boilers is defined as:

$$\eta = \frac{\mathsf{N_{boiler}}}{\mathsf{P \cdot LCV}} = \frac{\mathsf{G_{water} \cdot c_{water}(T_{out} - T_{in})}}{\mathsf{P \cdot LCV}} \tag{10.1}$$

where:

P	- fuel mass flow rate,	$\frac{kg}{s}$,
G_{water}	- water mass flow rate,	$\frac{kg}{s}$,
c_{water}	- specific heat of water,	$\frac{J}{kgK}$,
T_{out}	- water temperature at the water jacket inlet,	K,
T_{in}	- water temperature at the water jacket outlet,	K.

Thermal efficiency of the small scale retort boilers is usually in the 80 - 90%, range and it may drop to 70 - 80% if the boiler is derated or overrated. Then, pollutants emissions also increase. Experimental data (see Table 10.8), show that the retort boiler which is considered in this thesis, has an efficiency equal to 0.84.

In the numerical simulations presented in Chapter 9 the radiative section of the boiler, has been considered the radiative section of the boiler only. However, in order to calculate the boiler thermal efficiency using the developed CFD - based model, it is imperative to include also the convective section of the boiler. The boiler exit parameters listed in Table 10.8, correspond to the convective section outlet.

Fuel input	
LCV, kJ/kg	28549
flow rate, kg/h	3.83
fuel input, kW	30.37
excess air ratio	1.6
Hot water	
flow rate, kg/s	0.34
inlet temperature, K	323
outlet temperature, K	341
enthalpy rate, kW	25.65
Boiler exit	
flue gas temeprature, K	498.11
chimney draft, Pa	4.6
CO_2, vol. %	12.85
O_2, vol. %	8.15
CO, mg/m_n^3	2291.40
Boiler Efficiency	
0.84	

Table 10.8: Measurements of retort boiler efficiency [145]

Comparison of the experimental and predicted data (boiler exit values)		
Flue gas		
	Measured	Predicted
flue gas temeprature, K	498	532
chimney draft, Pa	4.6	4.6
CO_2, vol. %	12.85	11.72
O_2, vol. %	8.15	8.75
CO, mg/m_n^3	2291.40	139.71
rated power, kW	25.65	24.01
thermal effciency	0.84	0.79

Table 10.9: Comparison of predicted and measured data

Figure 10.24 shows the whole boiler unit, as it has been set up in an additional computational run that includes both boiler sections. Table 10.9 shows the calculated and measured parameters at the boiler outlet. The predicted thermal efficiency is 79% while 84% has been measured. The observed 5% difference is due to a number of factors mainly due to discrepancy in the wall temperature and emissivity, simplified radiative heat transfer calculations, and imperfections in CFD model for the convective section. Obviously, such a 5% difference is visible on the predicted boiler exit temperature that is by 34K higher than the measured value. The measured and predicted oxygen and carbon dioxide volume fractions are in good agreement. As it has been already discussed in Section 9.2, the carbon monoxide concentration at the outlet exceeds by far the measured value.

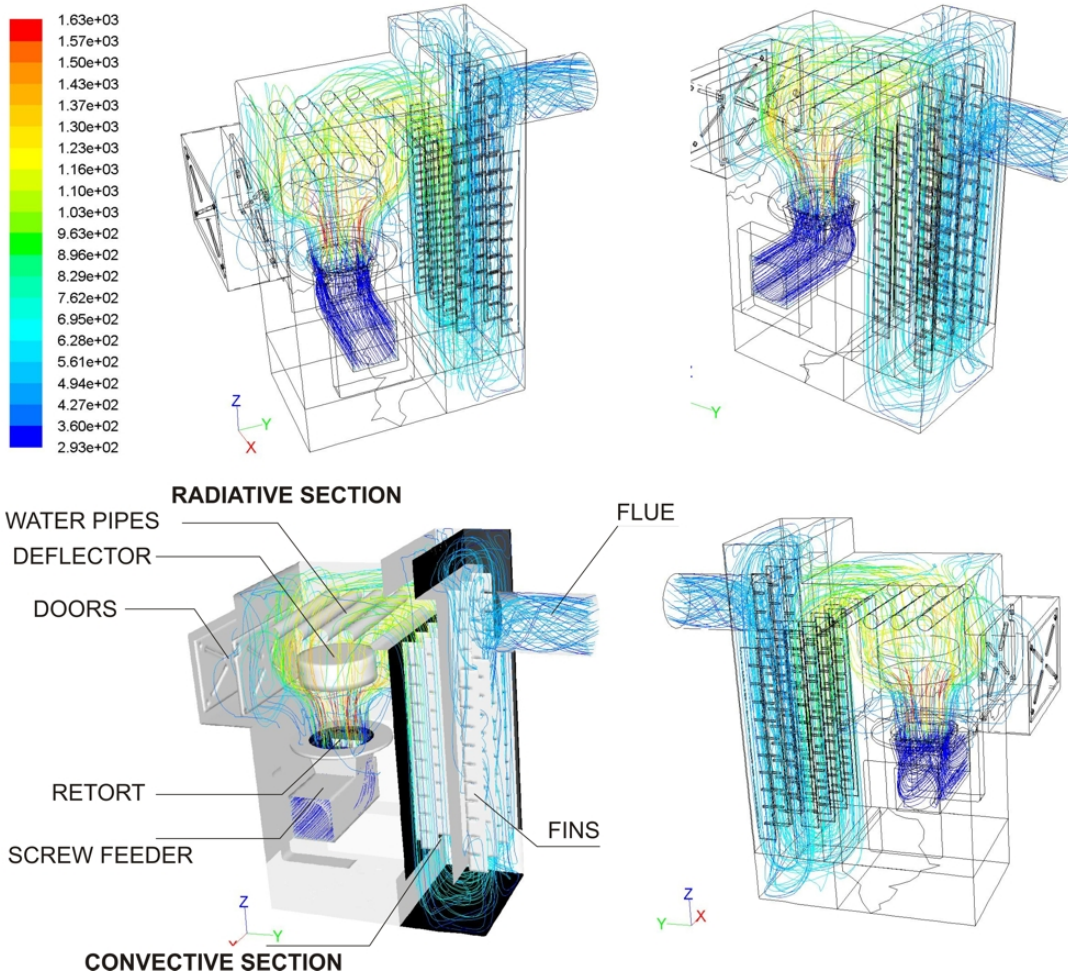

Figure 10.24: The boiler unit - path lines colored by temperature (temperature in Kelvin)

It is informative to consider again Case R (λ=1.8) where the boiler geometry and combustion conditions have been optimized so that the convective section has been removed. The thermal efficiency of the radiative section of Case R is 69% which is by 19% larger than the radiative section efficiency of the original retort boiler operated at 1.8 excess air ratio. Thus, this confirms again the superiority of Case R design over the commercial unit.

11 Summary and Conclusions

This study is dedicated to examining of combustion processes in a small - scale retort boiler fired with specially prepared coal (or biomass pellets). Such units are operated in many houses, both in Poland and in Europe. The boilers are designed on the basis of experience and intuition of manufacturers.

The present study aims at improving the combustion process in such boilers. Herein, the searching for design improvements is based on scientific background, which is a new approach in this boiler sector. In order to find out the best design solutions a CFD - based mathematical model has been developed. The fixed-bed sub-model developed in this thesis constitutes the heart of the overall CFD-based boiler model. The fixed-bed sub-model has been validated against measurements of temperature and gas composition of a fixed-bed of EKORET coal.

The validation process has demonstrated satisfactory agreement between predictions and measurements. The correlation coefficient for temperature ranges from 0.858 to 0.957 while the same coefficients for the gas composition varies within the 0.871 to 0.906 interval. The lowest values of correlation coefficients are obtained for CO at the level of 0.6. The sensitivity analyses revealed that the pre-exponential factor and the activation energy of the combustion reaction affects the obtained results to the most significant degree.

The newly developed fixed-bed sub-model has been implemented into the CFD Fluent code to simulate a commercial boiler unit. Numerical calculations have been carried out for the non-structural mesh comprising about $1,000,000$ cells. The boiler is operated at $25kW$ (nominal power), with the value of excess air ratio $\lambda = 2,0$ that is typical for units of that type. The validation procedure for the overall boiler model has been carried out using the temperature and gas composition measurements in the commercial unit. The validation has indicated satisfactory correlation for both temperatures and gas composition. The correlation coefficients are at the level of 0.94 for temperatures and 0.7 - 0.99 for species. The correlation coefficient for CO has been as high as 0.99. The validation procedure has demonstrated that the model is suitable to predict performance of real boilers with sufficient accuracy and confidence. Then, the model is used to optimize the boiler performance.

The numerical model is used to improve boiler operation. Perfecting the boiler design resulting in reduced emission of pollutants, (CO, unburned hydrocarbons and fly ash) can be achieved by repositioning of the deflector, redirection of air supply paths into the combustion chambers as well as reshaping of the combustion chamber. According to the model predictions, lowering of the deflector by 0.065 m with respect to its initial position results in a decrease of CO emission by more than 60% (compared to the emission of the commercial unit). When an additional screen is used to protect the combustion zone together with the deflector against cold walls of the combustion chamber the emission of CO can be reduced by 67%.

Other modifications related to redistribution of the combustion air have also been beneficial and lead to substantial improvements. Swirling of the secondary air has resulted in 72% reduction of the CO concentration. The swirl has enhanced the mixing, and it prolonged the residence time both resulting in equalization of temperature inside the boiler. The model calculations have shown that reshaping of the combustion chamber from the initial cubicoid to the cylinder-shaped form leads to 86% reduction of CO emission.

Finally, an optimized boiler design has been proposed (Case R), which features the circular combustion chamber and combustion air swirling. The decrease of CO emission by more than 90% is foreseen at excess air ratio of 2.0. According to the model predictions, the optimized boiler can operate at 1.5 excess air ratio (Case R2) with 80% reduced CO, unburned hydrocarbons and particles emissions. The overall boiler efficiency is then increased since 30% more energy is extracted from the radiative part (combustion chamber) of the boiler than in the commercial unit.

There is no doubts, the newly developed model has proven to be a useful tool in both analyzing and optimizing the boiler performance.

References

[1] Coal Industry Advisory Board, World Coal Demand and Supply Prospects, Meeting with IEA Governng Board, 2003.

[2] Gawlik L., Grudziński Z., Projection of coal prices in international turnover in comparison, Międzynarodowa Konferencja "Przyszłość węgla w gospodarce świata i Polski", 136-144, 2004.

[3] EIA, Annual Energy Outlook 2004 with projections to 2025, Energy Information Administration, Washington, 2004.

[4] IEA, Coal information 2003, International Energy Agency, Paris, 2003.

[5] IEA, Energy Policies of IEA Countries, International Energy Agency, 2009.

[6] IEA, Worldwide Engagement for Sustainable Energy Strategies, International Energy Agency, 2010.

[7] Coal Information 2010, International Energy Agency, 2010.

[8] Blaschke W., Przyszłość węgla kamiennego przeznaczonego dla użytkowania w energetyce, Zakład Ekonomii i Badań Rynku Paliwowo-Energetycznego, PAN, Kraków 2006.

[9] Ney R., Ocena zasobów, wydobycia i zużycia węgla kamiennego i brunatnego w Polsce, Mat. Konf. Przyszłość węgla w gospodarce świata i Polski. PK ŚRE, GIPH. Katowice 2004.

[10] Brendow K., Global and regional coal demand perspectives to 2030 and beyond, Mat. Konf. Przyszłość węgla w gospodarce świata i Polski. PK ŚRE, GIPH. Katowice, 2004.

[11] Nowaczyk M, Zasuń R., Mamy największe złoża węgla brunatnego na świecie, Gazeta Wyborcza, 2008.

[12] Ocena jakości powietrza w Polsce za rok 2003, Główny Inspektorat Ochrony Środowiska. Warszawa, 2004.

[13] Niska emisja, Górnicza Izba Przemysłowo-Handlowa, Nr 9-10 (87-88), Wrzesień - Październik 2002.

[14] Sprzedaż Węgla, Ekogroszek workowany, strona internetowa <http://www.sprzedazwegla.pl/ekogroszek/>.

[15] Katowicki Holding Węglowy S.A., Ekoret i Ekofins - węgiel do kotłów niskoemisyjnych, strona internetowa <http://wegiel.katowice.pl/ekoret_i_ekofins/>.

[16] Firma Ekogroszek, Czym jest ekogroszek i gdzie ma zastosowanie?, strona internetowa <http://www.ekogroszek.info.pl/content/view/3/2>.

[17] Wach. E, Polski rynek pelet w 2007 roku, Bałtycka Agencja Poszanowania Energii S.A, 2008.

[18] Firma Barlinek, Co to jest Pelet?, strona internetowa <http://www.pelet.com.pl/Pelet/pelet-informacje-ogolne>

[19] Chrapka R., Kotły na ekogroszek, strona internetowa, <http://www.info-ogrzewanie.pl>, 2006.

[20] Kurczabiński L., Nowoczesne technologie spalania węgla w małych i średnich źródłach wytwarzania ciepła - aspekty ekonomiczne i ekologiczne, strona internetowa, <http://www.khw.pl/237?p=7>.

[21] Matuszek K., Zawistowski J., Spalanie węgla w kotłach małej mocy. Organiczne związki, strona internetowa, <http://www.ogrzewnictwo.pl>.

[22] Tomeczek J., Zgazowanie węgla, Gliwice, Wydawnictwo Politechniki Śląskiej, 1991.

[23] Tomeczek J., Spalanie węgla, Gliwice, Wydawnictwo Politechniki Śląskiej, 1992.

[24] Chiew Y., Glandt E., Simultaneous conduction and radiation in porous and composite materials: effective thermal conductivity, Ind. Eng. Chem. Fundamen., 1983, 22 (3), 276-282, 01 May 2002.

[25] Hütter E. S., Kömle N. I., Determination of the radiative contribution to the effective thermal conductivity of a granular medium under vacuum conditions, 5^{th} European Thermal-Sciences Conference, The Netherlands, 2008.

[26] Schotte W., Thermal conductivity of packed beds, AIJChE Journal, 6:63-67, 1960.

[27] Atkinson B., Merrick D., Mathematical models of the thermal decomposition of coal 4. Heat transfer and temperature profiles in a char-oven charge National Coal Board, Coal Research Establishment, Stoke Orchard, Cheltenham, Glos., GL52 4RZ, UK, 1982.

[28] Shadle L., Shamsi A., Spontaneous Combustion of Char Stockpiles, Energy & Fuels, 12 (6), pp 1305-1312, 1998.

[29] Badzioch S., Gregory D., Field, M., Investigation of the Temperature Variation of the Thermal Conductivity and Thermal Diffusivity of Coal, Fuel, 43, 267-280, 1964.

[30] Merrick D., Mathematical models of the thermal decomposition of coal, 2. Specific heats and heats of reaction, National Coal Board, Coal Research Establishment, Stoke Orchard, Cheltenham, Glos., GL52 4RZ, UK, July 1982.

[31] Merrick D., Mathematical models of the thermal decomposition of coal 1. The evolution of volatile matter National Coal Board, Coal Research Establishment, Stoke Orchard, Cheltenham, Glos., GL52 4RZ, UK, July 1982.

[32] Nussbaumer T., Combustion and Co-combustion of Biomass: Fundamentals, Technologies, and Primary Measures for Emission Reduction, Energy&Fuels, 17 (6), pp 1510-1521, 2003.

[33] Perkins G., Sahajwalla V., A Mathematical Model for the Chemical Reaction of a Semi-infinite Block of Coal in Underground Coal Gasification, Energy&Fuels, 2005, 19 (4), 1679-1692, 29, April 2005.

[34] Tsang T. , Modeling of Heat and Mass Transfer During Coal Block Gasification, Ph.D. Thesis, The University of Texas at Austin, Austin, TX, 1980.

[35] Roberts D., Harris D., Char Gasification with O_2, CO_2 and H_2O: Effects of Pressure on Intrinsic Reaction Kinetics, Energy&Fuels , 14, 483-489, 2000.

[36] Tomita A., Mahajan O., Walker Jr., P., Reactivity of Heat-Treated Coals in Hydrogen, Fuel, 56, 137-144, 1977.

[37] Chomiak J., Combustion: a study in theory, fact and application, New York, Gordon and Breach Science Publishers, 1990.

[38] Kostowski E., Przepływ ciepła, Wydawnictwo Politechniki Śląskiej, Gliwice, 2000.

[39] Boardman R., Smooth L., Fundamentals of Coal Combustion for Clean and Efficient Use, Amsterdam, Elsevier, 1993.

[40] Bes A., Dynamic Process Simulation of Limestone Calcination in Normal Shaft Kiln, Ph.D thesis, Magdeburg University, 2005.

[41] VDI Warmeatlas. 8^{th} Edition. Springer Verlag, Berlin, Heidelberg, 1997.

[42] Jeschar R., Specht E., Alt R., Grundlagen der Warmeubertragung. Viola-Jeschar-Verlag, Goslar 1990.

[43] Matuszek K, Duża emisja z małych, Instytut Chemicznej Przeróbki Węgla, Zabrze, 2005.

[44] Wall et al., PECS, 5, 1-29, 1979.

[45] Jeżowiecka-Kabsch K., Szewczyk H., Mechanika płynów, Oficyna Wydawnicza Politechniki Wrocławskiej, Wrocław, 2001.

[46] Bogusławski A., Drobniak S., Tyliszczak A., Turbulencja - od losowości do determinizmu, Instytut Maszyn Cieplnych, Politechnika Częstochowska, 2001.

[47] Prandtl L., Bericht uber Untersuchungen zur Ausgebildeten Turbulenz. Z. Angew. Math. Mech., N0 5, S. 136-169, 1925.

[48] Harlow F., Nakayama P., Transport of turbulence energy decay rate, University of California, Rep. LA-3854,1968.

[49] De Soete G., Overall Reaction Rates of NO and N_2 Formation from Fuel Nitrogen, Proc. Combust. Inst., 15:1093-1102, 1975.

[50] Wilk R., Podstawy niskoeminsyjnego spalania, Katowice, Wydawnictwo Gnome, Katowice, 2000.

[51] Melte P., Pratt D., Measurements of atomic oxygen and nitrogen oxides in jet stirred combustion, Proc. Combust. Inst., 15:1061-1070, 1974.

[52] Chen W., Smoot L., Fletcher T., Boardman R., Global Rate Expression for Nitric Oxide Reburning. Part II. Energy & Fuels, 10:1046-1056, 1999.

[53] Chen W., Smoot L., Hill S., Fletcher T., A computational method for determining global fuel-NO rate expressions, Part I. Energy & Fuels, 10:1036 -1046, 1999.

[54] Merrick D., Mathematical models of the thermal decomposition of coal 3. Density, porosity and contraction behaviour, National Coal Board, Coal Research Establishment, Stoke Orchard, Cheltenham, Glos., GL52 4RZ, UK, July 1982.

[55] Rezaei H., Gupta R., Bryant G., Hart J., Liu G., Baileya C., Wall T., Miyamae S., Makino K., Endo Y., Thermal conductivity of coal ash and slags and models used, Fuel, Volume 79, Issue 13, Pages 1697-1710, October 2000.

[56] Nosek R., Simplified method of solid fuels characterization and its application for modeling of fixed bed combustion, Politechnika Śląska,Wydział Inżynierii Środowiska i Energetyki, Instytut Techniki Cieplnej, Ph.D thesis, Zilina - Gliwice, 2009.

[57] Engineering Equation Solver, help files of the program.

[58] Szlęk A. Badanie procesu spalania paliw stałych w warstwie nieruchomej, Wydawnictwo Politechniki Śląskiej, Gliwice, 2001.

[59] Postrzednik S., Żmudka Z., Badania nad porowatością wkładów ceramicznych katalizatorów samochodowych, XI. Sympozjum Wymiany Ciepła i Masy. PAN, ITC Politechniki Śląskiej, Gliwice - Szczyrk, 2001.

[60] Sangtong-Ngam K., Narasingha M., Phil M., Kinetic Study of Thai-lignite Char Gasification Using the Random Pore Model, The Joint Graduate School of Energy and Environment, Thammasat Int. J. Sc. Tech., Vol. 13 No. 3, July-September 2008.

[61] Arias B., Pevida C., Rubiera F., Pis J., Changes In Coal Char Reactivity and Texture During Combustion in an Entrained Flow Reactor, Journal of Thermal Analysis and Calorimetry, Vol. 90 (2007) 3, 859-863, 2007.

[62] Gupta J., Bhatia S., A modified discrete random pore model allowing for different initial surface reactivity, Carbon 38 (2000) 47-58, 2000.

[63] Guo J., Lua A., Experimental and Kinetic Studies on Pore Development During CO_2 Activation of Oil-Palm-Shell Char, Journal of Porous Materials, Volume 8, Number 2, pp. 149-157(9), March 2001.

[64] Coelho P., Duic N., Lemos C., Carvalho, Modelling of a Solid Fuel Combustion Chamber of a Ramjet Using a Multi-block Domain Decomposition Technique, Aerospace Science and Technology, no 2, 107-I19, 1998.

[65] Zhou H., Jensen A., Glarborg P., Jensen P., Kavaliauskas A., Numerical modeling of straw combustion in a fixed bed, Combustion and Harmful Emission Control (CHEC) Research Center, Fuel 84 (2005) 389-403, 2005.

[66] Radulovic P., Usman Ghani M., Smoot L., An improved model for fixed bed coal combustion and gasification, Fuel, Vol 74, No. 4, pp. 582-594, 1995.

[67] Bruch Ch., Peters B., Nussbaumer T., Modelling wood combustion under fixed bed conditions, Fuel 82 (2003) 729-738, 2003.

[68] Cooper J., Hallett W., A numerical model for packed-bed combustion of char particles, Chemical Engineering Science 55 (2000) 4451-4460, January 2000.

[69] Ryu Ch., Shin D., Choi S., Effect of fuel layer mixing in waste bed combustion, Advances in Environmental Research 5 (2001) 259-267, 2001.

[70] Oman J., Tacer M., Tuma M., Overfeed fixed-bed combustion of wood, Bioresource Technology 67 (1999) 139-147, 1999.

[71] Ryan J., Hallett W., Packed bed combustion of char particles: experiments and an ash model, Chemical Engineering Science 57 (2002) 3873 - 3882, 2002.

[72] Kaer S., Straw combustion on slow-moving grates—a comparison of model predictions with experimental data, Biomass and Bioenergy 28 (2005) 307-320, 2005.

[73] Lin P., Yonghao L., Wang Y., A non-isothermal integrated model of coal-fired traveling grate boilers, Applied Thermal Engineering 29 (2009) 3224-3234, 2009.

[74] Sudiro M., Pellizzaro M., Bezzo F., Simulated moving bed technology applied to coal gasification, Bertucco A., Chemical Engineering Research and Design, 2009.

[75] Khan A., Bowen J., Analysis of Fixed Bed Reactors Using a Diffuse Interface Single Pellet Model, Trans IChemE, Vol 77, Part A, January 1999.

[76] Casajus C., Abrego J., Marias F., Vaxelaire J., Sanchez J., Gonzalo A., Product distribution and kinetic scheme for the fixed bed thermal decomposition of sewage sludge, Chemical Engineering Journal 145 (2009) 412-419 , 2009.

[77] Wiliams A., Backreedy R., Habib R., Jones J., Pourkashanian, Modelling coal combustion: the current position, Fuel, 81 605-618, 2002.

[78] Cho Y., Joseph B., Heterogeneous Model for Moving-Bed Coal Gasification Reactors, Ind. Eng. Chem. Process Des. Dev. 20 314-318, 1981.

[79] Agnew J., Zhang D., Gasification of a South Australian low-rank coal with carbon dioxide and steam: kinetics and reactivity studies, Ind. Eng. Fuel, Vol. 77, No. 11 1209-1219, 1998.

[80] Johansson R., Thumman H., Leckner B., Influence of intraparticle gradients in modeling of fixed bed combustion, Combustion and Flame, 149 49-62, 2007.

[81] Li L., Xiang J., Numerical studies on the combustion properties of char particle clusters, International Journal of Heat and Mass Transfer, 52 4785-4795, 2009.

[82] Radulovic P., Ghani M, Smoot L., An Improved model for fixed bed coal combustion and gasification, Fuel, Vol 74, 4 582-594, 1995.

[83] Sudiro M., Pellizzaro M, Bezzo F., Bertucco Alberto, Simulated moving bed technology applied to coal gasification, Chemical Engineering Research and Design, 88 465-475, 2010.

[84] Cui Y., Stubington J., In-bed char combustion of Australian coals in PFBC. 2. Char combustion without secondary fragmentation, Fuel, 80 2235-2243, 2001.

[85] Cooper J., Hallett W., A numerical model for packed-bed combustion of char particles, Chemical Engineering Science , 55 4451-4460, 2000.

[86] Gupta J., Bhatia S., A modified discrete random pore model allowing for different initial surface reactivity, Carbon, 38 47-58, 2000.

[87] He R., Suda T, Fujimori T., Sato J., Effect of particle sizes on transport phenomena in single char combustion, International Journal of Heat and Mass Transfer, 46 3619-3627, 2003.

[88] Boiko E., Pachkovskii S., A Kinetic Model of Thermochemical Transformation of Solid Organic Fuel, Russian Journal of Applied Chemistry,Vol 77, 9 1547-1555, 2004.

[89] Fermoso J., Arias B., Pevida C., Plaza M., Rubiera F., Pis J., Kinetic Models comparison for steam gasification of different nature fuel chars, Journal of Thermal Analysis and Calorimetry,Vol 91, 3 779-786, 2008.

[90] Oman J., Tacer M., Tuma M., Overfeed fixed-bed combustion of wood, Journal of Thermal Analysis and Calorimetry, Bioresource Technology, 67 139-147, 1999.

[91] Murphy J., Shaddix C., Combustion kinetics of coal chars in oxygen-enriched environments, Combustion and Flame, 144 710-729, 2006.

[92] Jones W., Lindstedt R., Global reaction schemes for hydrocarbon combustion, Combustion and Flame, 73(3) 233-250, 1988.

[93] Kim J., Schnell U., Scheffknecht G., Comparison of Different Global Reaction Mechanisms for MILD Combustion of Natural Gas. Combustion Science and Technology, 180(4) 565-592, 2008.

[94] Howard J., Wiliams G., Fine H., Kinetics of carbon monoxide oxidation in postflame gases, 14^{th} Symposium on Combustion, 975- 986, 1973.

[95] Johansson R., Thumman H., Leckner B., Sensitivity Analysis of a Fixed Bed Combustion Model, Energy & Fuels, 21 1493-1503, 2007.

[96] Field M., Rate of combustion of size-graded fractions of char from low-rank coal between 1200K and 2000K, Combustion and Flame, 13 237-252, 1969.

[97] Smoot, L., Smith P., Coal combustion and Gasification, New York, Plenum Press, 1985.

[98] Arthur, J., Reaction between oxygen and carbon, Transaction of the Faraday Society, 47, 164, 1951.

[99] Bruch C., Peters B., Nussbaumer T., Modelling wood combustion under fixed bed conditions, Fuel, 82 729-738, 2003.

[100] Zhou H., Peters B., Jensen A., Glarborg P., Jensen P., Kavaliaukas A., Numerical modeling of straw combustion in a fixed bed, Fuel, 84 389-403, 2005.

[101] Yu J., Zhang M., Experimental and modeling study on char combustion, Energy & Fuels, 23 2874-2885, 2009.

[102] Lu H., Robert W., Pierce G., Ripa B., Baxter L., Comprehensive study of biomass particle combustion, Energy & Fuels, 22 2826-2839, 2008.

[103] Thunman H., Leckner B., Niklasson F., Johnsson F., Combustion of Wood Particles - A Particle Model for Eulerian Calculations, Combustion and Flame, 129 30-46, 2002.

[104] Porteiro J., Granada E., Collazo D., Patino D., Moran J., F., A Model for the Combustion of Large Particles of Densified Wood, Energy & Fuels, 21 3151-3159, 2007.

[105] Yang Y., Sharifi V., Swithenbank J., Ma L., Darvell L., Jones J., Pourkashanian M., Williams A., Combustion of a Single Particle of Biomass, Energy & Fuels, 22 306-316, 2008.

[106] Agroskin, A., Goncharov, E., The Specific Heat of Coal, Coke Chem. U.S.S.R., 2 9-14 1965.

[107] Agroskin, A., Gonczarow, L., Thermal Capacity and Heat of Pyrolysis of Donbass Coal, Koks i Chimija, 5 8-13, 1970.

[108] Gladkov, L., Lebedev, A., Specific Heat of Solid Fuel and Coal Dust, Izv. VTI, 8 18-20,1948.

[109] Kirov, N., Specific Heats and Total Heat Contents of Coals and Related Materials at Elevated Temperatures, BCURA Month. Bull., 29 33-57, 1965.

[110] Postrzednik, S., Thermodynamic Analysis of Solid Fuel Devolatilization, Zesz. Nauk., 691, Politechnika SI., Gliwice, 1981.

[111] Wicke M., Peters W., Specific Heat Capacity, Heat and Temperature Transfer Coefficient of Solid Fuels (in German), Brennstoffchemie, 49 97-102, 1968.

[112] Thunman H., Leckner B., Niklasson F., Johnsson F., Combustion of Wood Particles-A Particle Model for Eulerian Calculations, Combustion and Flame, 129 30-46, 2002.

[113] Johnsson F., Thunman H., Leckner B., Sensitivity Analysis of a Fixed Bed Combustion Model, Energy & Fuels, 21 1493-1503, 2007.

[114] Boiko E., Pachkovskii S., A Kinetic Model of Thermochemical Transformation of Solid Organic Fuels, Russian Journal of Applied Chemistry, Vol. 77, No. 9 1547 - 1555, 2004.

[115] Chan W., Kelborn M., Krieger B., Modeling and experimental verification of physical and chemical processes during pyrolysis of large biomass particle, Fuel, 64 (11), 1505 - 1513, 1985.

[116] Turns S., An Introduction to Combustion: Concepts and Applications 2^{nd} ed., McGRAW-HILL, New York, 2000.

[117] Cooper J., Hallet W., A numerical model for packed bed combustion of char particles, Chemical Engineering Science, 55 4451- 4460, 2000.

[118] Johnsson R., Thunman H., Leckner B., Influence of intra particle gradients in modeling of fixed bed combustion, Combustion and Flame, 149 49 - 61, 2007.

[119] Ye D., Agrew J., Zhang D., Gasification of a South Australian low rank coal with carbon dioxide and steam: kinetics and reactivity studies, Fuel, Vol. 77, No. 11, 1209 - 1219, 1988.

[120] Pottgiesser C., Pyrolyse von Steinkohlen in einem Bereich von 1 bis 100 bar, Ph.D thesis, TH Aachen, 1980.

[121] Arendt P., Entgasung und hydrierende Vergasung von Steinkohlen im Druckbereich von 0,1 bis 90 bar bei Aufheizgeschwindigkeiten von 100 bis 1000 K/s, Dissertation TH Aachen, 1980.

[122] Lowenthal G., Kinetik der Korngrossenarderung von Steinkohlen bei der Pyrolyse und Hydropyrolyse, Bergbau-Forschung GMbH, Essen, 1984.

[123] Wiljenskij T., Hzmaljan D., Dinamika Gorenija Pyljewidnowo Topliwa, Energija, Moskwa, 1978.

[124] Ferziger J. Peric M., Computational Methods for Fluids Dynamics, Springer Verlag, 1999.

[125] Chung T., Computational Fluid Dynamics, Cambridge University Press, 2002.

[126] Magnussen B., Hjertager B., On Mathematcal Modeling of Turbulent Combustion with Special Emphasis on Soot Formation and Combustion. 16^{th} Symp. (Int.) on Combustion. Comb. Inst., Pittsburg, Pennsylvania, pp. 719-729, 1976.

[127] Magnussen B., Hjertager B., Olsen J., Bhaduri D., Effect of Turbulent Structure and Local Concentration on Soot Formation and Combustion in C_2H_2 Diffusion Flames, 17^{th} Symp. (Int.) on Combustion (1978). Comb. Inst., Pittsburg, Pennsylvania, pp.1383-1393, 1979.

[128] Magnussen B., On the Structure of Turbulence and a Generalized Eddy Dissipation Concept for Chemical Reaction in Turbulent Flow, 19^{th} AIAA Aerospace Science Meeting, St.Louis, Missouri, 12-15, 1981.

[129] Chern J., Hayhurst A., A model for the devolatilization of a coal particle sufficiently large to be controlled by heat transfer, Combustion and Flame, 146 553-571, 2006.

[130] Park K., Kim C., Park W., Modeling of gas-carbon reaction in pore diffusion control regime, Korean J. of Chem. Eng., 5(1) 35-40, 1988.

[131] Hzmaljan D., Kagen A., Teorija gorenija i topcznyje ustrojstwa, Energija, Moskwa, 1976.

[132] Hobler T., Ruch ciepla i wymienniki, WNT, Warszawa, 1968.

[133] Kolb T., Bleckwehl S., Gehrmann, Seifert H., Characterisation of combustion behavior of refuse derived fuel, Journal of Energy Institute, vol 81 no 1, 2008.

[134] Beckmann M., Scholtz R., Wiese C., Busch M., Peppler E., Gasification of waste minerals in grate systems, INFUB, vol. 2, Proceedings of the 4^{th} European Conference, Portugal, pp. 73 - 89, 1997.

[135] Scholz R., Jeschar R., Schopf N., Kloeppner G., Process Control and Process Engineering in the Nonpollutive Combustion of Wastes, Chemlnform, vol. 22 issue 12, 1991.

[136] Scholz, R.; Beckmann, M.; Schulenburg, F., Waste Incineration Systems, Current Technology and Future Developments in Germany, 3^{rd} European Conference on Industrial Furnaces and Boilers, Portugal, 1995.

[137] PN-EN 12809 Kotły grzewcze na paliwa stałe. Nominalna moc cieplna do 50 kW. Wymagania i badania.

[138] PN-EN 303-5 Kotły grzewcze – Część 5: Kotły grzewcze na paliwa stałe z ręcznym i automatycznym zasypem paliwa o mocy nominalnej do 300 kW – Terminologia, wymagania, badania i oznakowanie.

[139] Rozporządzenie Ministra Środowiska z dnia 20 grudnia 2005 r. w sprawie standardów emisyjnych z instalacji (DzU Nr 260, poz. 2181).

[140] Kubica K., Kryteria efektywności energetyczno-ekologicznej kotłów małej mocy i paliw stałych dla gospodarki komunalnej. Certyfikacja na znak bezpieczeństwa ekologicznego, Opracowanie IChPW, 1999.

[141] Kubica K., Dobre praktyki produkcji energii cieplnej dla indywidualnego i komunalnego ogrzewnictwa, Polski Klub Ekologiczny, Katowice, 2006.

[142] Behnke A., PM-Emissions and reduction measures in Germany, Dustconf, Feredral Environment Agency, 2007.

[143] Erste Verordnung zur Durchführung des Bundes-Immissionsschutzgesetzes (Verordnung über kleine und mittlere Feuerungsanlagen - 1. BImSchV) Vom 26. Januar 2010.

[144] Kim R., Ein Prozessodell zur Kokserzeung mit direkter Beheizung, PhD at Technical University of Clausthal, Faculty of Energy and Management, 2010.

[145] Kubica K., Private Communication, 2010,

[146] Weber R., Extracting mathematically exact kinetic parameters from experimental data on combustion and pyrolysis of solid fuels, Journal of the Energy Institute,vol. 81, no. 4, 2008.

Curriculum vitae

Personal data

Name	:	Rafał Buczyński
Born	:	05.08.1981
in	:	Brzozów (Poland)
Family status	:	bachelor
Address	:	Rafał Buczyński, Korfantego 9c/170
		41-100 Siemianowice Śląskie, Poland

School education

1988 - 1996 : Primary school, Siemianowice Śląskie (Poland)

1996 - 2001 : Technical College of Land Surveying, Katowice (Poland)
: **Degree**: Land Survey Technician,
Abitur (secondary school leaving examination)

Academic education

2001 - 2006 : Study at the Silesian University of Technology, Gliwice (Poland)
: Faculty of Environmental Engineering and Energy
: Institute of Thermal Technology
: **Specialization**: The Application of Computer Methods
: in Energy Engineering and Environmental Engineering
: **Degree**: M.Sc.
M.Sc. thesis title: High Steam Gasification of Coal and Biomass

2006 - 2011 : Ph.D. Studies at Silesian University of Technology, Gliwice (Poland)
: and Clausthal University of Technology, Clausthal-Zellerfeld (Germany)

Working experience

08/2005 - 10/2005 : MESCO, Computer simulations in industry and in science
Tarnowskie Góry (Poland)

01/2006 - 07/2006 : MSc Project, Combustion Engineering Laboratory,
University of Maryland (USA)

02/2009 - 05/2009 : Marie Curie Research Fellow at Clausthal University of Technology
Clausthal-Zellerfeld (Germany)

09/2010 - present : Research assistant at the Institute of Energy Process Engineering
and Fuel Technology, Clausthal University of Technology (Germany)